Tool Path Verification and Gouge Avoidance in Five-Axis Machining

by

Khalid R. Sheltami

A thesis
presented to the University of Waterloo
in fulfilment of the
thesis requirement for the degree of
Doctor of Philosophy
in
Mechanical Engineering

Waterloo, Ontario, Canada, 2000

©Khalid R. Sheltami 2000

National Library of Canada
Acquisitions and Bibliographic Services
395 Wellington Street
Ottawa ON K1A 0N4
Canada

Bibliothèque nationale du Canada
Acquisitions et services bibliographiques
395, rue Wellington
Ottawa ON K1A 0N4
Canada

Your file Votre reference

Our file Notre reference

The author has granted a non-exclusive licence allowing the National Library of Canada to reproduce, loan, distribute or sell copies of this thesis in microform, paper or electronic formats.

L'auteur a accordé une licence non exclusive permettant à la Bibliothèque nationale du Canada de reproduire, prêter, distribuer ou vendre des copies de cette thèse sous la forme de microfiche/film, de reproduction sur papier ou sur format électronique.

The author retains ownership of the copyright in this thesis. Neither the thesis nor substantial extracts from it may be printed or otherwise reproduced without the author's permission.

L'auteur conserve la propriété du droit d'auteur qui protège cette thèse. Ni la thèse ni des extraits substantiels de celle-ci ne doivent être imprimés ou autrement reproduits sans son autorisation.

0-612-53516-9

Canada

The University of Waterloo requires the signatures of all persons using or photocopying this thesis. Please sign below, and give address and date.

To My Parents

Abstract

In five axis machining of curved surfaces, the cutting surface of the tool, whether it is a sphere or a torus, lies very close to the design surface. Quite often the cutting surface falls below the design surface resulting in a gouge or overcut. These gouges are unacceptable. Thus, for a tool path to be acceptable it must be tested for gouging and corrected to avoid any gouges. The thesis of this work is to develop a swept volume generation method, which allow fast modeling of machined surface and quick detection of gouging. Subsequently, gouging tool positions can be corrected to generate a gouge free tool path. Rather than using the traditional boolean operations method, a new sweeping technique based on identifying "generating curves" along the tool path is developed. This technique reduces computation time significantly and consequently speeds up the simulation process. The new is augmented with a gouge-detection technique developed based on sectioning the generating curves by parallel planes. This results in planar representations of the moving tool, which enables the gouge detection and elimination to be done in two dimensions, thereby reducing complexity.

A computer program (Swept Volume Simulator *SVS*) has been implemented for five-axis machining based on the new techniques and was verified experimentally for different test pieces. It was also compared with the simulation results from the *Z-map* technique. The results of the experimental verification show the method to be accurate to within 15 μm for the test pieces. Furthermore, the computation time for the new technique is significantly less than the *Z*-map method. It is concluded that the new method allows fast simulations and accurate verifications of five-axis tool paths.

Acknowledgements

I would like to take this opportunity and offer my thanks to my supervisors Dr. F. Ismail and Dr. S. Bedi for their patience, understanding and encouragement throughout this project.

I would like to extend my thanks to my family and my wife, who continuously supported and encouraged me.

Financial support for the author was provided by *The Ministry of Scientific Research of Libya.*

Contents

1 Introduction 1

1.1 Thesis Outline 5

2 Literature Review 7

2.1 Introduction 7

2.2 Swept Volume 8

2.2.1 The Theoretical Methods 8

2.2.2 The Procedural Methods 11

2.3 Gouge Detection and Correction 17

3 The "Generating Circles" Technique 20

3.1 Introduction 20

3.2 Generating Circles 21

3.3 Implementation 28

3.3.1 The Solid Model 37

4 Numerical and Experimental Verifications for Generating Circles 42

4.1 Experimental Verifications 42

4.2 Comparison with Another Simulator 53

4.3 Effects of Changing the Step Size 57

5 The "Generating Curves" Technique 61

5.1 Introduction 61

5.2 The General APT Tool 62

5.3 Three-Dimensional Generating Curves for Toroidal Cutters 66

5.4 The Simulation Process 68

5.4.1 Equations of the Generating Curves in Toroidal Cutters . . . 72

5.4.2 The Swept Volume Simulator 74

5.4.3 Equations of the Generating Curves of Conical and Cylindrical Cutters 77

5.4.4 Equations of the Generating Curves of the General APT Tool 78

6 Numerical and Experimental Verifications for Generating Curves 87

6.1 Experimental Verifications 90

6.2 Numerical Verifications 93

7 Gouge Checking and Avoidance Methods 99

7.1 Introduction 99

7.2 The Sectioning Gouge-Detection Method 100

7.3 Gouge Elimination 104

7.3.1 Gouge Correction 104

8 Numerical and Experimental Verifications for Gouge Checking and Avoidance **109**

9 Conclusions and Recommendations **124**

9.1 Conclusions 124

9.2 Future Work 126

Bibliography **128**

List of Figures

1.1 Scallops Produced by ball-end mill cutters 2

1.2 Commonly Used Cutters 4

2.1 The Swept Volume for a Compact Two-Manifold Sweeping in R^3 . . 9

2.2 Ruled Surface Segments Generated by the Edges of a Sweeping Square Polygon 12

2.3 Toroidal Milling Tool Characteristic Profiles 13

2.4 The Z-map Method 15

2.5 The "Mow the Grass" Technique 16

3.1 The Toroidal Cutter 22

3.2 A Surface Generated by Rotating a Flat-End-Mill about a Point on the Tool Axis 23

3.3 A Toroidal Cutter Generating a Spherical Surface 24

3.4 The Flat End Mill Approximates a Toroidal Cutter as it Machines a Surface 26

3.5 The "Generating Circle" and its Projection onto the Cutting Plane 27

3.6 A four-axis Configuration of the CNC Machine 29

3.7 The Projection of the Tool at Two Consecutive Positions to Determine the Tangency Point for a *Concave Surface* 30

3.8 The Projection of the Tool at Two Consecutive Positions to Determine the Tangency Point for a *Convex Surface* 31

3.9 The Projection of the Tool at Two Consecutive Positions to Determine the Tangency Point for a *Flat Surface* 32

3.10 An Example of the "Generating Circles" in Consecutive Tool Positions 35

3.11 Various Components of Swept Volume of an Example Tool Path . . 38

3.12 Flow Chart to Generate The Swept Surface 39

4.1 Dimensions of the Circular Cut 44

4.2 The Solid Model of the Volume Swept by the Tool for the Circular Cut 45

4.3 The Solid Model of the Workpiece after the Subtraction of the Swept Volume of the Circular Cut 46

4.4 The Solid Model of the Volume Swept by the Tool for the Spiral Cut 47

4.5 The Sinusoidal Tool Path 48

4.6 The Solid Model of the Volume Swept by the Tool for the Sinusoidal Cut 49

4.7 The Difference Between Measured and Simulated Results for the Circular Cut at Two Sections 51

4.8 The Difference Between Measured and Simulated Results for the Spiral Cut at Two Sections 52

4.9 The Difference Between Measured and Simulated Results for the Sinusoidal Cut at Three Sections 54

4.10 Comparison Between the "Generating Circles" Technique and the Z-map Technique 56

4.11 The Change of Radius of the "generating circle" with respect to The Step Size for The Sinusoidal Cut 59

5.1 A Comparison Between Sweeping Profiles of the Generating Circles and the Generating Curves Methods 63

5.2 A Comparison Between Sweeping Profiles of the Generating Circles and the Generating Curves Methods, the Bottom View 64

5.3 A General Tool 65

5.4 Definition of the General Tool 66

5.5 The Splitting of the Front Half and Back Half of the Tool Procedure 67

5.6 The Concept of Corresponding Inserts 69

5.7 Two Consecutive Tool Positions of a Torus in Five-Axis Movement 70

5.8 A five-axis Configuration of the CNC Machine 71

5.9 A Swept Surface by a Toroidal Cutter in Four Subsequent Tool Positions 75

5.10 The Swept Volume Simulator Algorithm 76

5.11 Approximating Conical and Cylindrical Cutters with an Infinite Number of Circular Layers 78

5.12 A Sweeping Profile of the Generating Curves of a Conical cutter in a Five-Axis Tool Motion 79

5.13 A Sweeping Profile of the Generating Curves of a Cylindrical cutter in a Five-Axis Tool Motion 80

5.14 Two Consecutive Tool Positions in Five-Axis Movement 81

5.15 A Sweeping Profile of the Generating Curves of the General APT Tool in a Five-Axis Tool Position 83

5.16 A Five-Axis movement with the Feed Direction angle $> \theta_{start}$ . . . 84

5.17 The Sweeping Profile of the Generating Curves when the Feed Direction Angle is Greater than θ_{start} in Three-Axis Motion 85

5.18 A Swept Volume of Four Subsequent Tool Positions When the Feed Direction Angle is Greater than θ_{start} 86

6.1 The Concave Turbine Blade Surface, Test Surface 1 88

6.2 Test Surface 2 89

6.3 The Difference Between Scanned and Simulated Results for the Turbine Blade at $X = 10\ mm$ and Parallel to Y Axis 92

6.4 The Difference Between Scanned and Simulated Results for the Test Surface at $X = 50\ mm$ and parallel to Y Axis 94

6.5 Comparison Between the "Generating Curves" and Z-map Techniques for The Turbine Blade at Three Sections 95

6.6 Comparison Between the "Generating Curves" and Z-map Techniques for The Test Surface at Three Sections 96

6.7 Comparison Between Swept Volume Representation in Generating Curves and Z-map Methods 98

7.1 Matching the Generating Curves Sections with the Corresponding Sections on the Surface 101

7.2 Difficulties in Identifying Surface Normals in the Triangularizaion Method 103

7.3 Positioning in the Inclined Tool Method 105

7.4 Tool Axis Plane for An Inclined Tool 106

7.5 The Gouge Detection and Elimination Procedure 108

8.1 A Test Surface Machined with The Inclined Tool Method. $\alpha = 3°$. 111

8.2 The Test Surface Simulated with $\alpha = 3°$ 112

8.3 Comparison of Scanned and Simulated Results for Inclined Tool Method at $Y = 20\ mm$, $\alpha = 3°$ 113

8.4 Comparison of Scanned and Simulated Results for Inclined Tool Method at $Y = 70\ mm$, $\alpha = 3°$ 114

8.5 Comparison of Scanned and Simulated Results for Inclined Tool Method at $Y = 110\ mm$, $\alpha = 3°$ 115

8.6 A Test Surface Machined with The Inclined Tool Method. $\alpha = 6°$. 117

8.7 Comparison of Scanned and Simulated Results for Inclined Tool Method at $Y = 20\ mm$, $\alpha = 6°$ 118

8.8 Comparison of Scanned and Simulated Results for Inclined Tool Method at $Y = 70\ mm$, $\alpha = 6°$ 119

8.9 Comparison of Scanned and Simulated Results for Inclined Tool Method at $Y = 110\ mm$, $\alpha = 6°$ 120

8.10 A Test Surface Machined with the Inclined Tool Method 122

8.11 A Test Surface Machined with the New Antigouging Method . . . 122

Chapter 1

Introduction

The increase in complexity of modern parts requires more sophisticated techniques to reduce the computer simulation time and increase the accuracy of the simulations.

Sculptured surfaces and other geometric entities of tools, dies and molds are commonly machined on 3 axis milling machines with ball-end mill cutters. However, as is well known, the machinability of these cutters is poor near the bottom, and sometimes, workpieces of complex geometry cannot be machined by three-axis milling; five-axis technology would have to be employed. Figure 1.1 shows the schematics of a ball-end mill cutter machining a curved surface. Typically the machined surface lies above the designed surface. If the machined surface falls below the designed surface, it results in gouging or over cutting. This gouging is acceptable if it is within pre-specified limits, otherwise, it can result in scraping the workpiece or expensive repair. The surface is machined with a number of tool passes generated using CAM package. The tool pass comprises of a numerous cut-

ter location points. The spacing between the tool passes is called cross-feed. The un-machined material between two passes is called scallop or cusp which requires a long time of hand finishing to produce the designed parts.

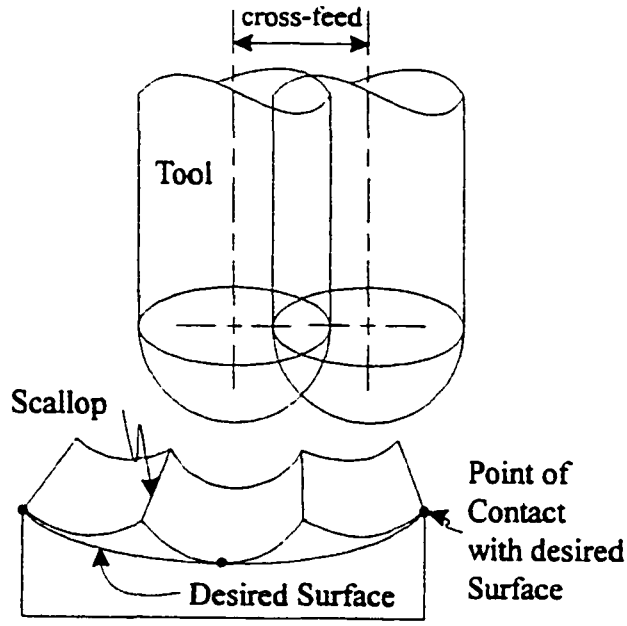


Figure 1.1: Scallops Produced by ball-end mill cutters

To decrease cusp heights when machining sculptured surfaces with a ball-end mill, the tool path cross feed must be adjusted in consideration of the cusp height. This method normally requires a long machining time, because of the large number of passes of the tool, and a manual polishing is required to remove the cusps.

The making of tools, dies and molds from stock is done in phases, namely, rouging, finish machining and hand polishing. Typically, for large dies the percentage of total machining time spent in: the rouging phase is around 10%: the finish ma-

chining phase is around 25%, and; the hand polishing phase is around 50%. The percentage of total machining time in the respective phases for small and medium size dies is about the same as above. The time spent in the finish machining phase, however, is the largest among these.

For all these reasons, five-axis CNC milling with radiused end mills and/or toroidal cutters is becoming increasingly popular. Generally, five-axis milling yields smaller cusp heights at greater feeds than three-axis milling. Figure 1.2 shows the cutters commonly used in machining of surfaces: ball nose, flat bottom and toroidal end mills.

In most countries, the mold and die industry consists of small companies (less than 100 employees) [1]. In the United States, there are about 15,000 tool and die companies representing an annual sales of $20 billions. The main reasons for using the five-axis technology are to: produce parts quickly; reduce the manufacturing cost and lead times; and; improve the overall quality. However, some issues remain unresolved in machining of complex surfaces using these methods.

Recently, work advocating the use of five-axis machines to reduce machining time (by up to 85%) has become available in the literature [2-9]. Some five-axis machining methods are based on tilting the tool with a certain angle in the feed plane (*The Inclined Tool Method*) [10], other methods are based on matching the geometric characteristics of the surface with that of a toroidal tool (e.g. in the *Principal Axis Method* (PAM)) [5, 6, 7, 11, 12]; and on machining a surface by utilizing two points of contact between the tool and workpiece (e.g. in the *Multi-Point Machining*) [9]. Some issues pose special difficulties in machining of complex

surfaces using these methods. One critical issue is the production of a gouge and interference free tool path. The key difficulty is the determination of the surfaces generated by the tool as it moves relative to the workpiece. This problem, called *"the swept volume"* of a tool, is an ongoing research challenge.

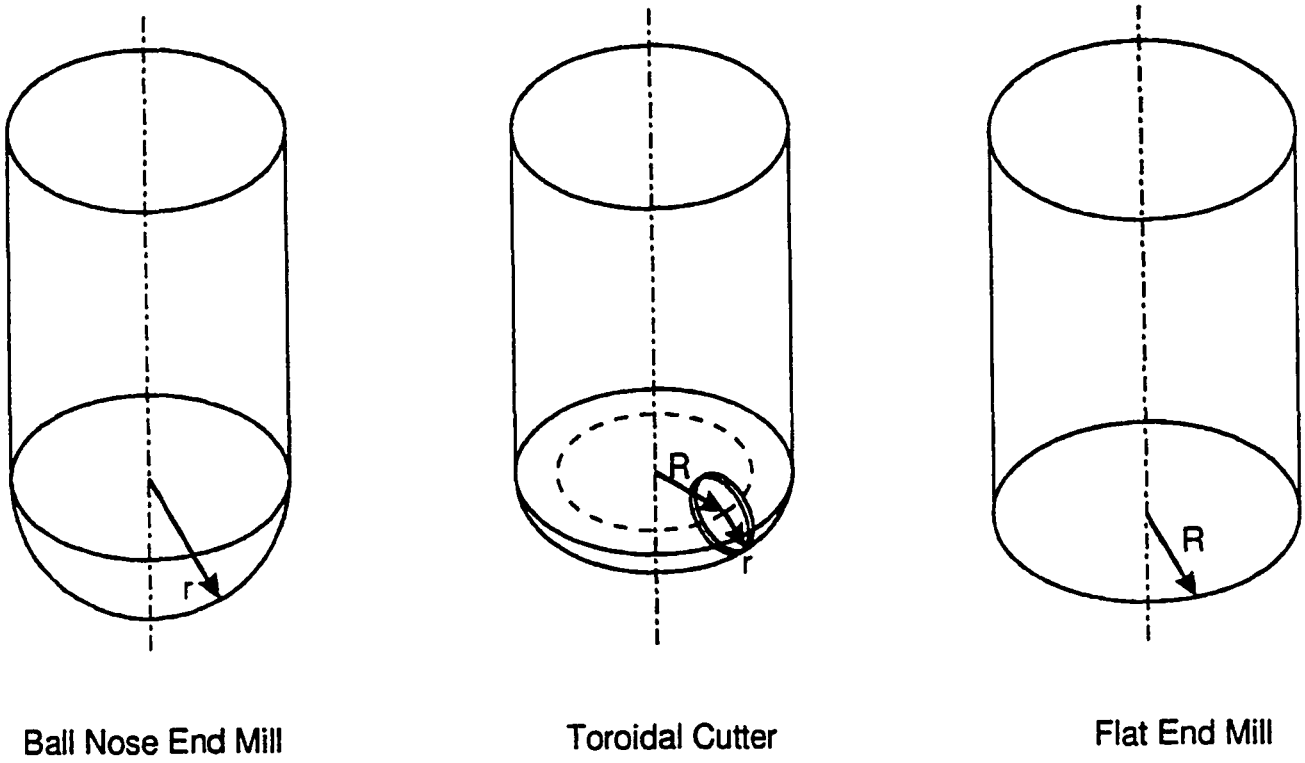


Figure 1.2: Commonly Used Cutters

The typical way of calculating the swept volumes is by using Boolean operations technique. However, this method uses a huge computer memory and a long simulation time.

To overcome the speed and memory problems, in this work, new methods were

developed to generate swept volumes. The speed of the new techniques was exploited to quickly check and avoid gouging and interference at each and every point of the tool path.

The new methods were integrated with a modified version of the "*Inclined Tool*" positioning technique [10] and implemented on a precise NC verification tool kit, the SVS program. Several tool paths were simulated on the implemented SVS program. These paths have also been used to produce actual test pieces. The SVS program was verified experimentally and numerically (against the Z-map method [13]). The comparisons are in close agreement, thereby validating the new methods.

1.1 Thesis Outline

Chapter 2 presents a survey of work related to swept volumes and gouge detection and correction.

Chapter 3 presents *The Generating Circles* new method of generating swept volume of special surfaces followed by a discussion of the implementation. Chapter 4 presents the experimental and numerical verifications of the generating circles technique.

Chapter 5 presents the new method of generating swept volumes for any kind of sculptured surface in five-axis machining. Chapter 6 presents the experimental results and numerical verifications of the generating curves method.

Chapter 7 presents the new gouge detection and avoidance techniques. Chapter 8 shows the experimental and numerical verification of those techniques. The last chapter presents conclusions and recommendations for future work.

Chapter 2

Literature Review

2.1 Introduction

Three dimensional surfaces of automobiles, ship propellers and turbine blades are often composed of free-form surfaces. The generation of a gouge-free cutter locations (CL) path on this kind of surfaces, for non-spherical cutters, is a difficulty with which technicians and researches into NC programming have been confronted.

Gouge detection and correction is an essential tool for any CAD/CAM package. An accurate NC verification requires simulating the volume swept by the tool and comparing it to the design surface. Nonetheless, simulating the swept volume for five-axis machining is not an easy task.

The first part of this chapter briefly discusses the different methods presented in the literature related to the swept volume problem. This is followed by highlights of the advantages and disadvantages of each method.

The second part discusses the work that has been presented in the literature associated with the gouging problem.

2.2 Swept Volume

Attempts to solve the swept volume problem can be classified into theoretical methods and procedural methods. The theoretical methods include the Lie group and differential manifold method and the envelop method. The procedural methods include the sum of volumes, the intersection of vectors, and the ray casting methods. These methods as related to NC machining are briefly discussed below.

2.2.1 The Theoretical Methods

The Lie Group and Differential Manifold Method

This approach is mainly presented in the work of Blackmore et al. [14-17] and Warner [18]. Swept volume in this method is determined by utilizing the Lie group structure of the set of Euclidean motions via the theory of differential equations. They have proven that every smooth Euclidean motion, or sweep, can be identified with a system of first order linear differential equations. Based on the differential equations theory, the swept volume of an object can be completely determined by the sweep differential equations and the initial position of the object. Therefore, sweeps can be dealt with as a function of the properties of sweep differential equations. These sweep differential equations provide useful insight into the topological

and geometrical nature of the swept volume of an object or a tool. The generation of the sweeps of the individual algebraic surfaces and then combining them requires a method for generating surface points and lines of intersection, which are complex issues but are further complicated by the presence of surfaces defined by differential equations. Also, there is a difficulty in representing the swept volume for a compact n-manifold because the interior and boundary point sets of the swept volume do not consistently form the interior and boundary point sets of the sweeping compact n-manifold. There may exist points along trajectories formed by interior points of n-manifold that are boundary points of the swept volume. Furthermore, there may exist points along trajectories formed by boundary points of n-manifold that are interior points of the swept volume. For example, let us consider the swept volume of a compact two-manifold sweeping in R^3 (see figure 2.1 [21]).

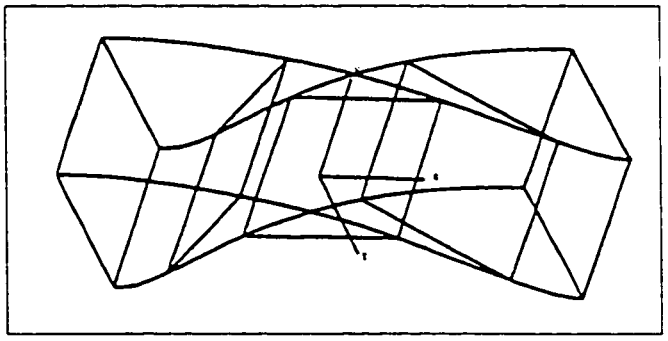


Figure 2.1: The Swept Volume for a Compact Two-Manifold Sweeping in R^3

The compact two-manifold simultaneously undergoes a straight-line translation and a continuous rotation about an axis that is perpendicular to the direction of translation. There exist points along trajectories formed by interior points of the compact two-manifold that are boundary points of the swept volume and points along the trajectories formed by the boundary points of the compact two-manifold that are interior points of the swept volume. Therefore, only for restricted sweeps

will the interior and boundary points sets of the swept volume for a compact n-manifold be generated from one specific point set of the compact n-manifold. Thus, the practicality of this method for a fast tool path swept volume generator is limited.

The Envelop Method

The envelope theory is used to determine the boundary surfaces of the swept volume as presented by Zeng et al. [19] and Ling et al. [20]. They have used the *Envelope Theory* together with the *Instantaneous Screw Axes* to generate the swept volume. The envelope of a moving surface keeps touching the surface at every instant of time as they move along a specified path, and produces a family of continuous surfaces. This family is time dependent. The motion of the object can be defined by its instantaneous screw axis. There is only one instantaneous screw corresponding to an object at any instant of time. The swept volume is then generated by the tangent envelope surface to all members of the family of the moving surfaces.

In four and five-axis motion, circles, cylinders and tori sweep complex surfaces. A generalized expression of these surfaces can be generated using symbolic computation programs. But these complex equations need to be solved to determine points on the envelop surface. Furthermore, intersections of the complex surfaces are required to generate the edges of the swept volume. Other than for simplified motions, so far, this method has not been practical to implement.

In the above methods, the swept volume for a moving toroidal tool would be generated by combining the volumes swept by a model of the tool shank (cylinder), the tool cutting edges (torus) and the bottom (circle). The individual swept

surfaces are generated using different theories. These swept entities must first be realized and then combined by finding intersection curves, into a valid model. Since the swept volumes are represented by complex algebraic/trigonometric equations, finding intersection curves is a computationally heavy task. Furthermore, realizing these volumes into a solid model (which can represent only a limited number of primitives) may require approximation methods for both topology and geometry. It is these two steps that take up a considerable amount of time and make the above methods impractical.

2.2.2 The Procedural Methods

The Sum of Volumes Method

The swept volume of an object can be generated by a sum of the volumes of its components through which the tool is swept [21-27]. The sum of swept volumes problem suffers on the same grounds as the previous methods. However, for polyhedron objects it is a viable method since representing the swept volume of a polyhedral object can be reduced to representing the swept volume of its boundary surfaces, which consist of finite number of planar polygons. Nonetheless, the sweeps of planar shapes must be restricted such that the plane of the shape is continuously at some fixed angle to the tangent of some sufficiently smooth space curve. This restriction guarantees that the boundary point set and interior point set of the tool are generated by the boundary and interior point sets of the planar shapes respectively.

The ruled surface segments formed by the edges of a sweeping polygon form portions of the boundary surfaces of its swept volume. Figure 2.2 [21] shows that

ruled surface segments formed by the edges of a square polygon. The shape of the ruled surface segments is dependent on the shape of the polygon and its sweep.

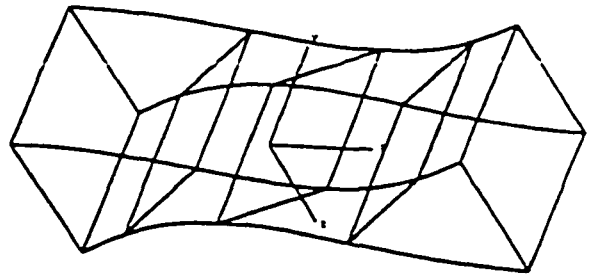


Figure 2.2: Ruled Surface Segments Generated by the Edges of a Sweeping Square Polygon

In order to generate a reasonable approximation of the tool it must be modelled by numerous planar faces. The method would require sweeping each of these faces and then summing the volumes appropriately. Each summation is a simple task but a large number of these operations is required, which increases the overall time of computation significantly. This method, however, can be implemented on any solid modelling tool kit. One alternative to this method is the creation of numerous images of the tool from the start to the end of the pass and combining them to generate the swept volume for the move. The implementation is fast, but every view requires regeneration and gouge detection is manual. Although it is simple to implement, the method is time consuming. For one of the test tool paths used in the early stages of the current work, this method was implemented on a Pentium 75 MHz PC. For this tool path with 140 moves (each move is 1 mm) it took 14 hours when the tool was represented with exact surfaces. The time was reduced to 7 hours when the tool was modelled using faceted models.

The Intersection of Vectors Method

In the intersection of vectors approach [28], the swept volume is created by intersecting rectangular and circular sections with the surface. To calculate the intersection of a vector with a solid, the intersection must be performed for several characteristic profiles. For example, a cylindrical milling tool can be presented by three profiles: two circular profiles representing the top and the bottom faces and a rectangular profile connecting the top and the bottom. In the same manner, a toroidal milling tool can be presented by five profiles: a rectangular profile, two circular profiles for the inserts (labeled A and B) and two circular profiles for the top and the bottom (labeled C and D) as shown in figure 2.3.

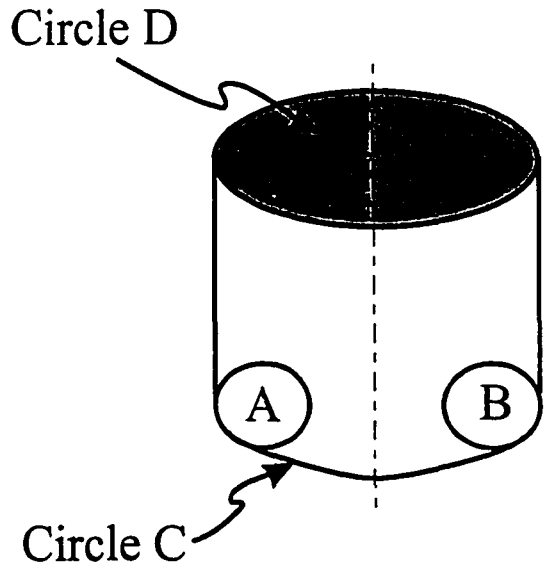


Figure 2.3: Toroidal Milling Tool Characteristic Profiles

For three-axis milling, an assumption can be made of linear tool path and constant tool axis direction. However, the introduction of parametric tool axis variation

in five-axis results in having a nonlinear system of equations. The resulting equations can be solved numerically using Dekker-Secant algorithm [28]. The difficulty in this technique is to find a valid search interval of the independent variables to be used in the highly nonlinear and complex differential equations.

The ray casting [25, 29, 30, 31] method uses a large number of rays emanating from the part surface and intersects them with the tool at any given position. To generate the swept volume, numerous images of the tool are placed between the starting point and the end point. The intersection process is repeated for each of these positions and a good approximation of the swept surface can be generated. This method has been converted to work on parallel processor based systems [32] and gives good performance. However, the cost of the system is high. This method has also been implemented by Rao et al. [33] to generate instantaneous swept volumes for gouge avoidance and determination of cutting forces. Kim et al. [34] implemented a modified version of the ray casting method; they called it Z-map. In this method, the workpiece is represented as a set of discrete columns as shown in figure 2.4. Each column is stored as a number in an array. Lines defined by z-columns are then intersected with the tool movement. If the intersection result is less than the Z-map value, the value in Z-map is replaced by the intersection result. The disadvantage of this method is that the accuracy of the simulation requires a huge size of the Z-buffer.

Jerard et al. [35, 36, 13] and Drysdale et al. [37] proposed new methods, based on "mow the grass" concept, to overcome the size problem in the Z-map method. In these methods, vectors grow from the design surface, in the normal direction, and are intersected with the tool motion as shown in figure 2.5. The length of the

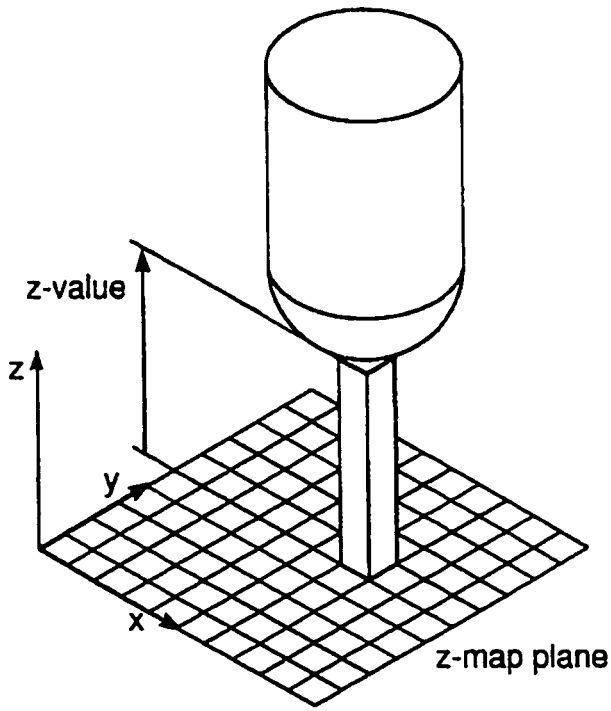


Figure 2.4: The Z-map Method

vectors are reduced to the intersection point. After completing the simulation, the surface can be computed from the length of the grass. Mow the grass technique reduces the memory requirements and increases the speed of simulations.

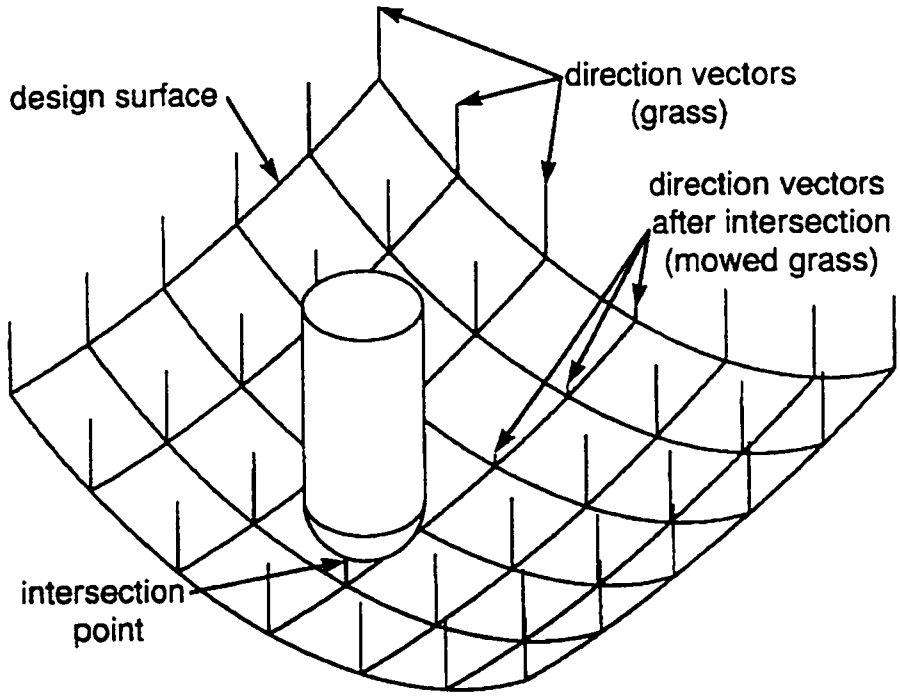


Figure 2.5: The "Mow the Grass" Technique

Sheltami, Bedi and Ismail [39] presented a new fast method to approximate the swept volume for toroidal cutters. They have shown that a swept volume can be constructed using the locations of the tool along the tool path (CL data) with planar generating circles. These generating circles can be thought of as numerous flat-bottom cutters. The whole technique is presented in chapter 3. The errors resulting from approximating the imprint of the toroidal cutter with planar circles increase drastically, especially near the outside of the tool, because the normals of

surface and the tool axis throughout the tool path are far apart, which is the case in most of the five-axis cuttings as explained in chapter 5. A considerable amount of time was spent to modify this technique by digitizing the five-axis motion into different combinations then using the superposition to determine the final curve, however, the errors were still large.

Roth et al. [42] pursued the idea presented in [39] further and presented a method to simulate the movement of a toroidal cutter in five-axis. They have digitized the toroidal cutter into a number of pseudo inserts and then the same tangency concept that had been applied in [39] was used between each two corresponding pseudo inserts. Each two corresponding inserts are determined based on positions and orientations of the tool along the tool path. The tangency points between the corresponding inserts are the contact points between the cutter and the surface. These points can be used to generate a swept volume.

In chapter 5, a more general, novel method is presented to simulate the swept volume in five-axis machining.

2.3 Gouge Detection and Correction

Five-axis machining of sculptured surfaces offers many advantages over three-axis machining, including faster material-removal rates, improved surface finish, and the elimination of hand finishing. However, five-axis machining suffers from a major drawback, which is related to gouging. Attempts to solve this problem in the literature are limited; they are discussed below.

Yu, Deng, Duan and Liu [43] have presented a method to generate a series of gouge-free CL points. These points are constructed by generating a sequence of tangent planes to the surface at each programmed point on the surface and then tilting the tool to avoid gouging. For complex surfaces, the equation of the tangent will eventually be complicated and this will pose difficulty in the adjustment of the tool orientation. Also, this approach may result in producing large cusp heights.

In [44], the authors presented a method to avoid gouging using the curvature catering technique for a special disc cutter with a concave end. In this method, the envelop formed by the trace of the tool nose in each tool pass is matched with the envelop of the surface. The matching of the envelops is achieved by matching their derivatives. This technique requires heavy computations to determine and match the derivatives, up to the third degree, for even simple surfaces.

Another technique is presented in [45] for gouge avoidance for flat-bottom end-mills. This method is based on triangularizing the parametric surface then placing the cylindrically shaped tool over the surface and checking locally for gouging and interference using a set of check points on the tool. The gouge checking method is done using the so called inside/outside test between check points and design surface. If gouging occurs, check points are used to determine the direction and magnitude of rotation to eliminate gouging. A similar method is implemented for toroidal cutters is presented in [46].

Veeramani and Gau [47] proposed eliminating gouging by dividing the surface into several surface patches and dealing with each patch as a separate surface. The design surface is then modeled using these compound surface patches. Each patch

is machined by different tool size based on the so called up-down procedure. The up-down procedure is a technique to determine the maximum gouge free tool size for each surface patch. However, using different tool sizes may gouge adjacent surface patches when machining the boundaries of the patches of a compound surface. If the CL-data between two surface patches is continuous, gouging will not occur, otherwise it may occur. In the case of discontinuity between surface patches, the authors suggested correcting some CL-boundary points using two different algorithms.

Rao et al. [33] used the "mow the grass" method at the contact point between the cutter and the surface to detect gouging using PAM. PAM utilizes the minimum curvature of the surface to calculate the tool inclination angle. This guarantees that gouging does not occur provided that curvature of the surface does not change below the tool. If the curvature below the surface increases, gouging will occur. The curvature used in the tool positioning calculations has to be increased till gouging in eliminated. Wang and Tang [48] presented a similar technique by matching the local curvatures of the surface and the tool geometry.

In chapter 7, a novel, fast and accurate gouge detection and correction method for five-axis machining for a general APT tool is presented.

Chapter 3

The "Generating Circles" Technique

3.1 Introduction

In this Chapter, a new technique for simulating the volume swept by toroidal cutters, for special surfaces[1], is presented. This technique has been published in the International Journal of Machine Tools and Manufacture [39]. The idea of this method is to generate circles milled by the bottom of the tool, and to combine these circles with some information about the cutter side to generate the swept volume.

The model of the tool considered in this study is shown in figure 3.1. It represents a cylindrical shank and carbide inserts. The cutting edge in this model subtends an arc larger than 90°, indicating that the tool can cut with a part of its

[1]Surfaces with normals that coincide with the tool axis at each point of the tool path

bottom face. The equation of the swept surface of the insert as it rotates is a torus and is given by

$$\vec{T}(\theta,\phi) = \begin{pmatrix} x \\ y \\ z \end{pmatrix} = \begin{bmatrix} (R + r\sin\theta)\cos\phi \\ (R + r\sin\theta)\sin\phi \\ -r\cos\theta \end{bmatrix} \tag{3.1}$$

where R is the radius of the circle swept by the insert centers, r is the radius of the inserts, θ and ϕ are angles indicated on figure 3.1.

3.2 Generating Circles

To understand the concept of establishing swept volumes by toroidal cutters using "generating circles", one must first look at the simpler case of a flat bottom end mill generating a spherical cavity. Warkentin et al. [9] have shown that when the mill rotates about a point on the tool axis as shown in figure 3.2, it produces a part of a sphere. It is the bottom circular end of the cutter that generates the spherical surface; it is called here the "generating circle".

The radius of this circle is R, which is the major radius of the cutter, and it remains unchanged regardless of the radius of the spherical cavity. A toroidal cutter rotating about a point on its axis also generates a spherical surface at the bottom. The sphere is also produced by a circle that is centered on the tool axis and lies in a plane perpendicular to the tool axis. This circle is identified by joining the center of rotation and the center of inserts and extending the line to intersect the boundary of the insert as shown in figure 3.3.

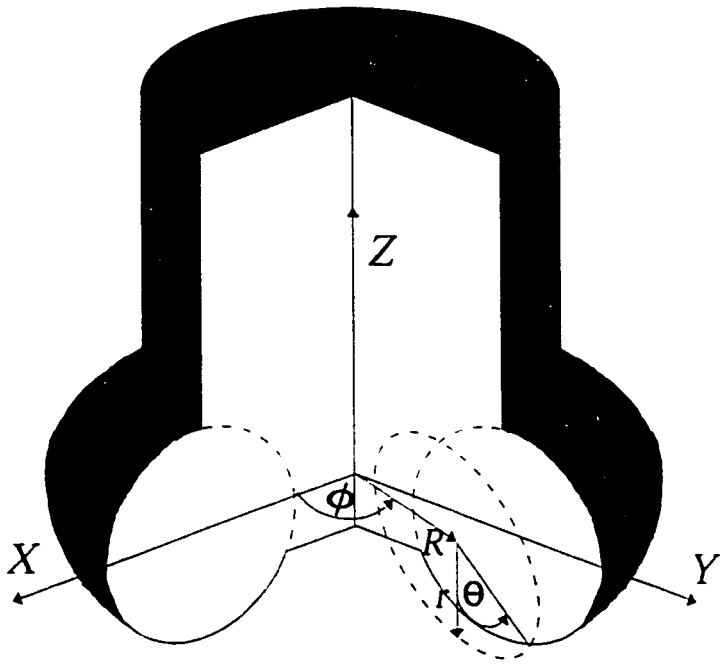


Figure 3.1: The Toroidal Cutter

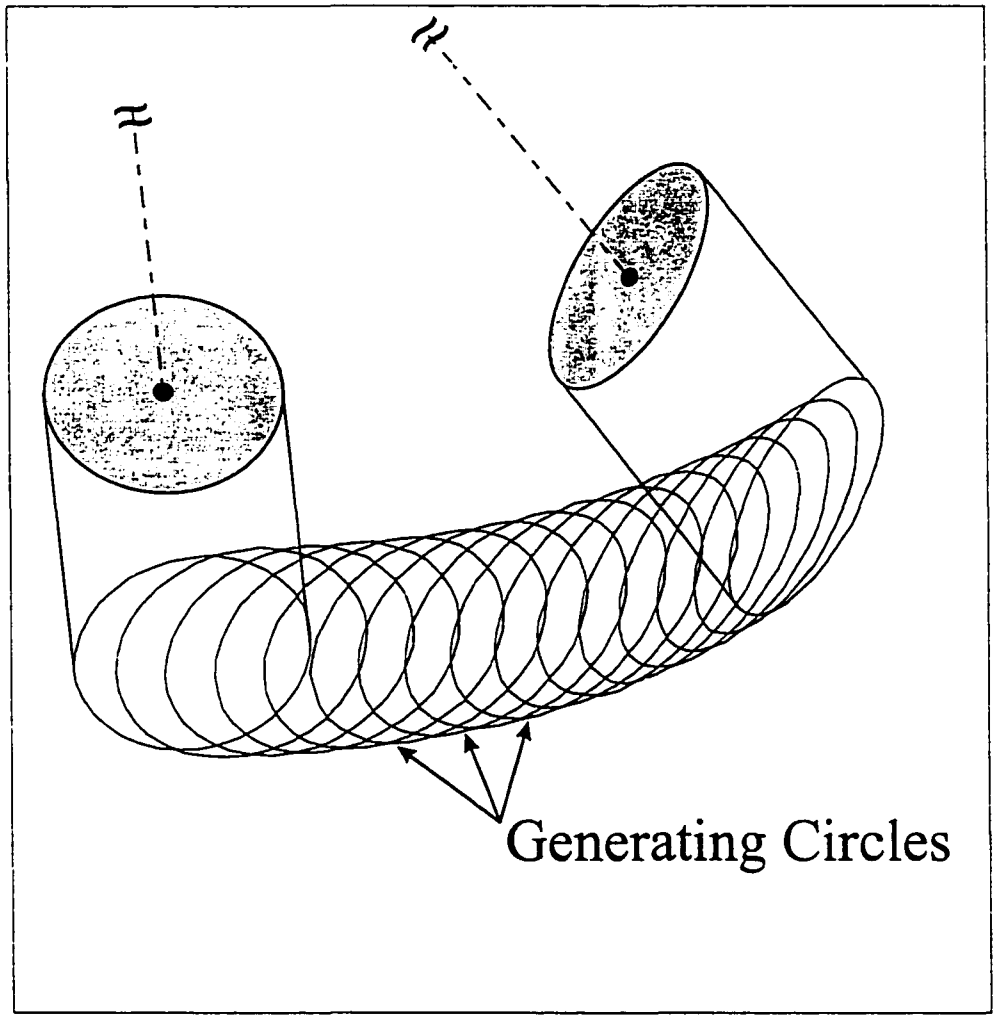


Figure 3.2: A Surface Generated by Rotating a Flat-End-Mill about a Point on the Tool Axis

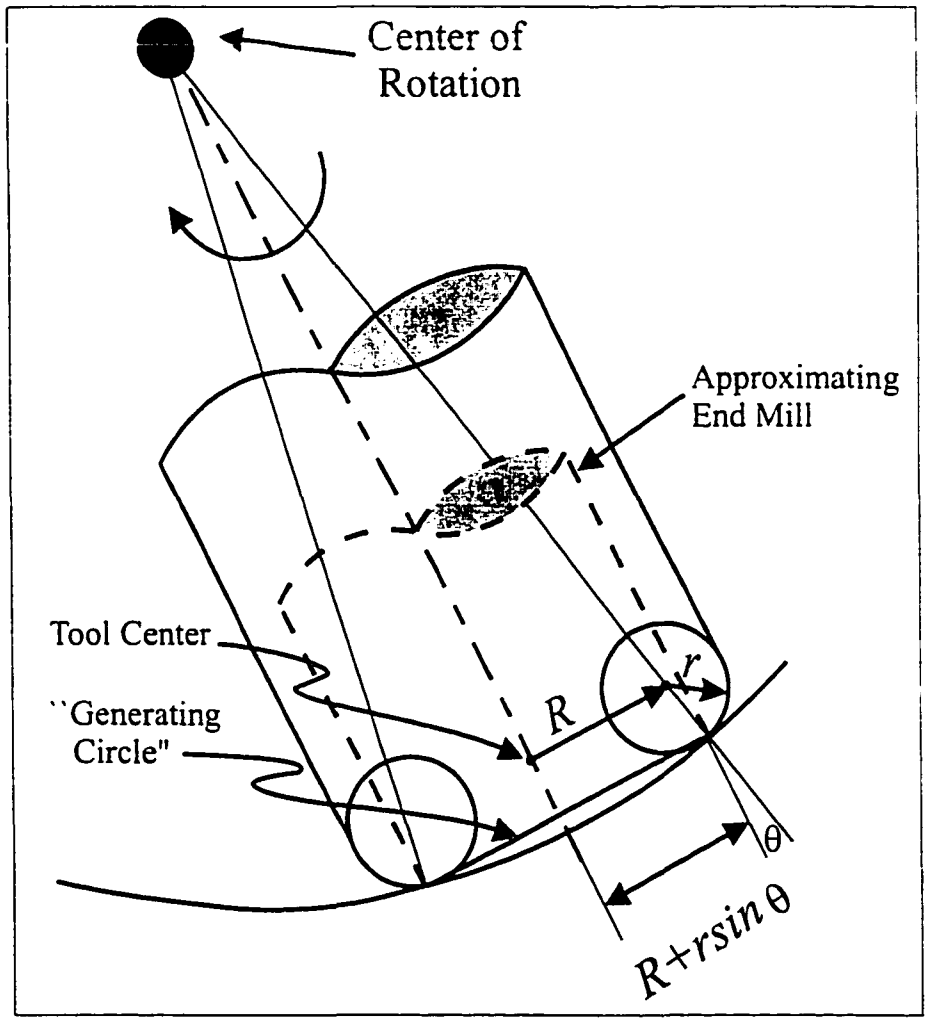


Figure 3.3: A Toroidal Cutter Generating a Spherical Surface

This point on the boundary lies on a circle of radius $R + rsin\theta$ where R is the distance between the center of the tool and center of the insert, and r is the radius of the insert. This is the "generating circle" that generates the spherical surface: it is as if the toroidal cutter has been replaced by a flat end mill. The radius of the generating circle, however, varies according to the radius of the circular path, or to put it in general terms, according to the curvature of the surface to be machined. In effect, one can accurately simulate the toroidal cutter by numerous flat end mills: at any point along the tool path, only one of these flat end mills approximates the toroidal cutter as depicted in figure 3.4.

Finding the swept volume using the "generating circles" is exact when the normal of the surface coincides with the tool axis, as it was verified experimentally by Warkentin et al. [9]. In this study, it is assumed that during this short movement, the tool axis remains in one plane that includes the feed direction. This plane is designated as the *"feed plane"*. Across the feed direction, it is not the "generating circle" but rather its projection onto the "osculating plane" (cutting plane) that determines the swept volume profile, see figure 3.5. The osculating plane, or the cutting plane, is a plane normal to the feed direction at the point of contact between the tool and workpiece. This profile matches the intended surface profile exactly at the center of the tool in the feed plane, and deviates from it as we move sideways to other sections.

With the idea behind the circles technique now explained, the implementation of the technique is described next.

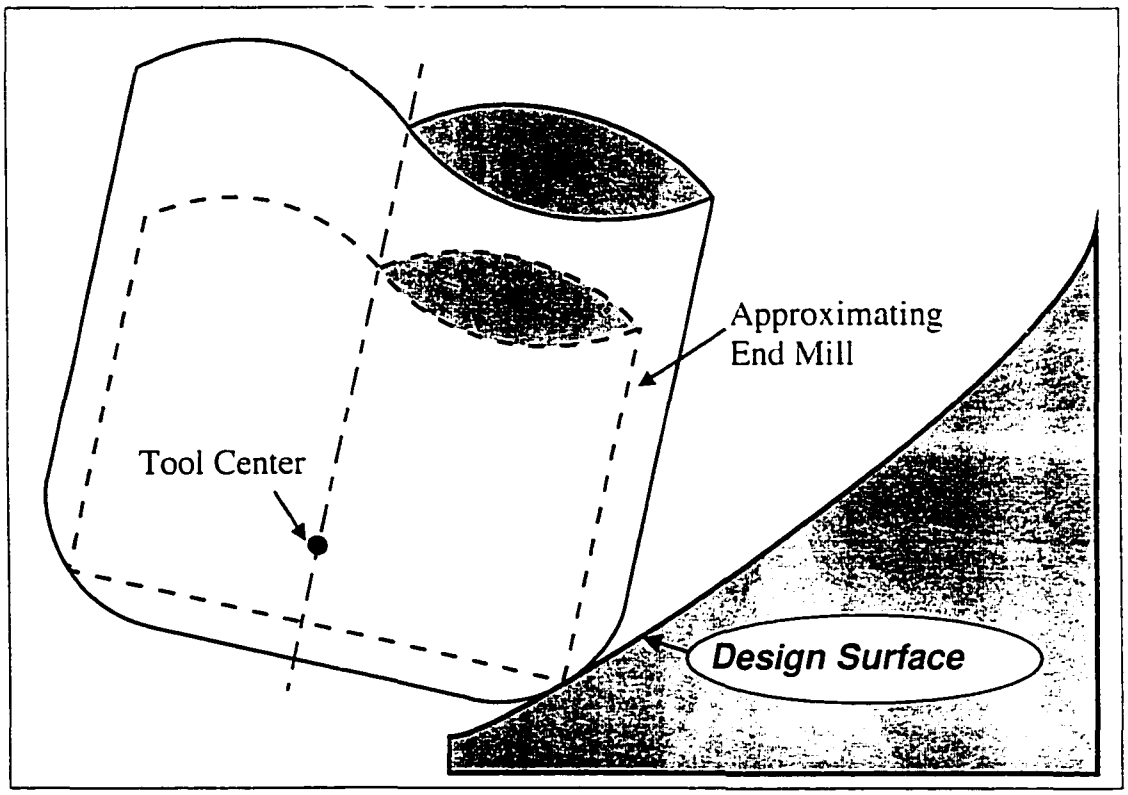


Figure 3.4: The Flat End Mill Approximates a Toroidal Cutter as it Machines a Surface

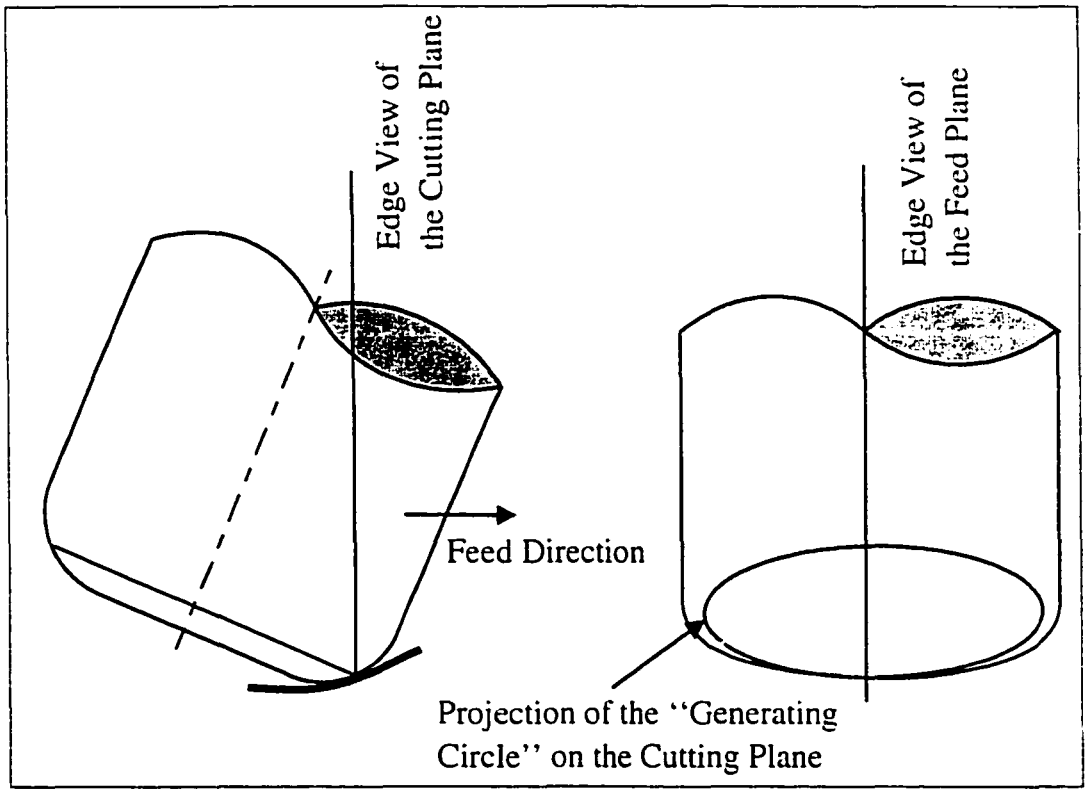


Figure 3.5: The "Generating Circle" and its Projection onto the Cutting Plane

3.3 Implementation

A tool path that lies in one plane that includes the tool axis can be obtained in up to four-axis machine configuration. Such a configuration is shown in figure 3.6. Actually this is the same configuration employed in the experimental work to be described later. It has 3 translational axes, X, Y, and Z, and a rotary axis A. The axis A is provided by a rotary table.

The computation of the swept volume starts with the given tool path described in terms of G-code or in APT format. In both cases the location of the tool and its orientation can be determined from the information in the code, the parameters of the tool including its length, and the kinematics of the NC machine.

The second step in the computations is to identify the "generating circles". This is accomplished by dealing with the tool in two consecutive positions. The movement of the tool between these positions is assumed to be linear. This is a valid assumption for small interpolation steps ($1\ mm$) which are the main concern in the present investigation. Between the two consecutive steps, the tool could move on a concave surface batch as shown in figure 3.7, on a convex batch as in figure 3.8, or on a flat surface as shown in figure 3.9. For any given tool path, like the one shown in figure 3.7, the parameters known at the two consecutive positions, i and $i+1$, include the center of the tool, $\vec{W}_i$, and a second point on the tool axis, $\vec{P}_i$. The second point dictates the orientation of the tool and if not explicitly given, it can be generated from the orientation of the tool axis. All parameters are defined with vectors with respect to the global frame xyz as shown in figure 3.7. The corresponding points for the $(i+1)^{th}$ positions are $\vec{W}_{i+1}$ and $\vec{P}_{i+1}$. The location of

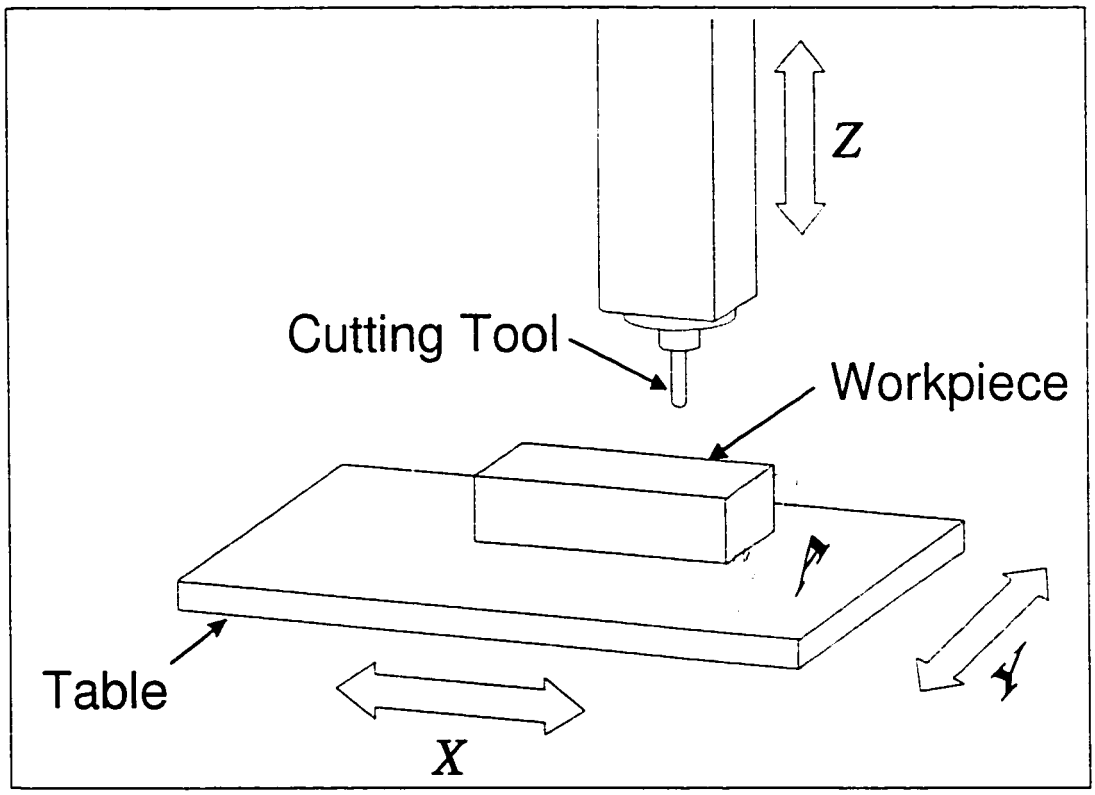


Figure 3.6: A four-axis Configuration of the CNC Machine

the center of the inserts in this plane can be obtained from the following equation:

$$\vec{M}_i = \frac{\vec{A} \times \vec{L}_i}{|\vec{A} \times \vec{L}_i|}.R \tag{3.2}$$

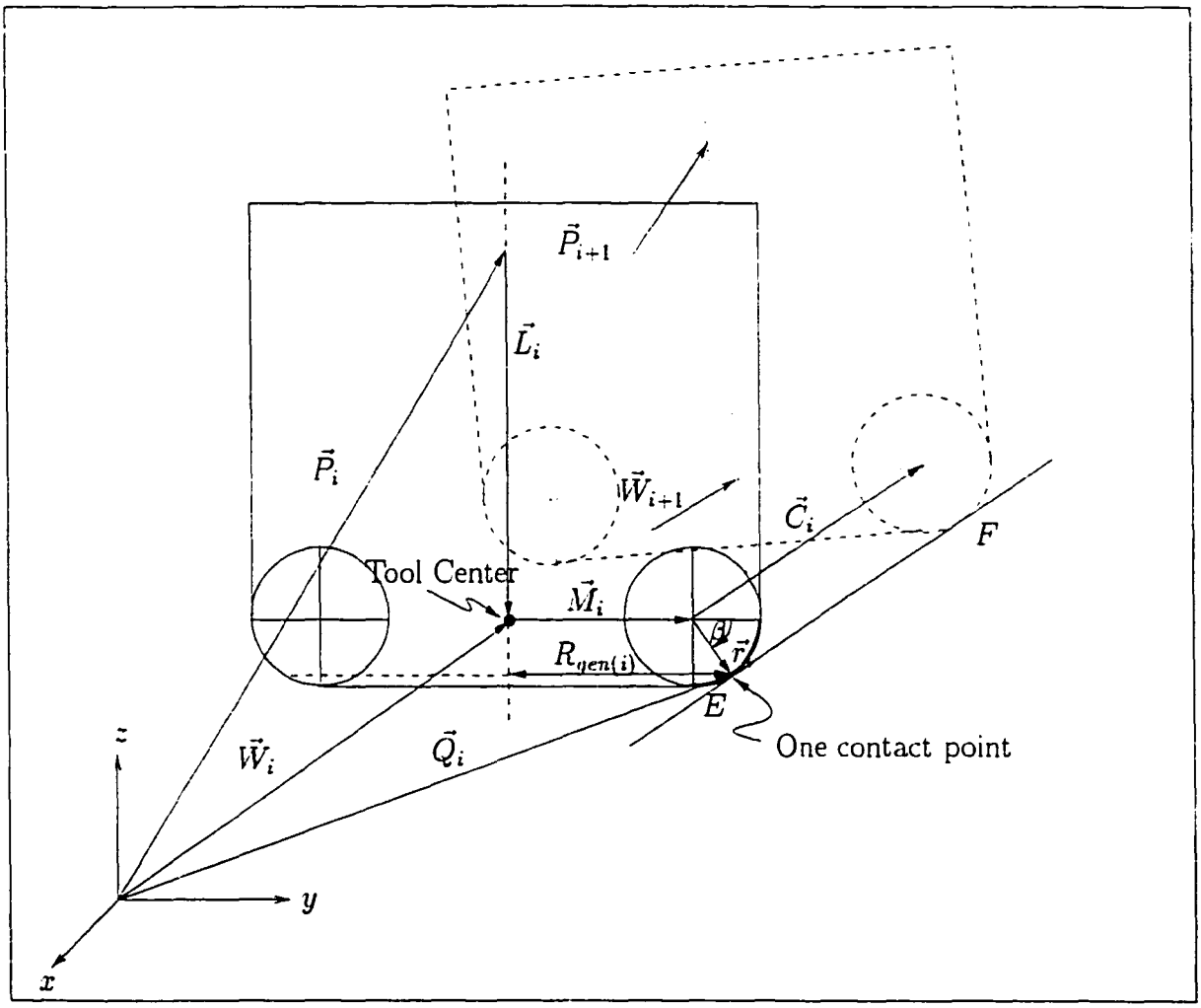


Figure 3.7: The Projection of the Tool at Two Consecutive Positions to Determine the Tangency Point for a *Concave Surface*

where

$\vec{A}$ is a unit vector along the fourth axis (rotation axis), and.

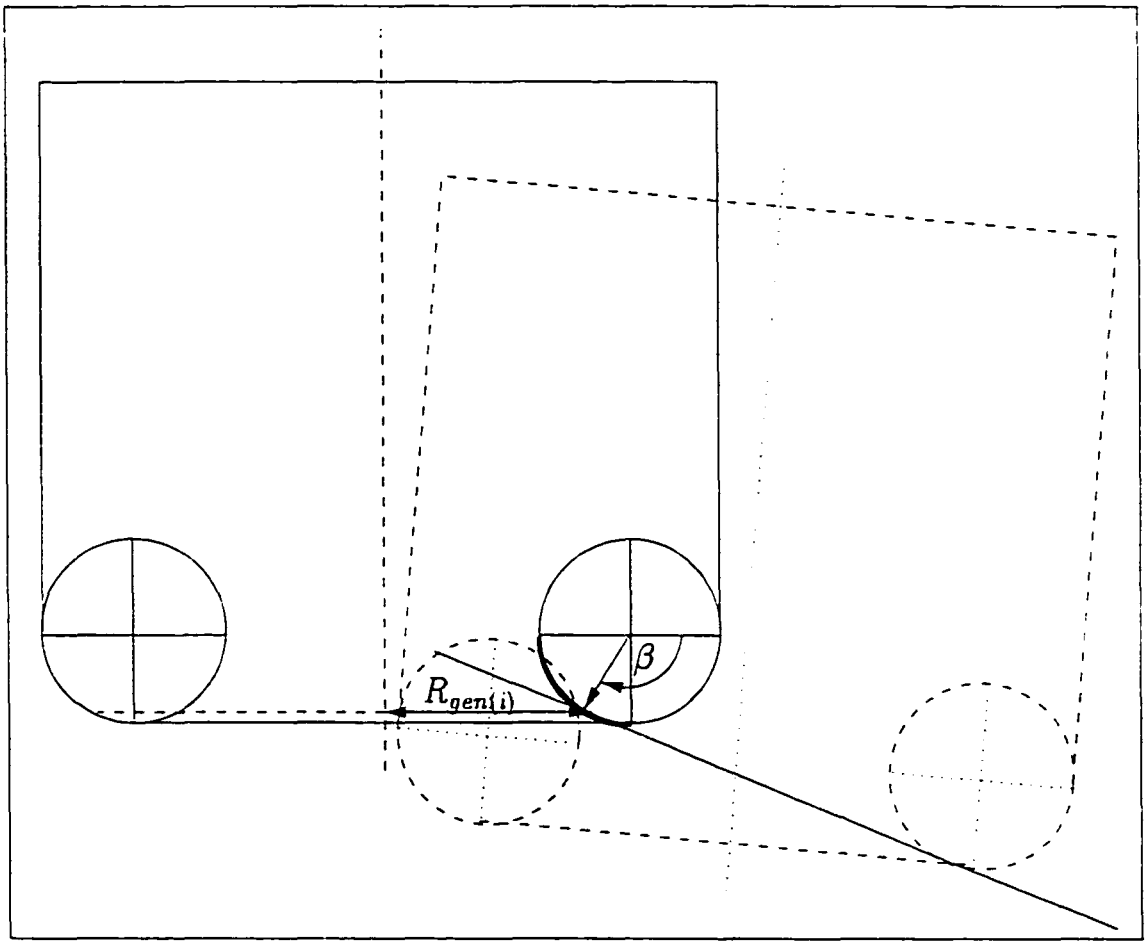


Figure 3.8: The Projection of the Tool at Two Consecutive Positions to Determine the Tangency Point for a *Convex Surface*

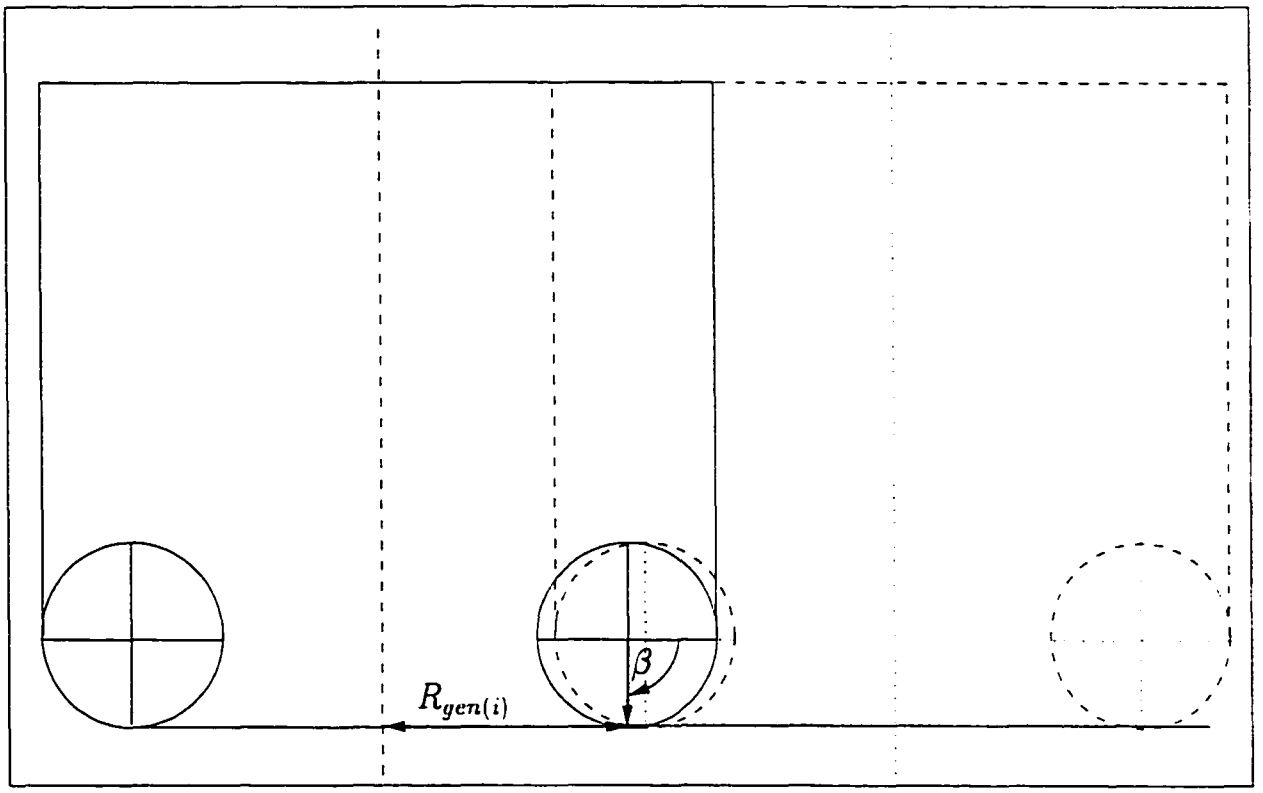


Figure 3.9: The Projection of the Tool at Two Consecutive Positions to Determine the Tangency Point for a *Flat Surface*

$\vec{L}_i$ is a vector between $\vec{P}_i$ and $\vec{W}_i$. The vector between the center of the i^{th} and $(i+1)^{th}$ inserts, $\vec{C}_i$, can be obtained from:

$$\vec{C}_i = (\vec{W}_{i+1} + \vec{M}_{i+1}) - (\vec{W}_i + \vec{M}_i) \tag{3.3}$$

The location of the i^{th} point of contact is given by the vector $\vec{Q}_i$.

$$\vec{Q}_i = \vec{W}_i + \vec{M}_i + \vec{r}_i \tag{3.4}$$

where

$\vec{r}_i$ is a vector between the center of the insert and a contact point, and is perpendicular to the vector $\vec{C}_i$.

The vector $\vec{Q}_i$ depends on the radius of the "generating circle". The three cases, shown in figures 3.7, 3.8, 3.9, must be considered to determine this radius. In the first case, $R_{gen} > R$; the contact points lie in the range $0° \leq \beta < 90°$ on both insert images, or the cut is performed by the outside of the torus. In the second case, $R_{gen} < R$; the contact points lie in the range $90° < \beta \leq 180°$ on both insert images, or the cut is performed by the inside of the torus. The last case is a special case where $R_{gen} = R$; the tool axis is parallel in both positions, and $\beta = 90°$. In this case, the cut is performed by the bottom of the torus.

As shown in figure 3.7, the radius of the "generating circle" can be calculated as follows:

$$R_{gen(i)} = |\vec{M}_i| + \psi\sqrt{|\vec{r}_i|^2 - \delta_i^2} \tag{3.5}$$

where

ψ is a parameter which depends on the surface characteristics and is given by:

$$\psi = \begin{cases} +1 & \text{if the surface is concave} \\ -1 & \text{if the surface is convex} \\ 0 & \text{if the point on the surface is an inflection point} \end{cases}$$

δ_i is the projection of the vector $\vec{r}_i$ on the vector $\vec{L}_i$ and it can be calculated from

$$\delta_i = \frac{\vec{r}_i . \vec{L}_i}{|\vec{L}_i|} \tag{3.6}$$

The equation of the "generating circle" in parametric form is then given by

$$\begin{pmatrix} x \\ y \\ z \end{pmatrix} = \begin{bmatrix} A_x R_{gen} \cos(\omega) + B_x R_{gen} \sin(\omega) \\ A_y R_{gen} \cos(\omega) + B_y R_{gen} \sin(\omega) \\ A_z R_{gen} \cos(\omega) + B_z R_{gen} \sin(\omega) \end{bmatrix} \tag{3.7}$$

where

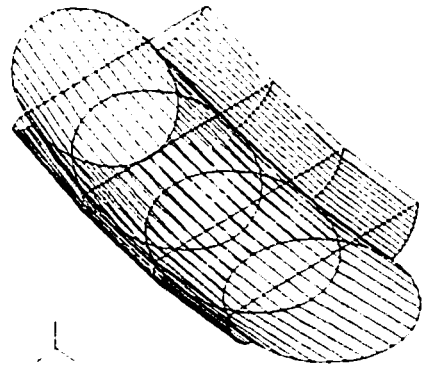
ω is the parameter which is actually the angle swept as we move around the circumference,

$\vec{A}$ is vector along the center of the rotary table,

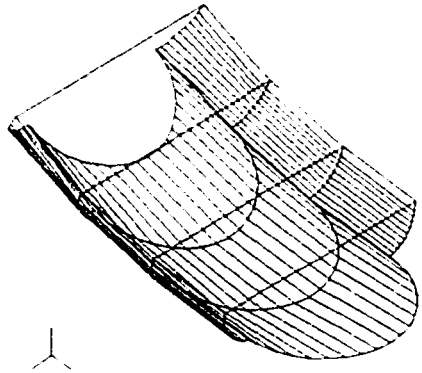
$\vec{B}$ is a unit vector parallel to the direction of feed and lies in the cutting plane, and,

R_{gen} is the radius of the "generating circle".

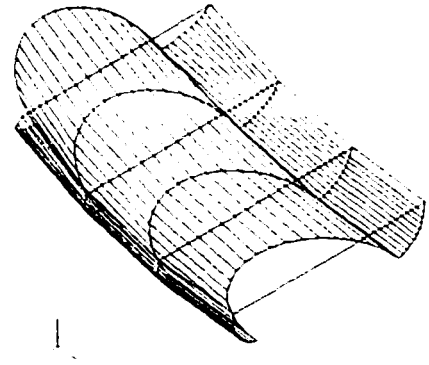
Figure 3.10.a shows an example of the "generating circles" in four subsequent tool positions. These circles describe the bottom surface of the swept volume. To generate the sides of that volume, the portion of the cutting surface of the inserts



a: The Bottom Surface Swept by the "Generating Circle"



b: Surface Swept by the Front of the Tool



c: Surface Swept by the Back of the Tool

Figure 3.10: An Example of the "Generating Circles" in Consecutive Tool Positions

above these circles must also be included as illustrated in figure 3.10. The cutting surface up to the center of the torus needs only to be considered.

Other than in simple situations, dealing with the whole "generating circles" shown in figure 3.10.a poses serious difficulties in determining the swept volume: the circles intersect with each other in such a way that it becomes difficult to discern what is on the outside or on the inside of the swept surface. To alleviate this problem, the "generating circle" is split into two halves, the front and the back. Now two surfaces are computed, one swept by the front of the tool, shown in figure 3.10.b, and the other one is swept by the back of the tool as shown in figure 3.10.c. The two surfaces are used in constructing two swept volumes that will eventually be combined using Boolean operations to get the final swept volume. The increased number of operations involved in treating halves of the "generating circle" was deemed necessary to offset the difficulties in dealing with the whole circle, and thus to make the developed technique more robust.

The "generating circles" described above are determined at all intermediate points along the tool path. The start and end positions are treated differently. At the starting position, the "generating circle" radius is simply R. At the end position, the radius of the "generating circle" is calculated based on the last two points of the given tool path (only for the part generated by the back of the tool). The toroidal cutting surface (only the bottom half) is split into two halves, the back half is added to the surface in figure 3.10.c at the start point, and the front half is added to the surface in figure 3.10.b at the end point. In this way the bottom surfaces (front and back) swept by the toroidal cutter from start to finish are fully described. These surfaces are used to generate the swept volumes by dividing the

circumference of all semi-circles, including the profile of the inserts, into segments, and connecting the same point in two subsequent tool positions by a straight line. In this way, we generate two planar faceted volumes, one swept by the front of the tool and the other one swept by the back. The final step involves taking the union of these two volumes to arrive at the final swept volume. Figure 3.11 is an exploded diagram of an example swept volume; it shows the bottom surface swept by the "generating circles", the front of the toroidal cutting surface at the end of the cut, the back toroidal surface at the beginning of the cut, and the sides swept by the inserts. This figure also shows the volume swept by the cylindrical shank of the tool.

3.3.1 The Solid Model

Creation of generic solid model primitives requires access to low level Euler functions in a solid modelling system. For this part of the work, an in-house solid modeller (*GWB*) based on the work of Mantyla [40] was used. This modeller provides access to low level Euler functions and can be compiled with a custom 'C' code. Figure 3.12 outlines the procedure of generating the swept surface.

Swept Volume Primitive

Once the "generating circles" (which include the sides) are identified at all tool positions, they are broken into equal number of points. Care is taken to ensure that each component within each generating curve has the same number of points. The number of points used to simulate each semi-circle is 19. Each side was simulated with ten points and the side line was simulated with two points (representing the

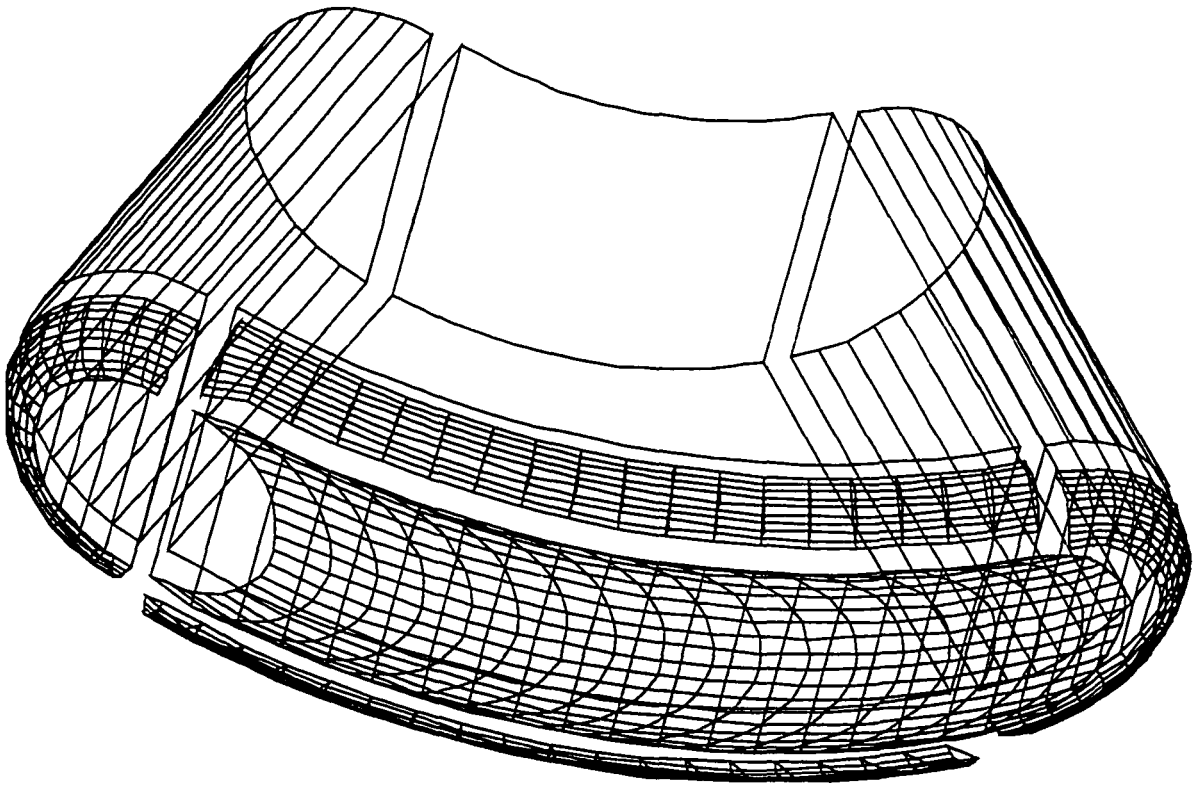


Figure 3.11: Various Components of Swept Volume of an Example Tool Path

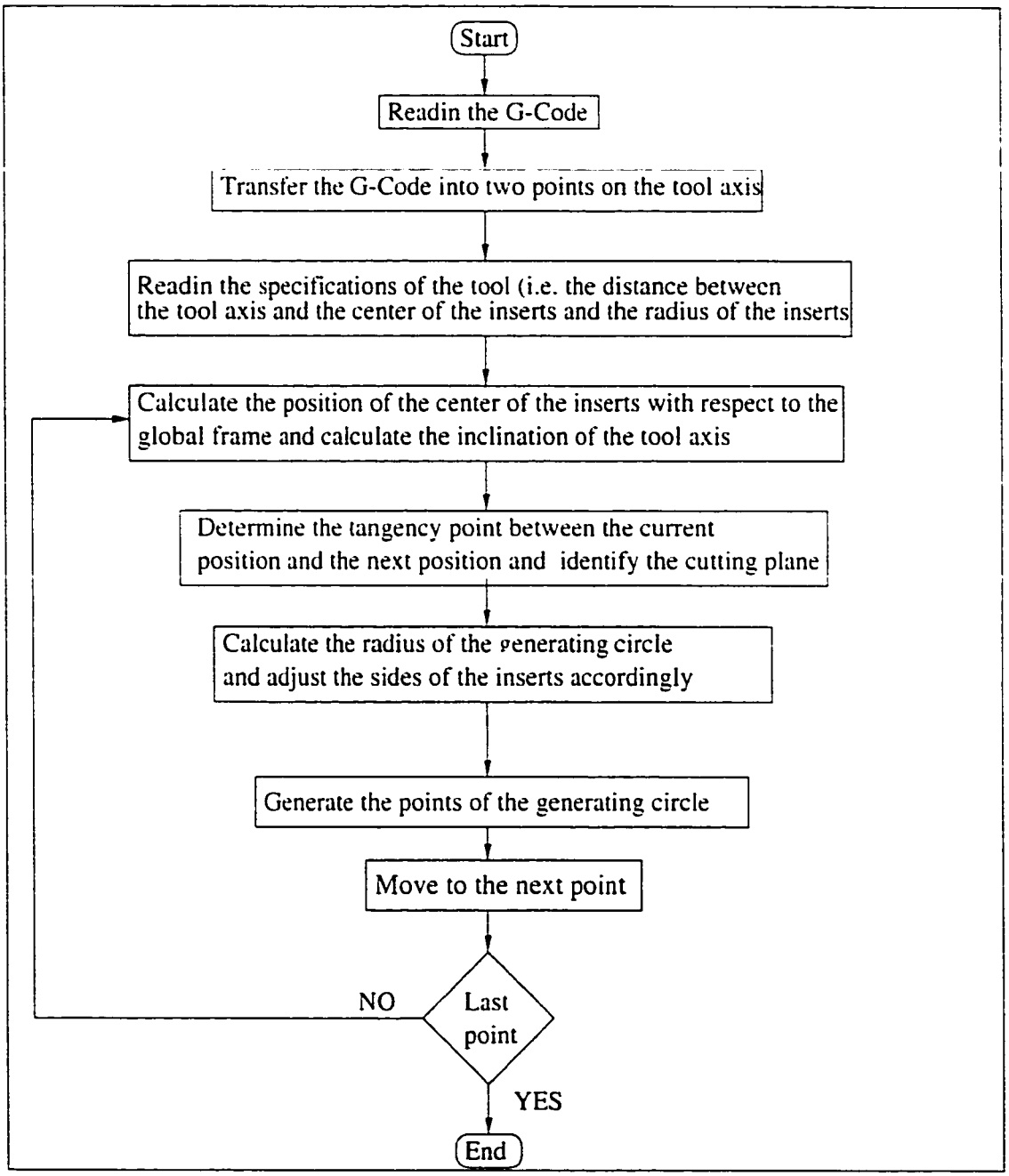


Figure 3.12: Flow Chart to Generate The Swept Surface

shank of the tool). These numbers may vary according to the desired accuracy.

The swept volume is generated by creating a solid with the *mvfs* (make vertex face solid) Euler operator. The position of the first point of the first generating curve is used in this model. In the second step the first point is connected with the second point on the same generating curve by creating an edge between them. This is done with the *lmev* (make edge vertex) Euler operator. This step is repeated for all points on the first generating curve. The last point of this generating curve is joined to the first point which results in creating a new face using the *lmef* (make edge face) Euler operator. In the third step, the vertices on the newly created face are connected to the points on the next generating curve by creating new edges with the *lmev* Euler operator. In the fourth step, the newly created edges from step three are connected into new planar faces. This is done by starting from the first point on the generating curve and connecting every set of three edges into a new face by creating a new edge using the *lmef* Euler operator. Step 3 and 4 are repeated until no more generating circles are available. At this point, step 4, the topology of the start and end points need to be connected by adding parts of the toroidal cutter as discussed earlier. This process of adding a split cutter at the first point is achieved by sweeping the vertices of the first face about the axis of the tool at the staring point. Each vertex is rotated by a known angle and connected to the previous vertex with an edge using the *lmev* Euler operator. Once this has been done for half of the vertices in the first face, the newly created edges are connected into faces by connecting every set of three edges into a face adding a fourth edge using the *lmef* Euler operator. Steps three and four are repeated on the newly created edges and in the final step the newly created edges are connected to the later half of the vertices of the first face (which were not rotated in the first step). Similar set of steps are

repeated at the end point to complete the solid representation of the swept volume. This procedure gives the swept volume for the front and the back of the tool. These two volumes must be combined together to produce the actual swept volume.

Having now described the theory behind the circles technique and its implementations, the accuracy of this technique is checked both experimentally and numerically as discussed in the next chapter.

Chapter 4

Numerical and Experimental Verifications for Generating Circles

4.1 Experimental Verifications

The circles technique was used to simulate three cuts: a circular, a spiral, and an inclined sinusoidal wave. Each cut was made in a single plane to avoid turns and twists, which are addressed in the new generating curves technique presented in chapter 5.

The circular cut was simulated as shown in figure 4.1. the axis A rotated by 45° while the center of the arc remained at the same location on the tool axis. The radius of the arc, R_s was 88.65 mm, and the tool involved had the dimensions. R = 12.7 mm, and r = 6.35 mm. In this special case the radius of the generating

circle, the effective radius, remains constant. In effect, it is like using the same flat end mill of that radius for the entire cut. Figure 4.2 shows the simulated swept volume, and figure 4.3 shows the resulting workpiece.

The spiral cut was performed exactly like the circular cut, except the tool moved uniformly upward for a distance of 10 mm in the Z direction during the rotation of axis A. This then caused a linear variation in the radius of the generating circle. Figure 4.4 shows the simulated swept volume.

The previous two cuts were easy to visualize and to predict the resulting workpiece surface. The third cut, the sinusoidal cut, was more challenging. In this cut, the axes X, Y, Z and A moved simultaneously to generate an inclined cosine wave, of wave length 100 mm, and an amplitude of 5 mm. The travel in the X direction for this cut was 50 mm. The bottom center of the tool was programmed to move along this cosine wave while ensuring that the bottom plane of the tool remained tangent to the curve as shown in figure 4.5. Because of symmetry, only half of the tool path is shown in figure 4.5. Unlike the first two examples of simulating concave surfaces, the current example includes concave and convex surfaces as well as an inflection point. The way the tool was deliberately programmed to cause gouging everywhere, and the resulting swept volume was generated partially by the front of the tool and partially by the back of the tool. The final outcome would be unknown apriori and the radius of the generating circle would change from point to point in an unknown fashion. The swept volume is shown in figure 4.6; it is more complicated than those in figures 4.2 and 4.4.

The three tool paths simulated above were also used in machining of three test

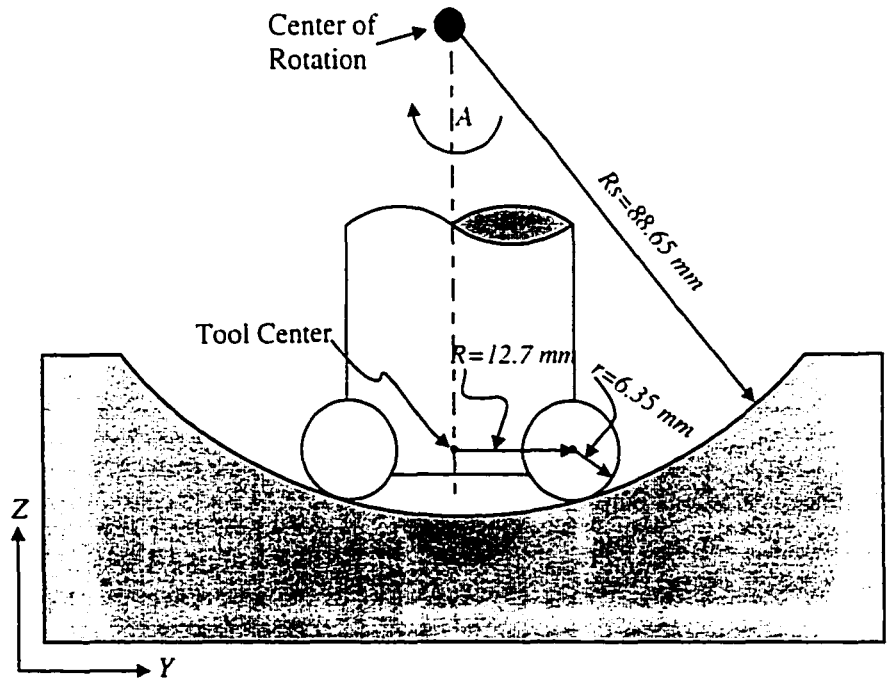


Figure 4.1: Dimensions of the Circular Cut

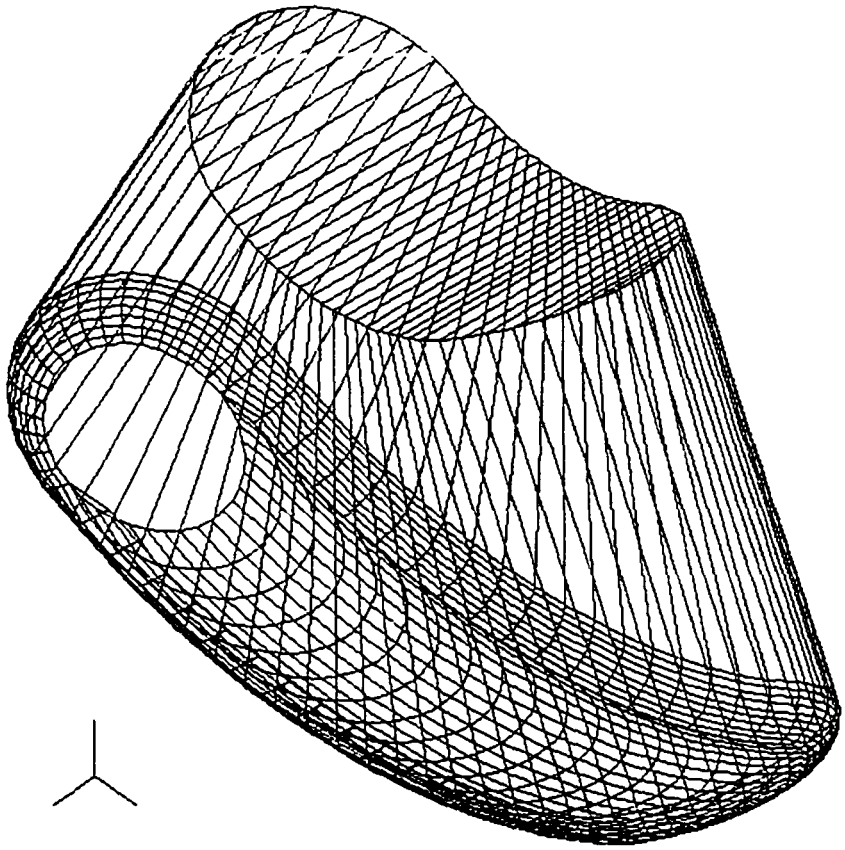


Figure 4.2: The Solid Model of the Volume Swept by the Tool for the Circular Cut

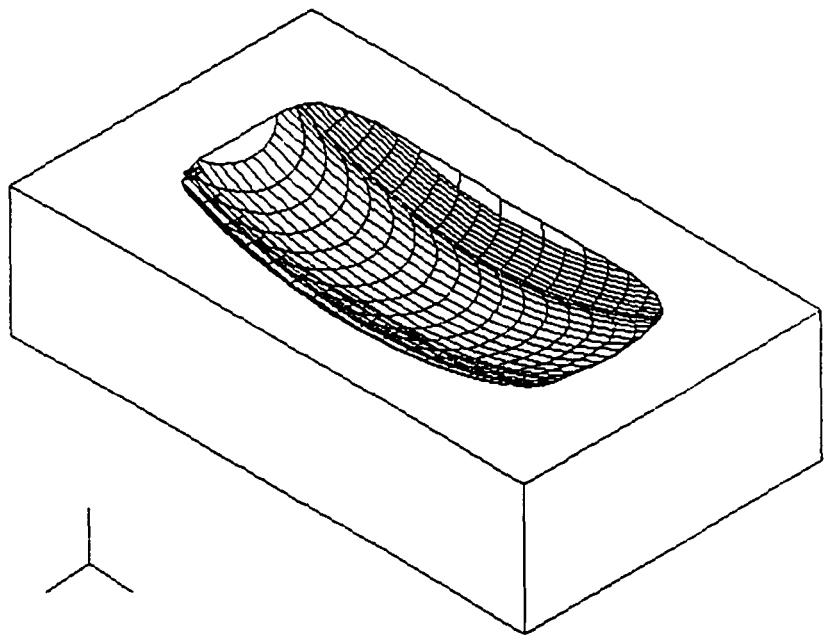


Figure 4.3: The Solid Model of the Workpiece after the Subtraction of the Swept Volume of the Circular Cut

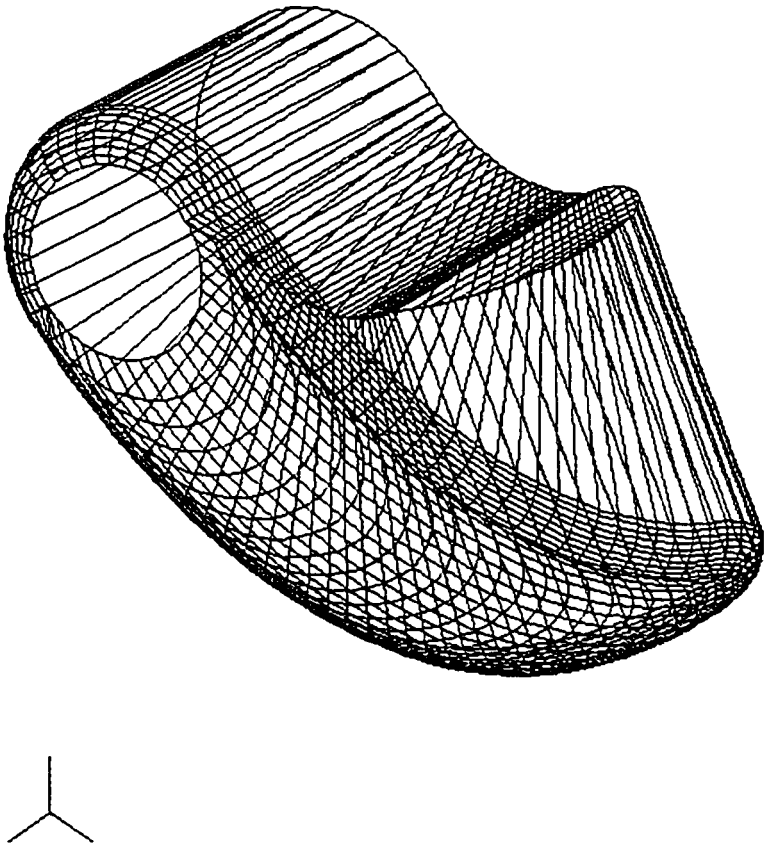


Figure 4.4: The Solid Model of the Volume Swept by the Tool for the Spiral Cut

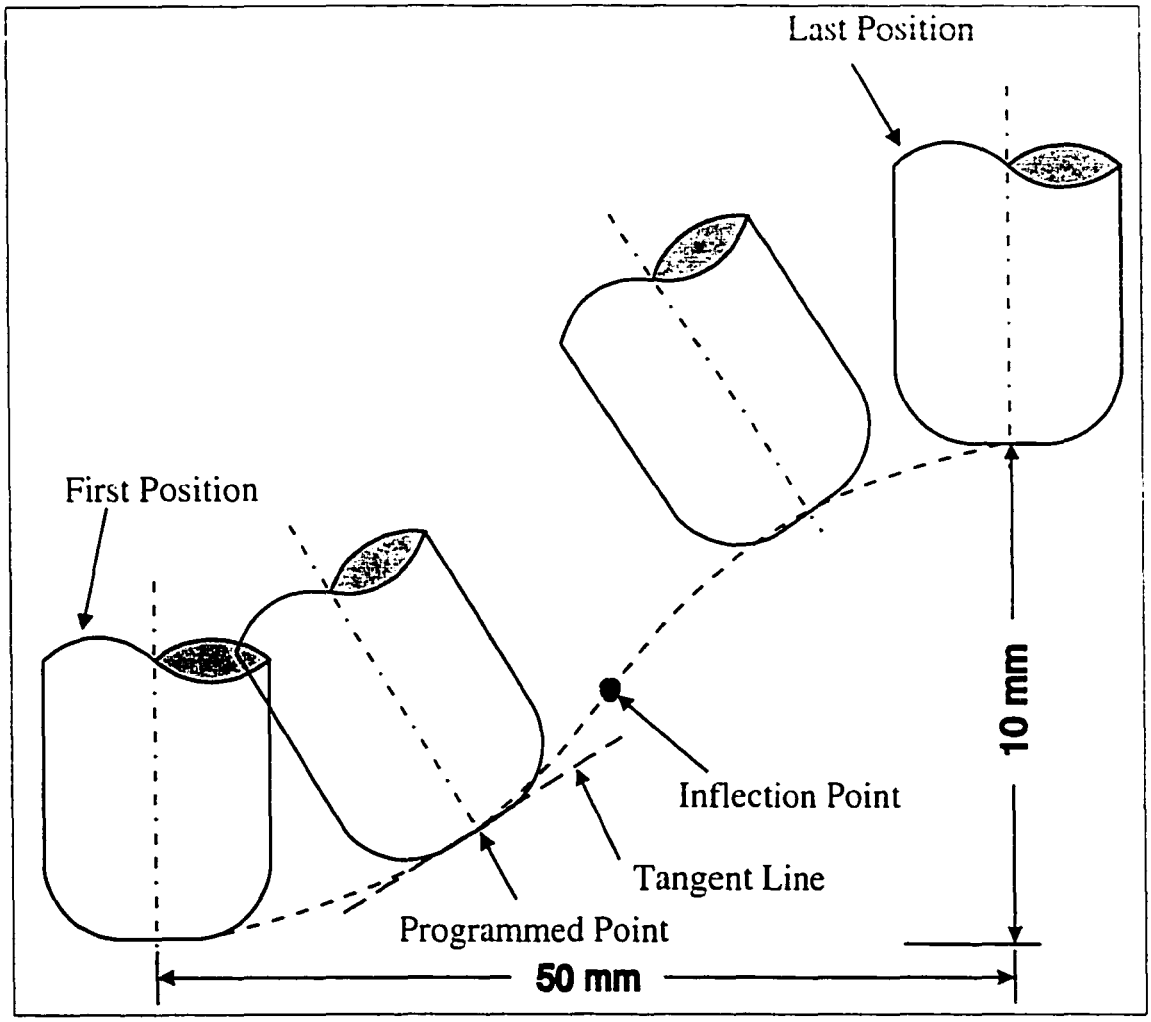


Figure 4.5: The Sinusoidal Tool Path

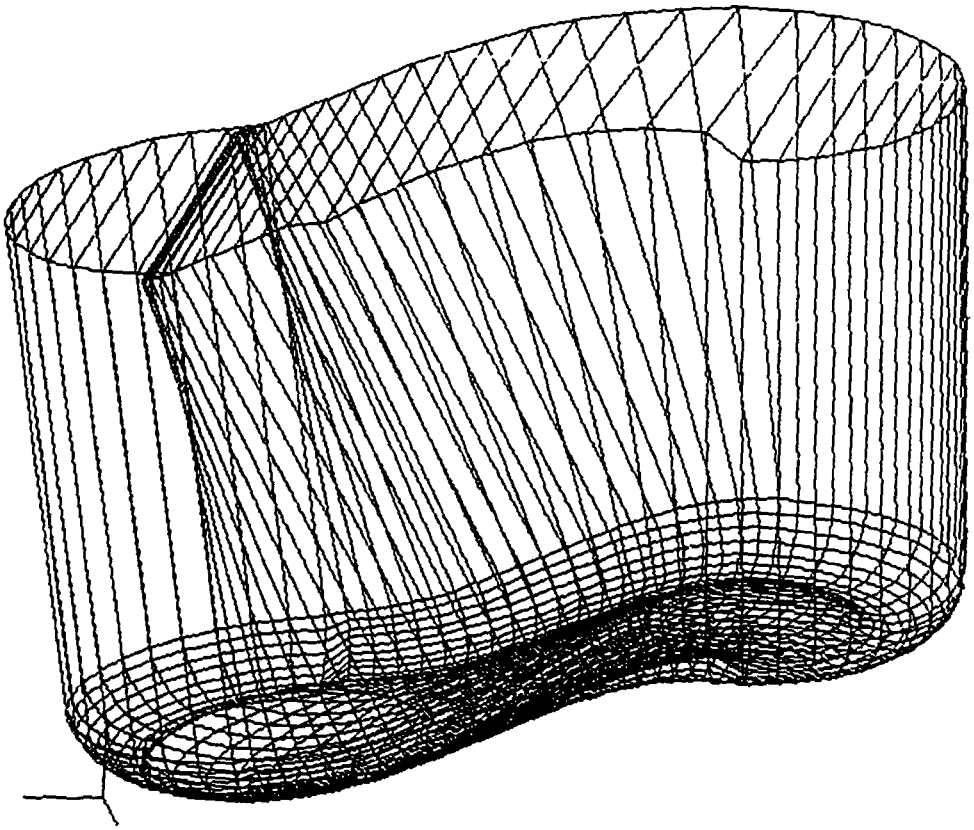


Figure 4.6: The Solid Model of the Volume Swept by the Tool for the Sinusoidal Cut

pieces. The machine used was an OKK MCV 410 four-axis machine, with the configuration shown schematically in figure 3.6. The workpiece was mounted in an overhang position in a fixture clamped to the rotary table. This arrangement was not particularly rigid, and for this reason machining wax was chosen for the workpiece material. The toroidal cutter used had 3 carbide inserts, and its dimensions were R = 12.7, and r = 6.35 mm. The cutting conditions used were: spindle speed $N = 1000\ rpm$, and feed = 150 mm/min.

The comparison between the simulation and the cutting tests was performed in terms of the Z coordinates of points on the workpiece obtained from the simulation with those measured on the machined part. The comparison was conducted for the feed plane (it contains the tool axis and the feed direction), as well as for another section in a plane parallel to the feed plane and offset from it by 6 mm. The measurements on the machined part were conducted on a Coordinate Measuring Machine, CMM, Mitutoyo model BMH305. Measurements were taken at 100 points along each section. It was not possible to match the locations of these points exactly with those generated in the simulation, and consequently some of the differences in the Z coordinates, albeit small, could be attributed to these deviations.

Figure 4.7 shows the comparison results for the circular path. The maximum difference is only 0.2 μm for the feed plane, and it is 0.8 μm for the offset plan. Although the agreement is excellent, yet it is expected because of the special nature of the cut.

Figure 4.8 shows the comparison results for the spiral cut. The maximum difference is 0.3 μm for the middle section, and it is about 1 μm for the offset section.

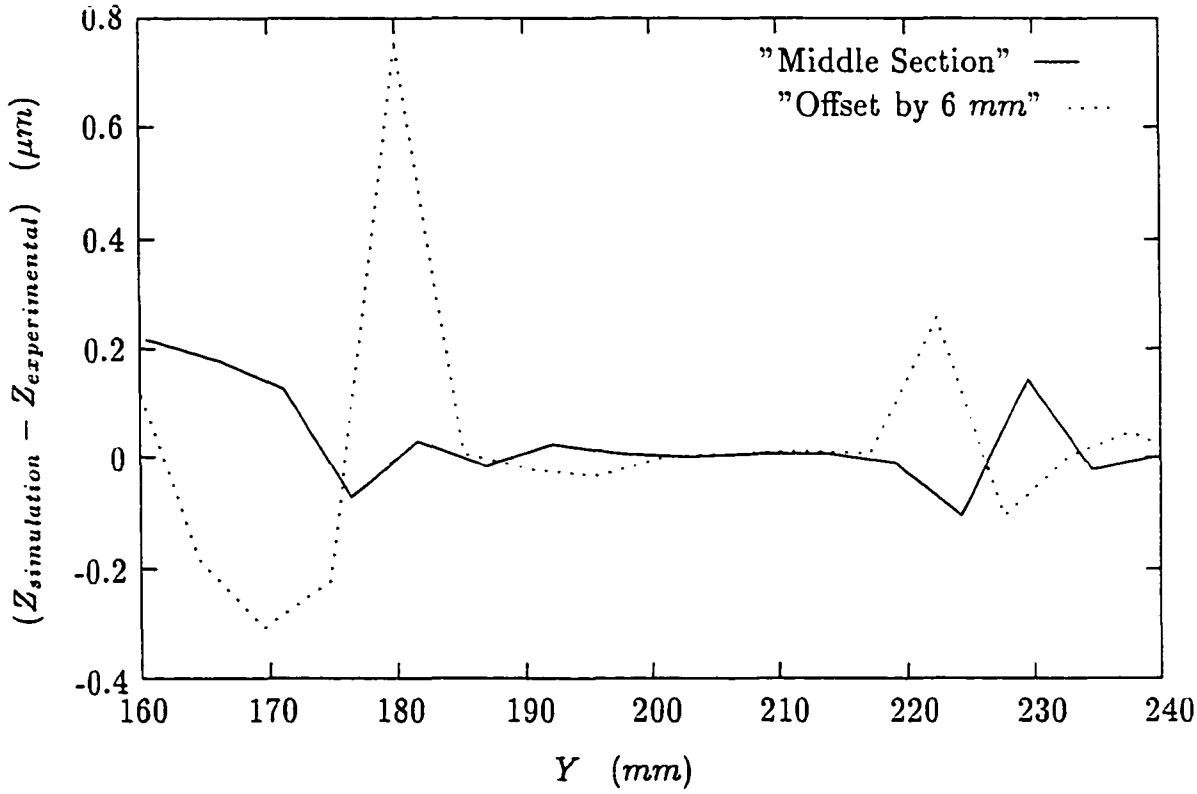


Figure 4.7: The Difference Between Measured and Simulated Results for the Circular Cut at Two Sections

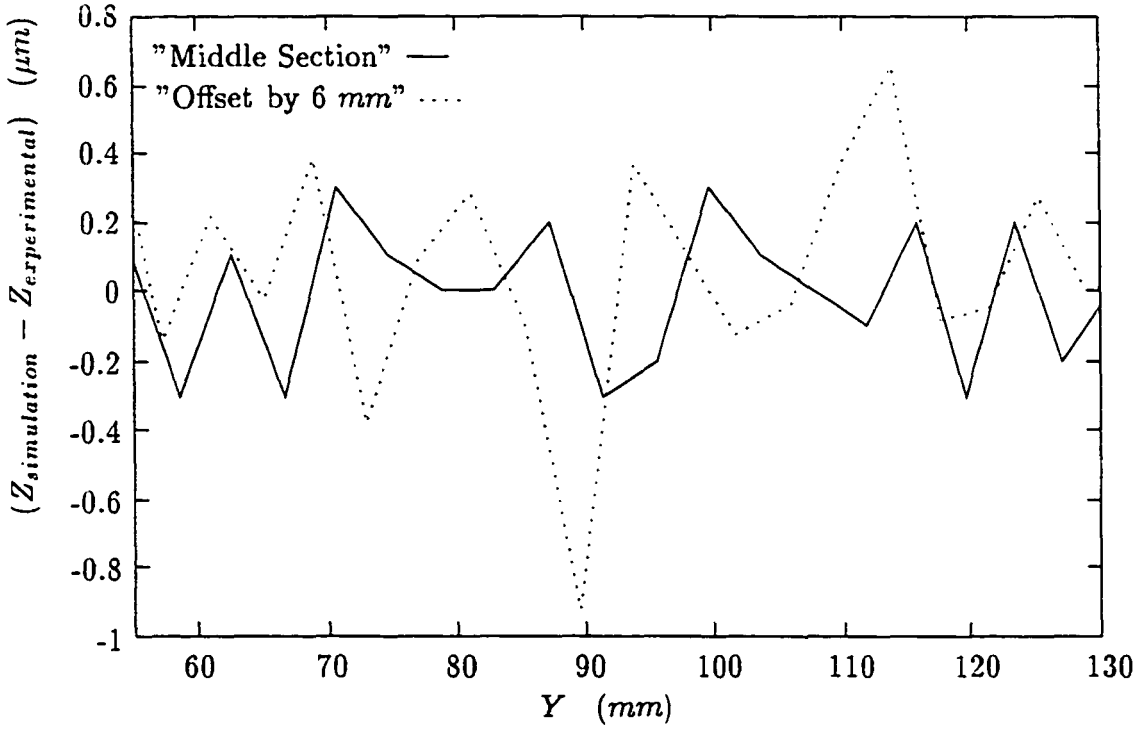


Figure 4.8: The Difference Between Measured and Simulated Results for the Spiral Cut at Two Sections

Again the differences are small and they do not follow any specific pattern. In this tool path, however, we should remember that the radius of the generating circle increased linearly from beginning to the end of cut. Such a trend did not manifest itself in the comparison results, and accordingly the differences in figure 4.8 could be attributed mainly to experimental errors.

Figure 4.9 shows the comparison results for the sinusoidal tool path. Because of the complexity of this tool path, comparisons were made at three sections: the middle, a plane offset by 6 mm, and a plane offset by 10 mm. The maximum difference at all sections is about 8 μm. This is an order of magnitude greater than the previous two examples. Nevertheless, it is still small, especially considering the fact that typical tolerances for sculptured surfaces are around ± 50 μm. Again, there is no apparent pattern in the results of figure 4.9, which means that the observed differences are due to random errors rather than systematic deviations associated with the circles technique.

4.2 Comparison with Another Simulator

The experimental results presented in section 4.1 indeed verify the circles technique for simulating swept volumes using the generating circles. The differences between simulated and measured results were negligible for simple cuts, in the order of 1 μm, and small, 8 μm, for the complex sinusoidal path. The differences could be attributed mainly to experimental errors, especially for the sinusoidal cut where all the four-axes moved simultaneously, and the mounting overhang was large. To eliminate these potential sources of errors, numerical comparisons were also conducted between the circles technique, and another simulation technique known as

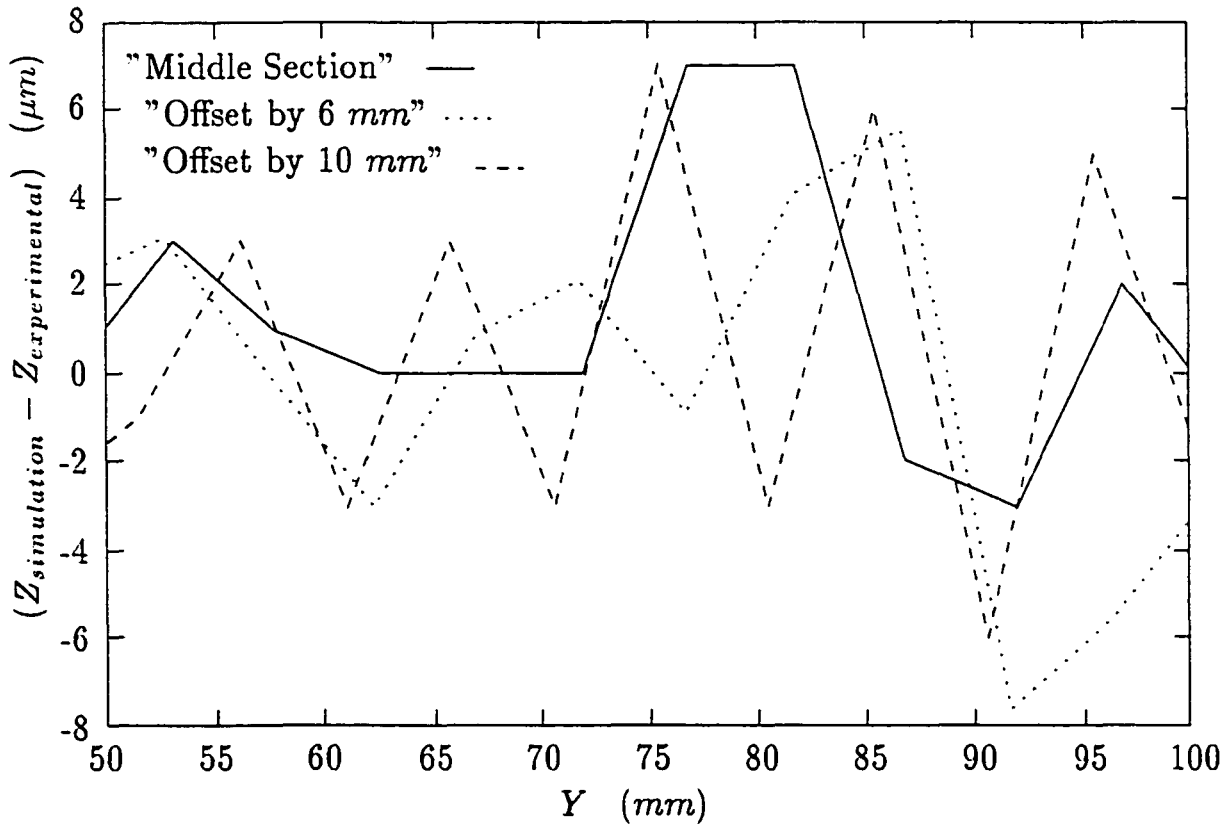


Figure 4.9: The Difference Between Measured and Simulated Results for the Sinusoidal Cut at Three Sections

the Z-map method.

The Z-map simulation has been established and used to determine surface finish in [32]. Rao et al. [33] also used it to determine gouging and to generate a gouge free tool path. The details of the method are described in [13], but a summary of the technique is given here. In the Z-map method, vertical rays (grass) of a specified height are constructed at closely spaced points along the region to be simulated. These rays are clipped by the tool as it moves from the starting point to the end point. At the end of the path, the height of the rays gives a good assessment of the existing surfaces. This method was implemented and used to simulate the resulting workpiece surface along the feed plane section, as well as for other offset sections. The grass density was 100 per mm, and the distance between the subsequent tool positions was 0.35 mm.

For both the circular and spiral tool paths, the agreement between the generating circles method and the Z-map method was almost perfect; differences were less than 0.1 μm. Figure 4.10 shows the differences between the two simulation techniques for the sinusoidal cut. They are within ± 1 μm, which provides another proof that the circles technique is indeed a viable one to generate swept volumes in multi-axis machining.

The objective of developing the new approach is to speed up the tool path simulation. The comparison with the Z-map method revealed that, the computation time, associated with the sinusoidal cut was 9 seconds for the new technique versus 27 seconds for the Z-map. It should be kept in mind that in the new approach, the whole imprint of the tool onto the workpiece surface was computed, whereas

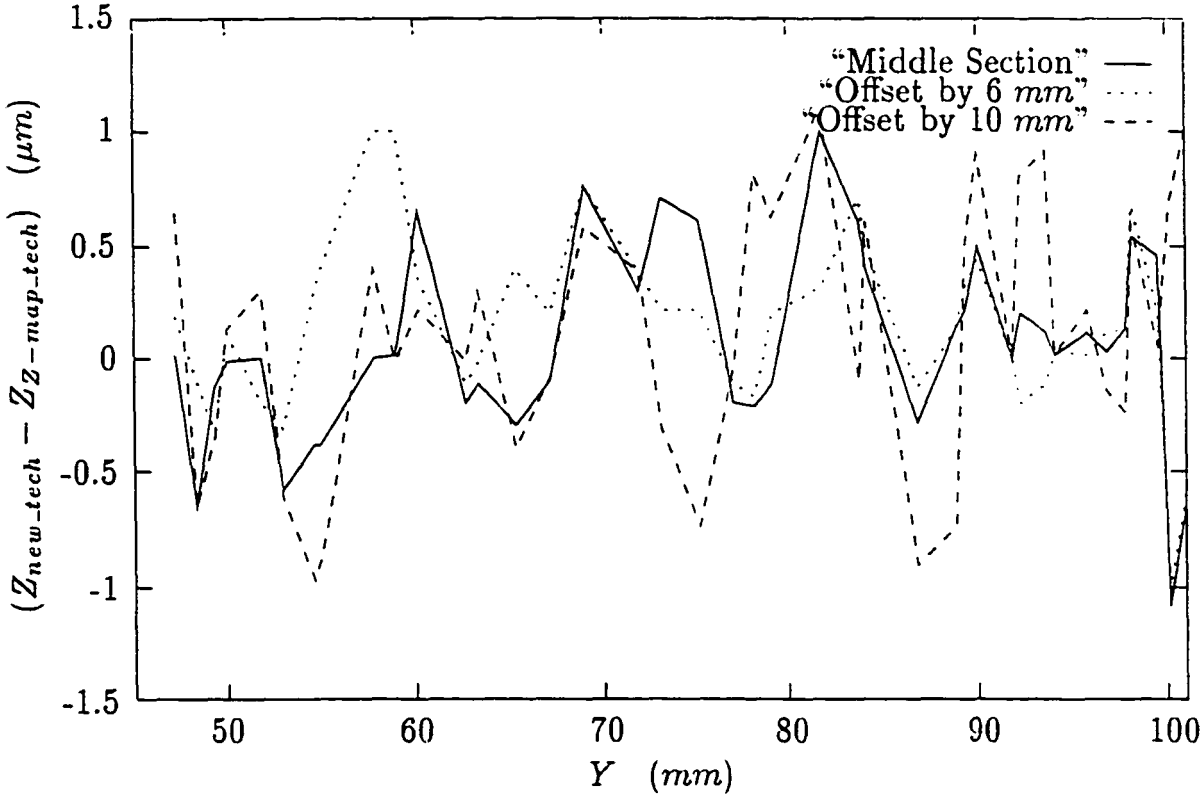


Figure 4.10: Comparison Between the "Generating Circles" Technique and the Z-map Technique

in the Z-map method the surface was simulated at 3 sections only. Computations were done in C on a Sun sprac 20 workstation. Another comparison was made for the sinusoidal cut in which Boolean operations were used at each tool position to simulate the resulting surface. The simulation was conducted using the package ACIS on a Pentium 75 MHz PC. It took 14 hours of computing time to generate half of the cosine curve. Even if we consider a factor of 50 for fair comparison taking into account the computing platforms, still the balance tilts heavily in favor of the generating circles.

The speed of the swept volume simulation is a function of the number of tool positions, the smaller the number of tool positions, the shorter the simulation time will be. For this reason, further analysis has been performed to determine the sensitivity of the swept volume to the number of tool positions in a given tool path, it is presented next.

4.3 Effects of Changing the Step Size

The sensitivity of the swept volume to changes in step size[1] was tested for three different step sizes; namely, 0.5 mm, 2.5 mm and 5 mm for all the three tool paths at different sections. Similar to the previous results, for the circular and the spiral cuts, the comparison was performed at two sections: a section in the feed plane and another parallel section offset by 6 mm. Again, for the sinusoidal cut, an additional section in a plane parallel to the feed plane and offset by 10 mm was also checked.

[1]The distance between two subsequent tool positions along a pass.

Swept volumes of the three cuts were generated for all three step sizes and a comparison was conducted between the swept volume for each cut in terms of Z coordinate and the maximum surface deviation was calculated.

In the circular cut, the radius of the "generating circle" varied slightly as expected. Although the change in step size is relatively large, the radius of the "generating circle" increased by only 0.200 mm, between 0.5 mm and 5.0 mm step sizes, and the maximum surface deviation was 0.070 mm.

In the Spiral cut, the "generating circle's" radius varied linearly, and increased by 0.250 mm. The maximum surface deviation was 0.080 mm.

The sinusoidal cut consists of a concave region, a convex region and an inflection point. It means that the machined surface is produced partly by the outside edges of the inserts (in the concave region), partly by the inside edges (in the convex region) and partly by the bottom of the inserts (in the flat region). Figure 4.11 shows the variation of the radius of the "generating circles" for the three step sizes, along the feed direction. The maximum variation of the radius in the concave region was 0.138 mm and the resulting surfaces deviated by 0.063 mm. In the convex region, the maximum variation of the radius was 0.181 mm and the resulting surfaces deviated by 0.071 mm. The change in the radius around the inflection point (change in curvature from concave to convex) was 0.201 mm and the resulting surfaces differed by 0.100 mm. This is expected since the "generating circles" changed from the outside to the inside of the inserts by passing the inflection point.

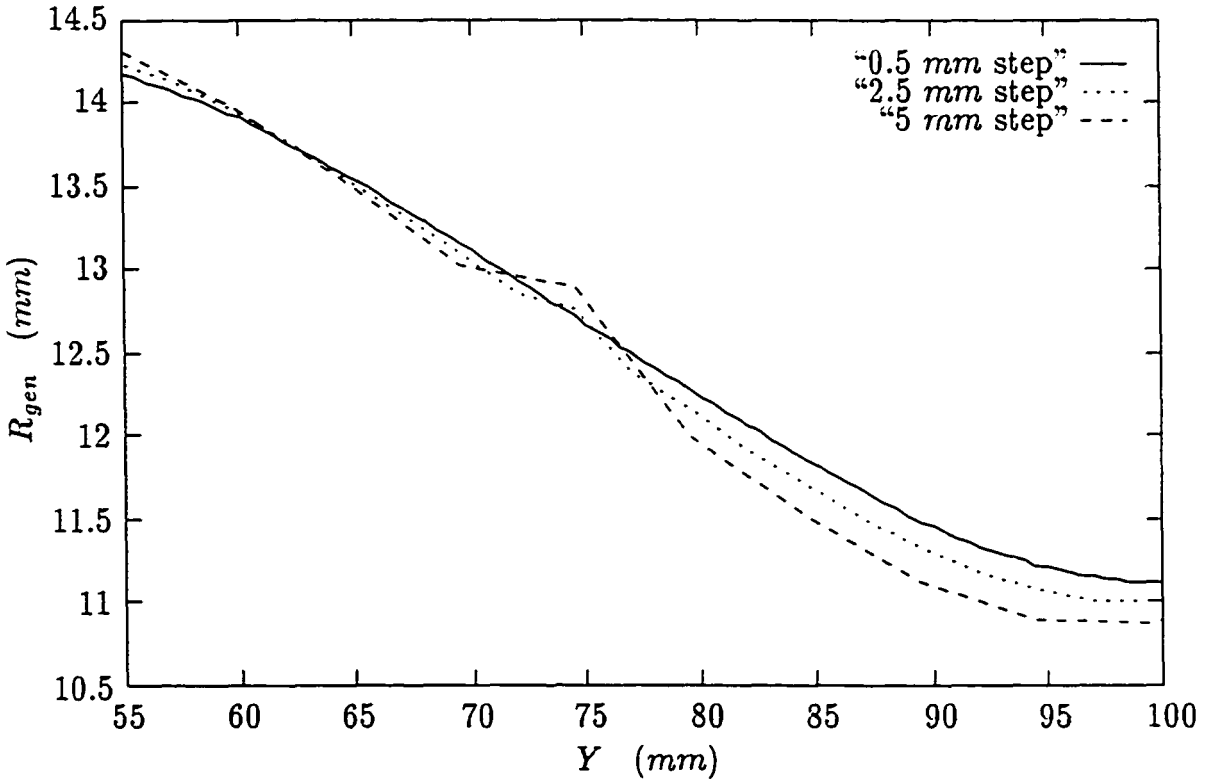


Figure 4.11: The Change of Radius of the "generating circle" with respect to The Step Size for The Sinusoidal Cut

From the above analysis, we can conclude that the radius of the "generating circles" is not very sensitive to the change in step size for surfaces with one type of curvature. Nevertheless, for concave-convex surfaces the radius of the "generating circles" is sensitive to the change in step size around the inflection points: the smaller the step size is, the more accurate the radius of the "generating circles" will be. For accurate representation of swept volumes, it is not necessary to have a very small step size for surfaces with one kind of curvature. In this work, a step size of about 2 mm was found to be adequate for this kind of surfaces.

Chapter 5

The "Generating Curves" Technique

5.1 Introduction

In chapter 3, a technique for simulating the swept volume of toroidal cutters, using planer generating circles, was presented. The generating circles method was applied successfully to special cases of three and four-axis tool paths, but it is inappropriate for five-axis tool paths.

As explained in chapter 3, the sweeping profiles of toroidal cutters, when the normal of the tool coincides with the normal of the surface, are exact circles. This is not the case in most five-axis tool paths. Thus simulating the sweeping profiles in five-axis machining based on just one point of contact between the tool and the surface results in losing a great deal of the swept volume information due to the fact that the sweeping profiles in five-axis tool paths are actually three-dimensional

curves. These curves, designated here as the "generating curves", are constructed based on many points of contact between the tool and the surface as discussed later in this chapter. To illustrate the difficulty in simulating the imprint of toroidal cutters when the normal of the tool does not coincide with the normal of the surface using the generating circles method, the sweeping profiles on the cutting surface of the tool, for a tool position in a three-axis tool path ($\Delta x = 3$ mm, $\Delta y = 20$ mm, $\Delta z = 10$ mm, $R = 24.35$ mm and $r = 13.06$ mm) were simulated using both the generating circles (figures 5.1a and 5.2a) and generating curves (figures 5.1b and 5.2b). The increments are large to exaggerate the differences. It is clear from figures 5.1 and 5.2 that, even for a three-axis motion, if the normal of the tool does not coincide with the normal of the surface, the trace of the toroidal cutter can not be accommodated in one plane using planar circles approximation: three-dimensional curves would have to be employed. Also, as shown in figure 5.2, the errors increased drastically as we moved towards the outside of the tool.

In this chapter, a technique based on three-dimensional generating curves for the general endmill shown in figure 5.3 is discussed. This technique was implemented for up to five-axis tool paths. A thorough study was conducted, with numerical and experimental verification, for toroidal cutters. Only numerical simulations are discussed for the general cutter.

5.2 The General APT Tool

The APT tool path programming language describes the general tool as a combination of two cones and a torus, as shown in figure 5.4. Using this combination, it

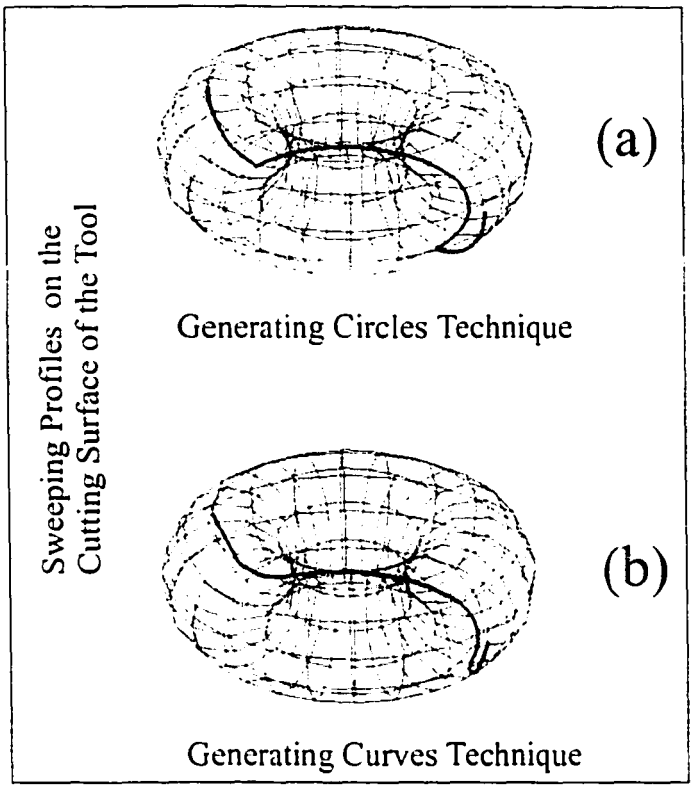


Figure 5.1: A Comparison Between Sweeping Profiles of the Generating Circles and the Generating Curves Methods ($\Delta x = 3\ mm$, $\Delta y = 20\ mm$, $\Delta z = 10\ mm$, $R = 24.35\ mm$ and $r = 13.06\ mm$)

is possible to model conical cutters, in addition to flat bottom cutters, ball nosed endmills and toroidal cutters, just by selecting appropriate values for the various parameters of the tool. This tool can be defined, with respect to the Z-axis, as follows:

$$x = \begin{cases} tm\cos\phi & \text{if } 0 < Z < n \\ (R + r\sin\theta)\cos\phi & \text{if } n \leq Z < n + r(\cos\theta_{start} - \cos\theta_{end}) \\ (R + r\sin\theta_{end} + ta)\cos\phi & \text{if } n + r(\cos\theta_{start} - \cos\theta_{end}) \leq Z \leq b \end{cases}$$

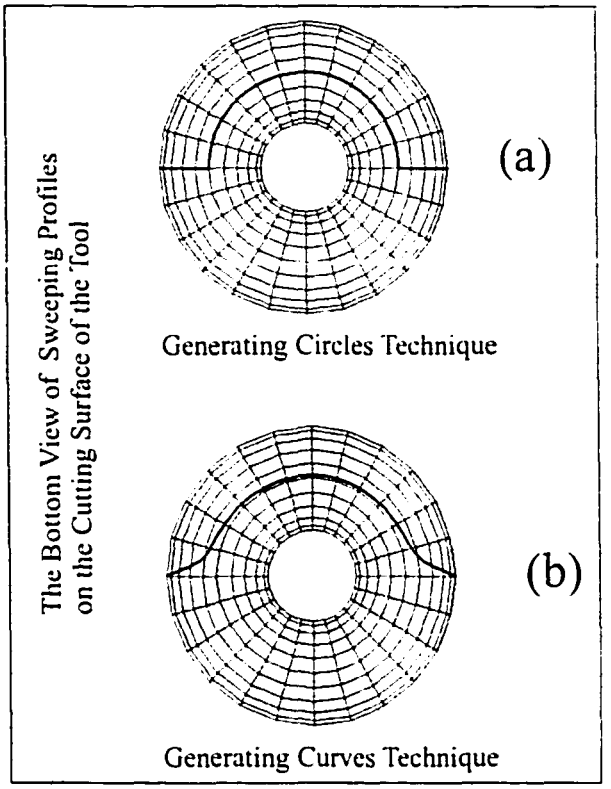


Figure 5.2: A Comparison Between Sweeping Profiles of the Generating Circles and the Generating Curves Methods, the Bottom View ($\Delta x = 3\ mm$, $\Delta y = 20\ mm$, $\Delta z = 10\ mm$, $R = 24.35\ mm$ and $r = 13.06\ mm$)

$$y = \begin{cases} tm \sin\phi & \text{if } 0 < Z < n \\ (R + r\sin\theta)\sin\phi & \text{if } n \leq Z < n + r(\cos\theta_{start} - \cos\theta_{end}) \\ (R + r\sin\theta_{end} + ta)\sin\phi & \text{if } n + r(\cos\theta_{start} - \cos\theta_{end}) \leq Z \leq b \end{cases}$$

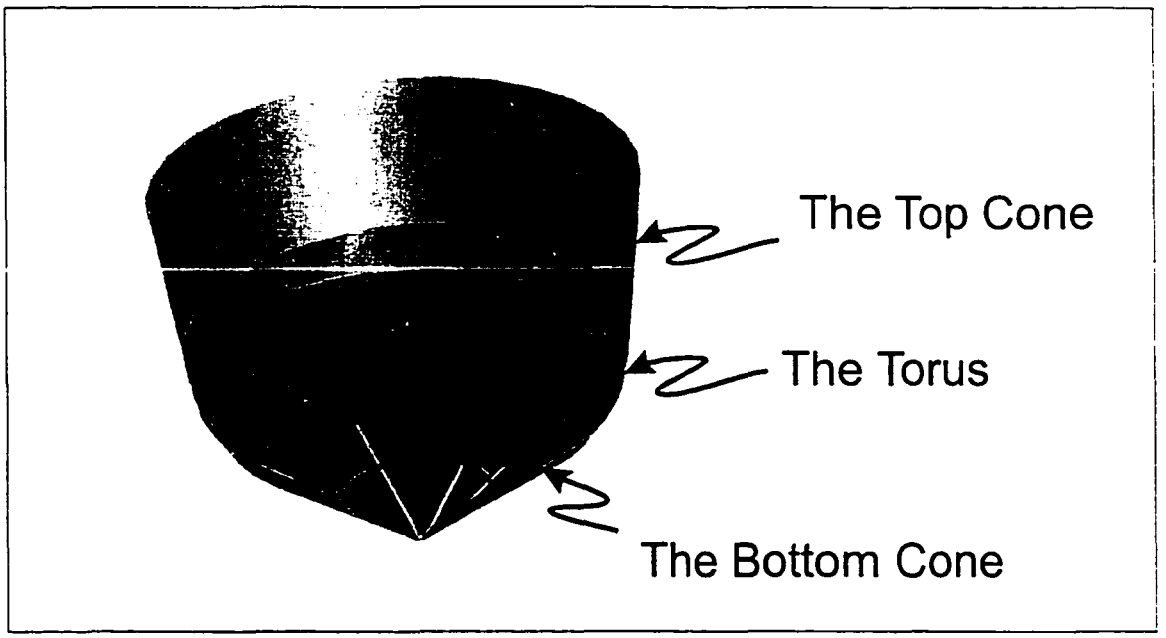


Figure 5.3: A General Tool

$$z = \begin{cases} tn & \text{if } 0 < Z < n \\ n + r(\cos\theta_{start} - \cos\theta) & \text{if } n \leq Z < n + r(\cos\theta_{start} - \cos\theta_{end}) \\ n + r(\cos\theta_{start} - \cos\theta_{end}) + tb & \text{if } n + r(\cos\theta_{start} - \cos\theta_{end}) \leq Z \leq b \end{cases} \tag{5.1}$$

where

$t \in [0, 1]$, $\theta \in [\theta_{start}, \theta_{end}]$,

$\theta_{start} = \tan^{-1}(n/m)$, $\theta_{end} = \tan^{-1}(b/a)$,

R is the radius of the torus, r is the radius of the inserts of the torus,

n, m, a, b, θ and ϕ are as illustrated in figure 5.4.

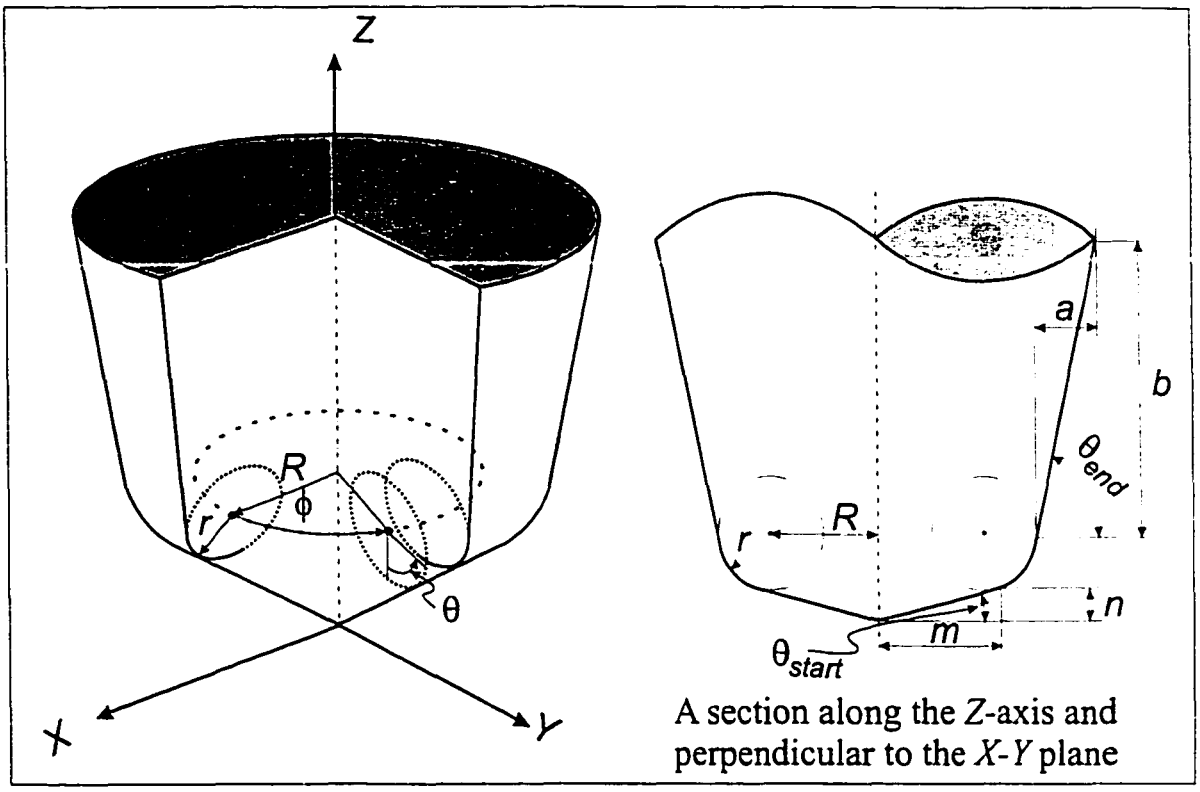


Figure 5.4: Definition of the General Tool

The generating curves concept for toroidal cutters is first explained, then it is extended to the general APT tool next.

5.3 Three-Dimensional Generating Curves for Toroidal Cutters

The technique of the generating curves is based on the tangency concept. As in the generating circles technique, a sequence of two consecutive tool positions has to be considered in order to identify the generating curves.

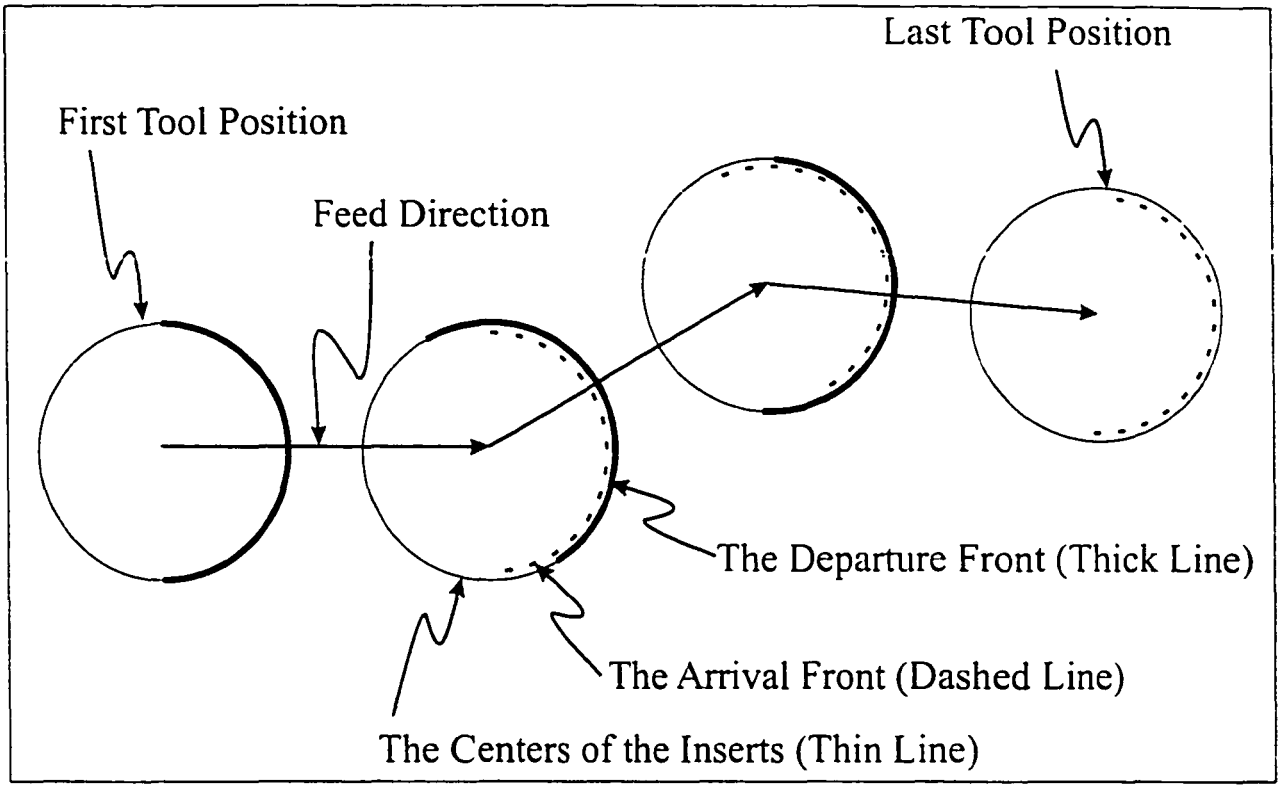


Figure 5.5: The Splitting of the Front Half and Back Half of the Tool Procedure

The first step in this new technique is the splitting of the tool into two halves, based on the feed direction and the orientation of the tool: the front half and the back half. For the purpose of explanation, let us consider four points in a five-axis tool path as shown in figure 5.5. To have a better understanding of the splitting procedure, we will concentrate on the front half of the tool and consider the motion to be two dimensional. As illustrated in figure 5.5, the cutter reaches the cutter locations from one direction and leaves them in another. Therefore, with the exception of the first and last tool positions, there are two fronts at each cutter location: one for the departure and one for the arrival. The complete thin circles in figure 5.5 are the circles that join the centers of inserts of the torus. The thick

semi-circles are the front halves of the tool as it proceeds from one tool position to another (departure fronts). The dashed semi-circles are the front half of the tool as it arrives from one tool position to another (arrival fronts). The next step is the digitizing of the tool into a number of inserts, each insert will contain a point on the generating curves. Thus, to increase the accuracy of the generating curves, the number of inserts should be increased. The equation of the generating curves is determined by dealing with a pair of departure and arrival front halves of the tool and taking the tangent between the corresponding inserts. The corresponding inserts are two sets of inserts in i^{th} departure front and $(i+1)^{th}$ arrival front of the tool path, separated by the same radial distance as shown in figure 5.6. The procedure of determining the tangency points between the correspond inserts is explained in section 5.4.1.

5.4 The Simulation Process

The simulation process starts with analyzing the given tool path, described in terms of G-code or CL data, and determining the locations and orientations of the tool throughout the tool path. The next step is determining the equations of the imprint of the tool at all the locations. This can be achieved by considering two consecutive tool positions, as shown in figure 5.7.

The movement of the tool between every two positions is assumed to be linear. For every two consecutive tool positions, like the ones shown in figure 5.7, i and $i+1$, the parameters Z_i, Z_{i+1}, $P_i(x_i, y_i, z_i)$ and $P_{i+1}(x_{i+1}, y_{i+1}, z_{i+1})$ are known. Vectors Z_i, Z_{i+1} represent the orientation of the tool, and points $P_i(x_i, y_i, z_i)$ and $P_{i+1}(x_{i+1}, y_{i+1}, z_{i+1})$ represent the position of the tool at the i^{th} and $(i+1)^{th}$ loca-

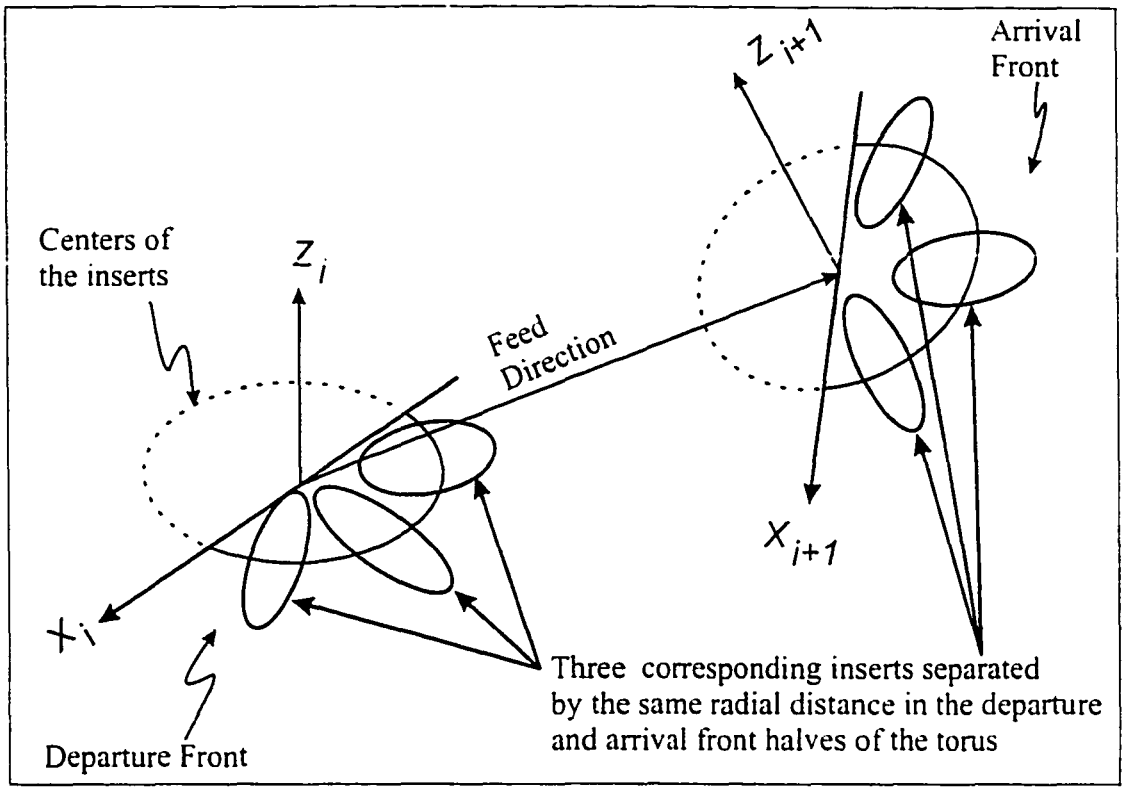


Figure 5.6: The Concept of Corresponding Inserts

tions respectively. Thus, the feed direction vector, ΔP_i, can be determined. As the tool moves along the tool path, the departure and arrival front halves of the tool at each position are identified. Vector ΔP_i divides the front half of the tool into two quarters, hence, the front half of the tool can be determined by defining a vector perpendicular to ΔP_i. At the i^{th} cutter location, the departure front is determined by taking the cross product of ΔP_i with Z_i. The arrival front at the $(i+1)^{th}$ tool position is obtained by taking the cross product of ΔP_i with Z_{i+1}. The resulting vectors define the local X axis at the two tool positions. The X axes at the i^{th} and $(i+1)^{th}$ locations are determined by

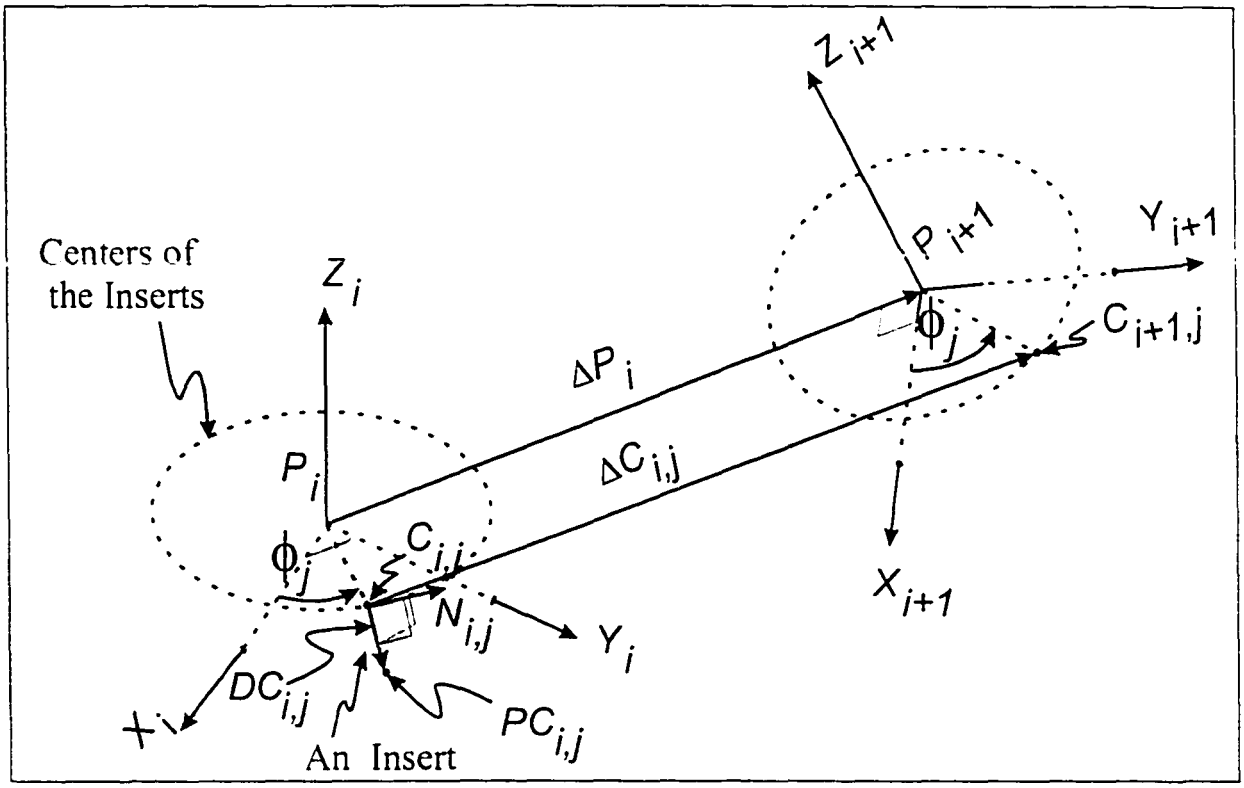


Figure 5.7: Two Consecutive Tool Positions of a Torus in Five-Axis Movement

$$X_i = \Delta P_i \times Z_i \tag{5.2}$$

$$X_{i+1} = \Delta P_i \times Z_{i+1} \tag{5.3}$$

To complete the two local frames, vectors Y_i and Y_{i+1} are determined as follows:

$$Y_i = Z_i \times X_i \tag{5.4}$$

$$Y_{i+1} = Z_{i+1} \times X_{i+1} \tag{5.5}$$

Having identified the front and the back of the tool, the determination of the imprint of tool can be achieved by dealing with a sequence of pairs of either front or back halves of the tool, depending on which half is actually cutting the surface, which can be determined by the tool orientation. To simplify the formulations, the equations are expressed with respect to X_t Y_t Z_t local frames.

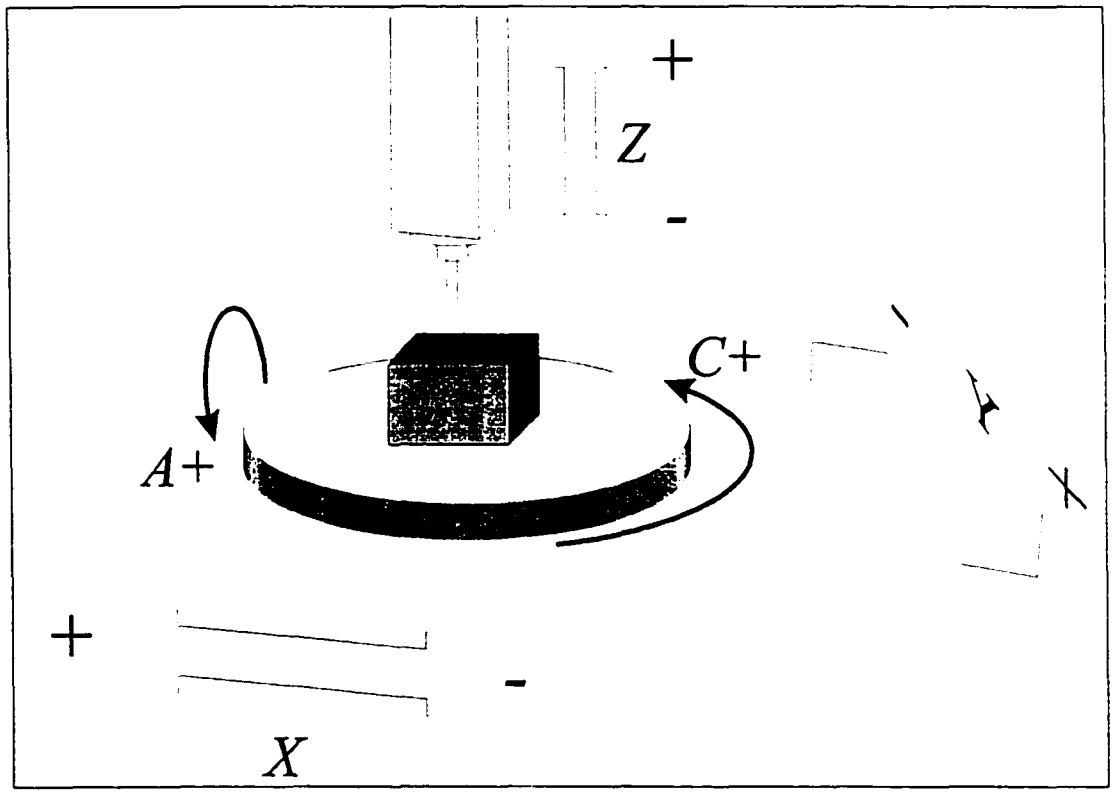


Figure 5.8: A five-axis Configuration of the CNC Machine

The configuration of the five axis machine used in machining the test pieces is shown in figure 5.8. It consists of three translational axes: X, Y, Z, and two rotational axes: A and C. The rotations are provided by a tilt-rotary table.

5.4.1 Equations of the Generating Curves in Toroidal Cutters

The generating curves produced by the torus, in toroidal cutters, is the main focus of the study in this chapter. As explained in section 5.3, the procedure of identifying the points on the generating curves starts with identifying a pair of departure and arrival fronts or backs and then slicing the torus into a number of inserts separated by a certain radial distance. The points of the generating curves are actually the tangency points between each two corresponding inserts. To simplify the understanding of the generating curves concept, we will concentrate on the front half of the tool for the rest of the study in this chapter. Let us consider figure 5.7 where we are dealing with two fronts. Angle ϕ_j determines the corresponding centers of inserts between each two consecutive tool positions.

A tangency point between two circles in one plane can be found by intersecting the circles with vectors perpendicular to the vector that joins the centers of the circles. If the two circles are in different planes, then the vectors that define the tangency point have to be in the same planes of the circles in addition to being perpendicular to the vector that joins the centers of the two circles. With this in mind, to find the tangency points for toroidal cutters in two subsequent tool positions, we first have to find the direction of vector $DC_{i,j}$ which defines where the torus touches the surface. Note that i and j correspond to the location of the tool and the location of the insert respectively. Finding the direction of $DC_{i,j}$ can be achieved by joining two corresponding centers of the inserts with vector ΔC_i and then finding a vector perpendicular to ΔC_i and at the same time lies in the insert plane. This can be accomplished by taking a cross product between ΔC_i and the

insert normal $N_{i,j}$. The cross product is then normalized and multiplied by r, the radius of the insert, to determine the point of contact, $PC_{i,j}$.

The equations of the two corresponding centers of the inserts, $C_{i,j}$ and $C_{i+1,j}$ shown in figure 5.7 are as follows:

$$C_{i,j} = (R_{torus} \cos \phi_j)\vec{i}_i + (R_{torus} \sin \phi_j)\vec{j}_i \tag{5.6}$$

where

R_{torus} is the distance between the center of the tool and the center of the inserts.

$$C_{i+1,j} = \Delta P + (R_{torus} \cos \phi_j)\vec{i}_{i+1} + (R_{torus} \sin \phi_j)\vec{j}_{i+1} \tag{5.7}$$

Now we can calculate $\Delta C_{i,j}$

$$\Delta C_{i,j} = C_{i+1,j} - C_{i,j} \tag{5.8}$$

The normal of the inserts $N_{i,j}$ can be expressed as follows:

$$N_{i,j} = (-\sin \phi_j)\vec{i}_i + (\cos \phi_j)\vec{j}_i \tag{5.9}$$

Now we can calculate the point of contact:

$$DC_{i,j} = \frac{\Delta C_{i,j} \times N_{i,j}}{|\Delta C_{i,j} \times N_{i,j}|}(r) \tag{5.10}$$

where

r is the radius of the inserts of the torus.

The equation of the generating curves is then defined in the global frame as

$$\sum_{i=1}^{n}\sum_{j=1}^{m}(C_{i,j})_{global} + (DC_{i,j})_{global} \tag{5.11}$$

where

n is the number of tool positions and

m is the number of the inserts.

The sweeping profile of the of the generating curves of toroidal cutters is shown in figures 5.1b and 5.2b and a swept surface of four subsequent tool positions are shown in figure 5.9.

5.4.2 The Swept Volume Simulator

A swept Volume Simulator (SVS) has been implemented in the C++ programming language based on the above formulations as outlined in figure 5.10. The program was developed using Microsoft Visual C++ 6.0 compiler in Windows NT environment. The main reason behind using this software is the powerful debugger of MS-Visual C++ 6.0. Porting the program to the Unix environment is a straight forward procedure. The SVS program requires the CL data and the tool parameters to produce generating curves of the swept volume. The input data can be either entered manually or read from a file. Two different kinematics configurations are implemented in this program:

- All rotational and translational axes are on the spindle.

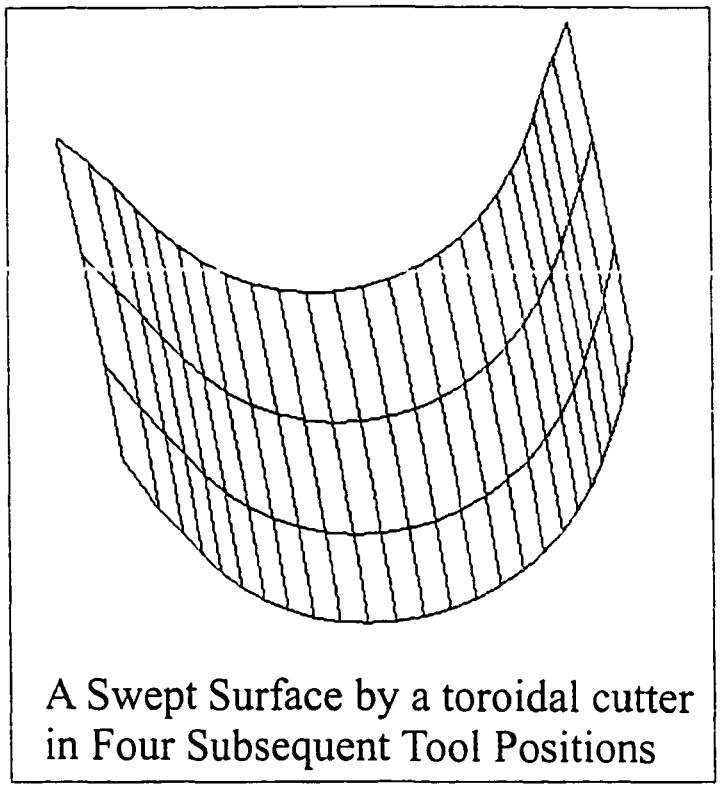


Figure 5.9: A Swept Surface by a Toroidal Cutter in Four Subsequent Tool Positions

- Two rotational and two translational axes are on the table and one vertical translational axis on the spindle.

The SVS program was verified numerically and experimentally as presented in the next chapter.

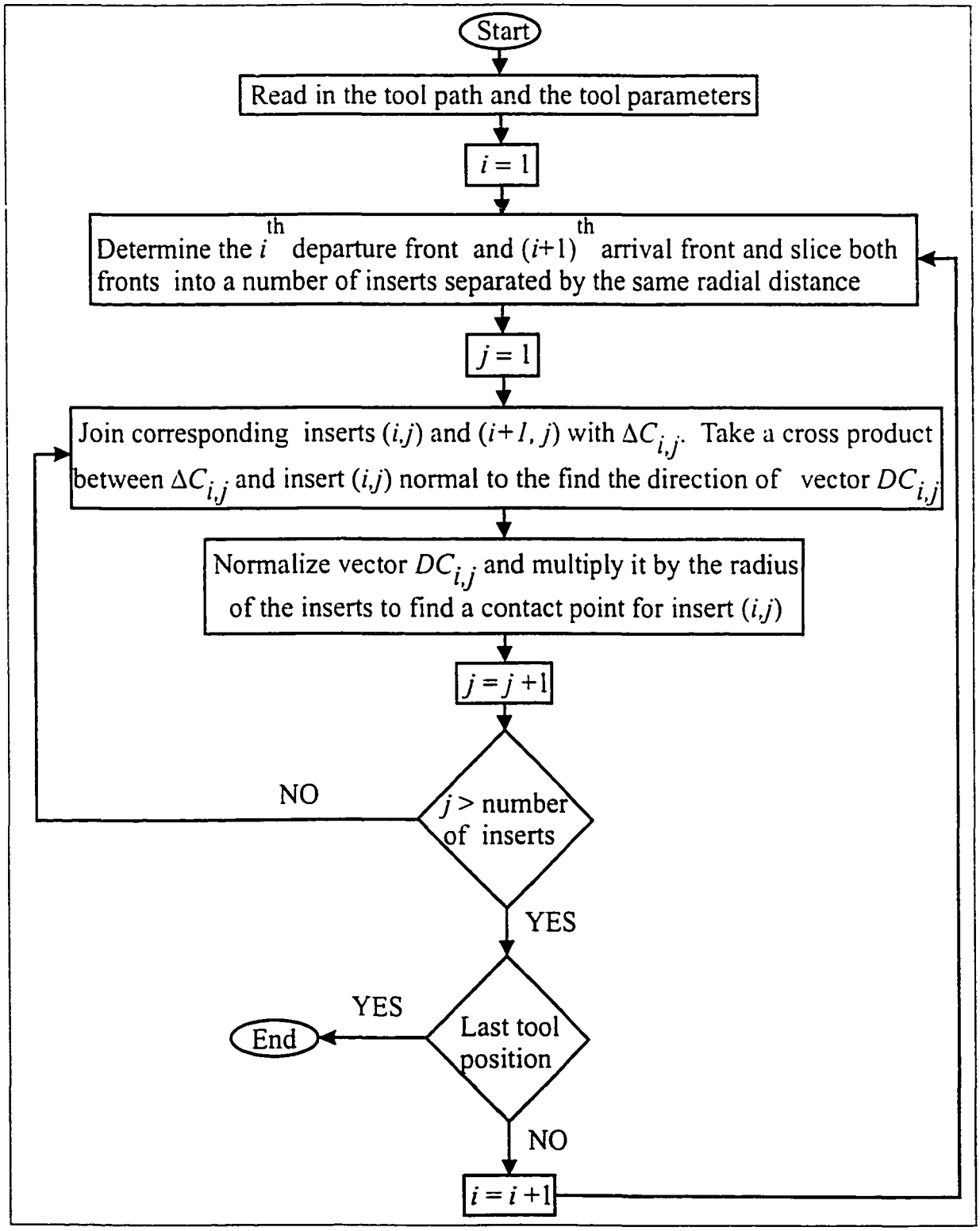


Figure 5.10: The Swept Volume Simulator Algorithm

5.4.3 Equations of the Generating Curves of Conical and Cylindrical Cutters

The generating curves procedure for conical and cylindrical cutters is slightly different than the one used with toroidal cutters. As shown in figures 5.11, a conical or cylindrical cutter can be approximated with an infinite number of circular layers, with different radii in the case of conical cutters, centered on the tool axis and lie in planes perpendicular to the tool axis. This approximation gives us the freedom of dealing with this kind of cutters as a bundle of circular layers which is a direct analogy to a deck of cards[1]. Each card could contain two points on the generating curves, therefore, the larger the number of the cards, the more accurate the approximation of the generating curves will be.

The method of finding the contact points between the cutter and the surface is by taking the tangent between pairs of corresponding cards. Two cards are said to be corresponding cards if they lie at the same height on the tool axis (have the same Z value). The procedure of finding the tangent between corresponding cards is explained in the next section. Figures 5.12 and 5.13 show the sweeping profile of the generating curves on the cutting surface of conical and cylindrical tools undergoing five-axis motions ($\Delta x = 5\ mm$, $\Delta y = 10\ mm$, $\Delta z = 10\ mm$, $\Delta A = 3°$ and $\Delta C = 3°$). The diameter of the cone is 35 mm and the height is 53 mm. The diameter of the cylinder is 38 mm. The sweeping profiles turned out to be not straight lines; rather, they are actually curved lines due to the nature of five-axis movement.

[1]From now until the end of this chapter, the circular layers are referred to as cards

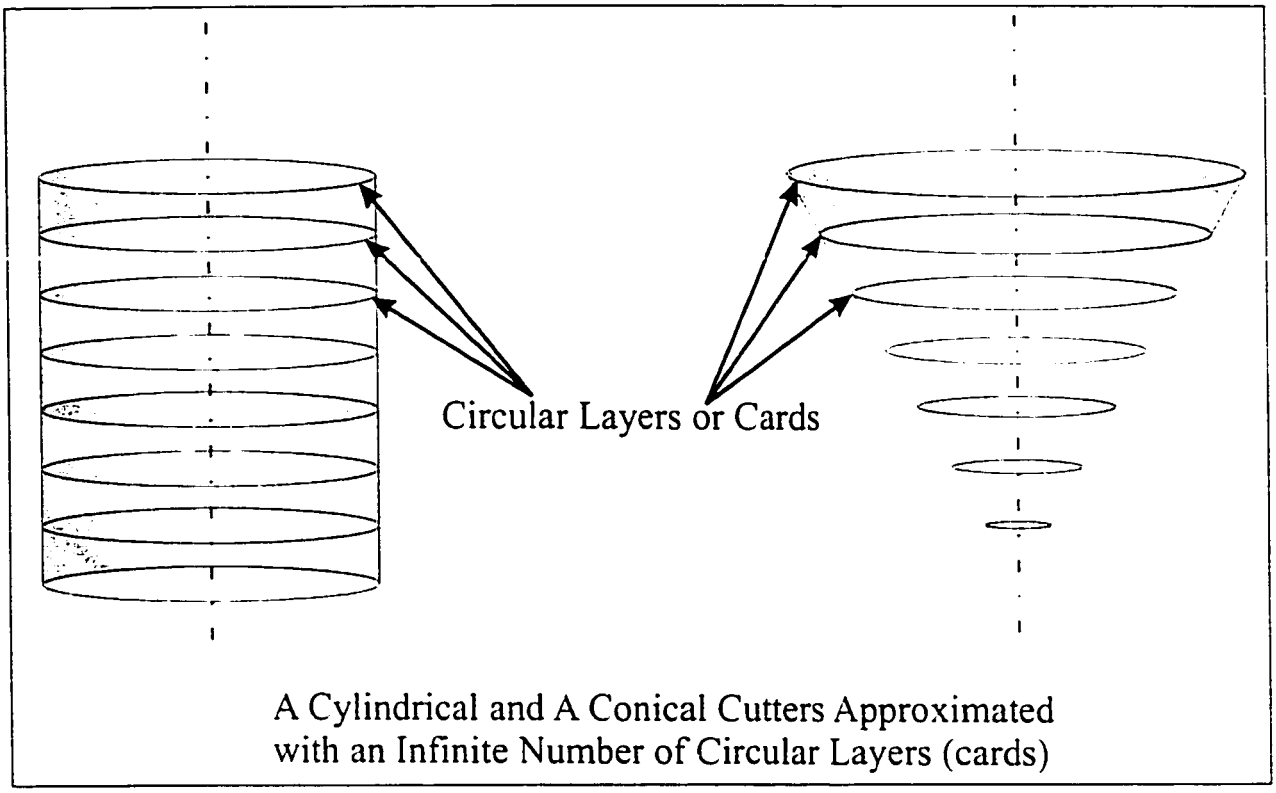


Figure 5.11: Approximating Conical and Cylindrical Cutters with an Infinite Number of Circular Layers

5.4.4 Equations of the Generating Curves of the General APT Tool

Similar to the cylindrical and conical tools above, the general APT tool can be best thought of as composed of infinite number of circular cards with different radii centered around the tool axis and lie in planes perpendicular to the tool axis. The tool is composed of two conical parts and a toroidal part as described earlier in equation 5.1.

To obtain the imprint of the tool on the surface, the equation of tangents be-

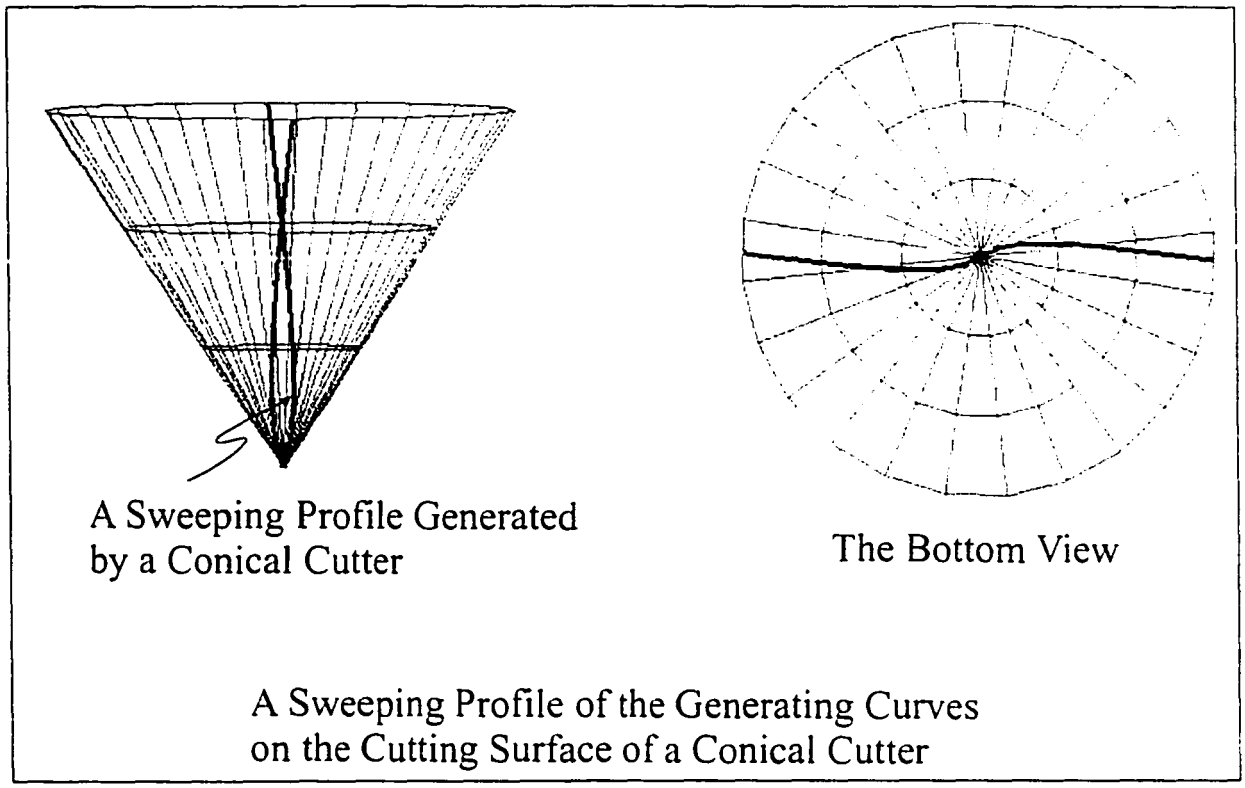


Figure 5.12: A Sweeping Profile of the Generating Curves of a Conical cutter in a Five-Axis Tool Motion ($\Delta x = 5\ mm$, $\Delta y = 10\ mm$, $\Delta z = 10\ mm$, $\Delta A = 3°$ and $\Delta C = 3°$)

tween every two corresponding cards, based on their Z location has to be determined as illustrated in figure 5.14.

The technique of finding the tangency points between a pair of corresponding cards is the same technique used with the torus calculations. The only difference is the method of identifying the corresponding cards, which is determined by vector $H_{i,j}$ shown in figure 5.14 in this case. Note that i corresponds to the tool position number and j corresponds to the cards number. As shown in figure 5.14, vector

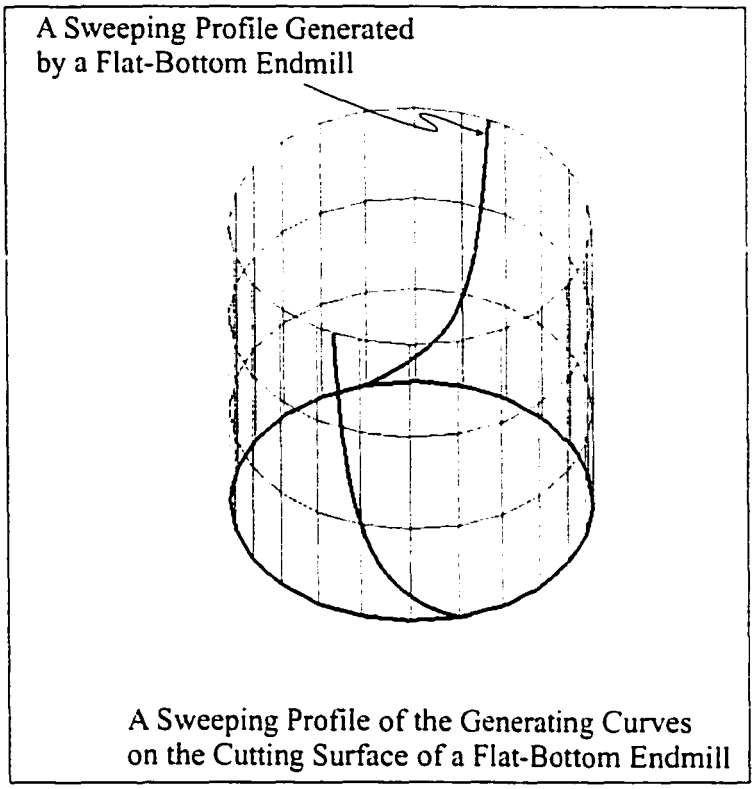


Figure 5.13: A Sweeping Profile of the Generating Curves of a Cylindrical cutter in a Five-Axis Tool Motion ($\Delta x = 5\ mm$, $\Delta y = 10\ mm$, $\Delta z = 10\ mm$, $\Delta A = 3°$ and $\Delta C = 3°$)

$L_{i,j}$ is the vector that determines where the tool touches the surface. To find the direction of this vector for a pair of corresponding cards, we have to find a vector perpendicular to $\Delta C_{i,j}$ and at the same time lies in the plane of the card. The centers of the two cards $C_{i,j}$ and $C_{i+1,j}$ are joined with vector $\Delta C_{i,j}$, which determines the movement of the cards from one tool position to another. Once $\Delta C_{i,j}$ is determined, finding a contact point can be achieved by taking a cross product between vector $\Delta C_{i,j}$ and the normal of the card, $N_{i,j}$ which is parallel to the tool axis. The cross product is then normalized and multiplied by the radius

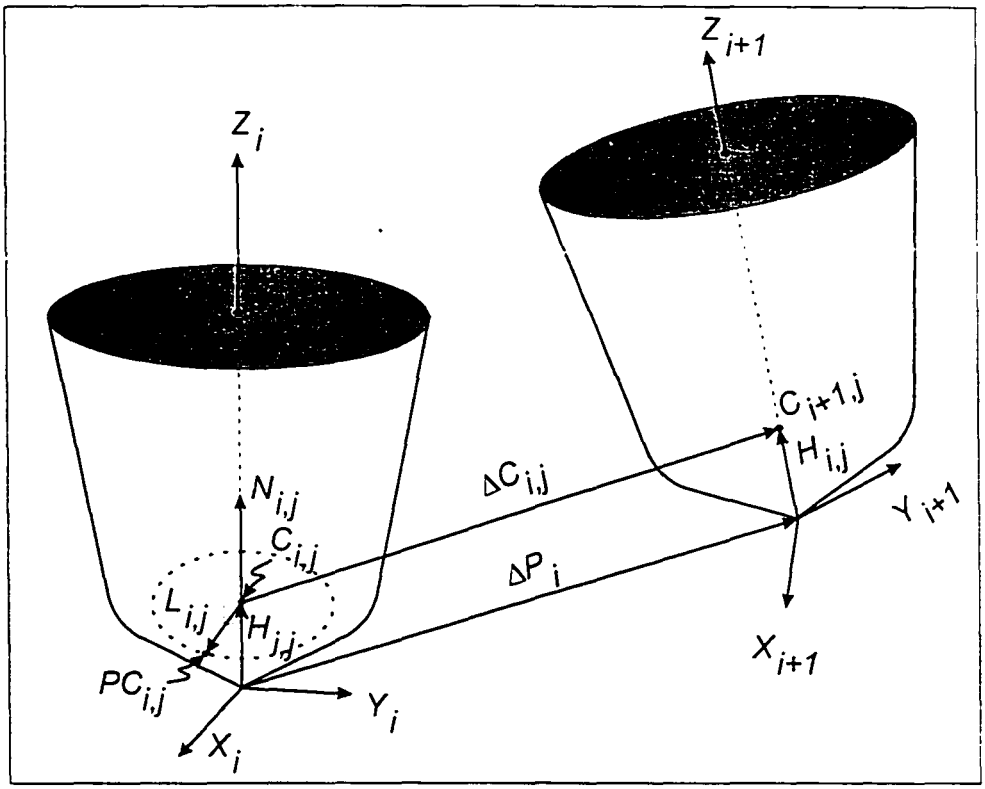


Figure 5.14: Two Consecutive Tool Positions in Five-Axis Movement

of the card to obtain the contact point.

The centers of the corresponding inserts are expressed as follows:

$$C_{i,j} = H_{i,j}\vec{k}_i \tag{5.12}$$

$$C_{i+1,j} = \Delta P_i + H_{i,j}\vec{k}_{i+1} \tag{5.13}$$

Vector $\Delta C_{i,j}$ can be defined as

$$\Delta C_{i,j} = C_{i+1,j} - C_{i,j} \tag{5.14}$$

The direction of the vector $L_{i,j}$ is then calculated by

$$D = \Delta C_{i,j} \times N_{i,j} \tag{5.15}$$

The resultant vector is then normalized and multiplied by radius of the card at the j^{th} point to determine the j^{th} point of contact at the i^{th} tool position.

$$L_{i,j} = \frac{D}{|D|}(R_{card}) \tag{5.16}$$

where

R_{card} is the radius of the card at the j^{th} point on the Z_i axis and is not constant. The equation of the generating curves is then defined in the global frame as

$$\sum_{i=1}^{n}\sum_{j=1}^{m}(C_{i,j})_{global} + (L_{i,j})_{global} \tag{5.17}$$

where

n is the number of tool positions, and,

m is the number of cards.

The generating curve, which is constructed by joining the tangency points, is shown in a five-axis motion in figure 5.15 ($\Delta x = 5\ mm$, $\Delta y = 10\ mm$, $\Delta z = 10\ mm$, $\Delta A = 3°$ and $\Delta C = 3°$). The tool dimensions as illustrated in figure 5.4 are $m = 28.32\ mm$, $n = 7.27\ mm$, $a = 10\ mm$, $b = 72.25\ mm$, $R = 24.35\ mm$ and $r = 5\ mm$.

As expected, the generating curves turned out to be curved lines in the conical portions not straight lines due to turning and twisting nature in general five-axis motions. The generating curves consist of three parts:

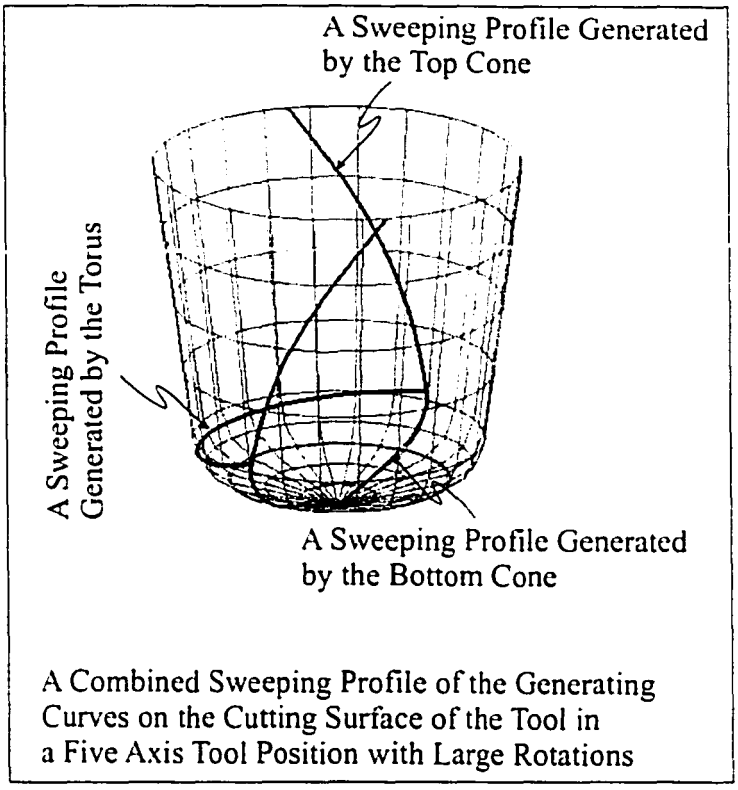


Figure 5.15: A Sweeping Profile of the Generating Curves of the General APT Tool in a Five-Axis Tool Position ($\Delta x = 5\ mm$, $\Delta y = 10\ mm$, $\Delta z = 10\ mm$, $\Delta A = 3°$ and $\Delta C = 3°$)

1. A portion generated by the bottom cone,
2. A portion generated by the toroidal part, and,
3. A portion generated by the top cone.

If the angle of feed direction vector ΔP_i, measured from the local $X_i - Y_i$ plane, is greater than θ_{start} and less than the angle θ_{end}, as shown in figure 5.16, the toroidal part replaces the bottom cone contribution to the cut as if the bottom cone does not exist. Figure 5.17 shows the sweeping profile on the tool of this special case

in a three-axis motion ($\Delta x = 2\ mm$, $\Delta y = 10\ mm$ and $\Delta z = 1\ mm$). The tool dimensions are the same as those in figure 5.15. To simplify the visualization of this particular movement in five-axis motion, a sequence of four points in a five-axis tool path of a sphere is simulated as shown in figure 5.18. The tool dimensions as illustrated in figure 5.4 are $m = 15\ mm$, $n = 3\ mm$, $a = 5\ mm$, $b = 25\ mm$, $R = 12\ mm$ and $r = 5\ mm$.

As can be clearly seen in figure 5.18, the toroidal portion dominated the bottom conical portion and the swept volume was generated only by the toroidal and top conical portions.

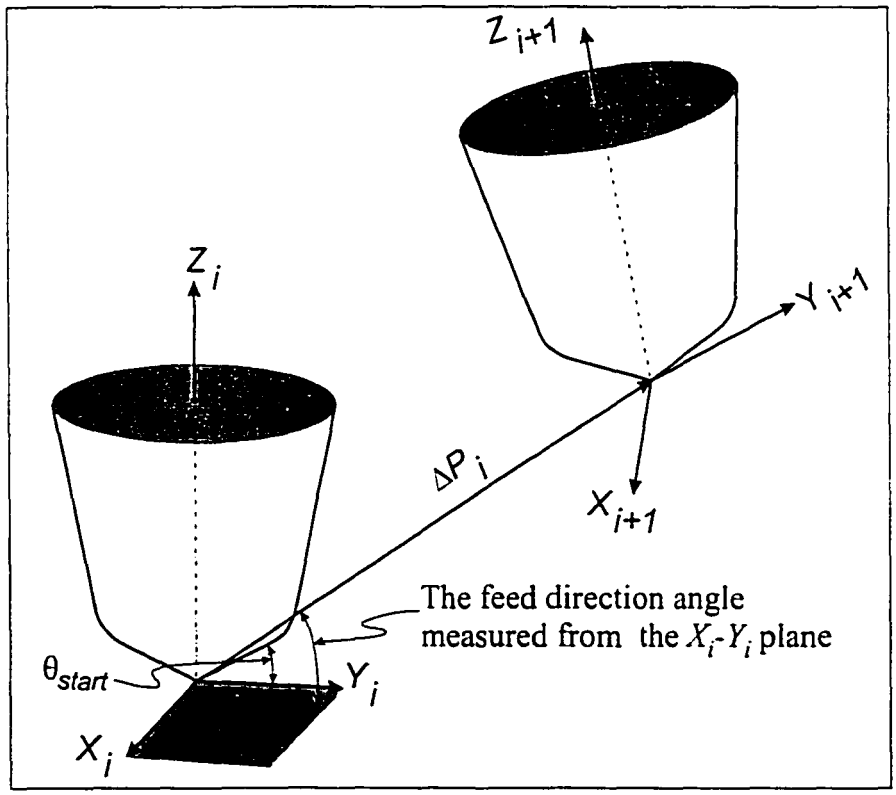


Figure 5.16: A Five-Axis movement with the Feed Direction angle $> \theta_{start}$

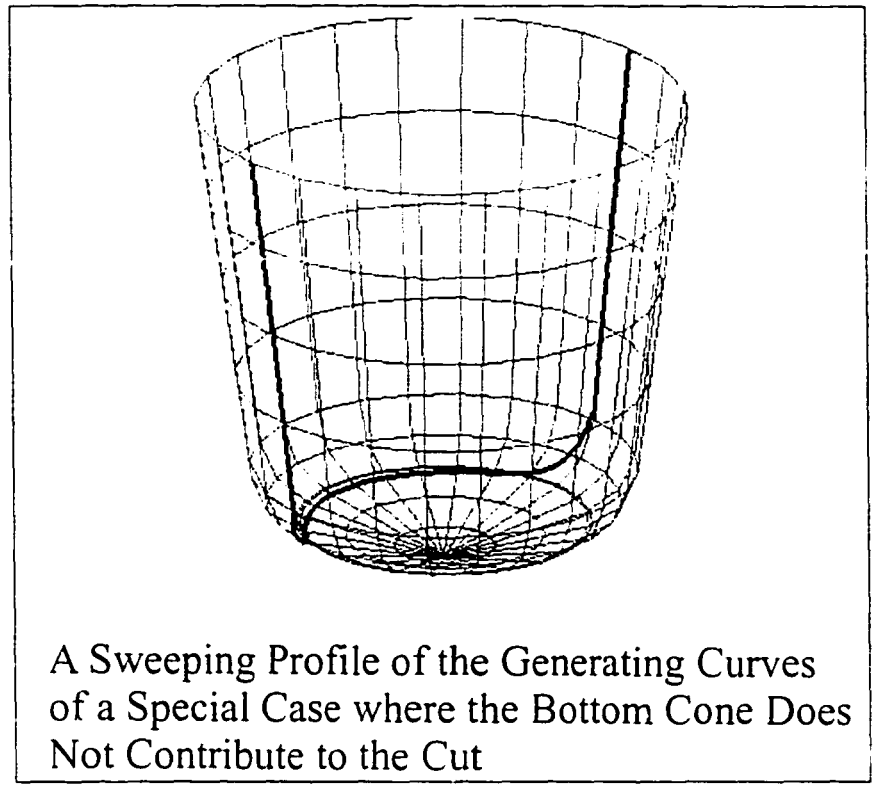


Figure 5.17: The Sweeping Profile of the Generating Curves when the Feed Direction Angle is Greater than θ_{start} in Three-Axis Motion

Having explained the generating curves technique, the numerical and experimental verifications for toroidal cutters are presented next.

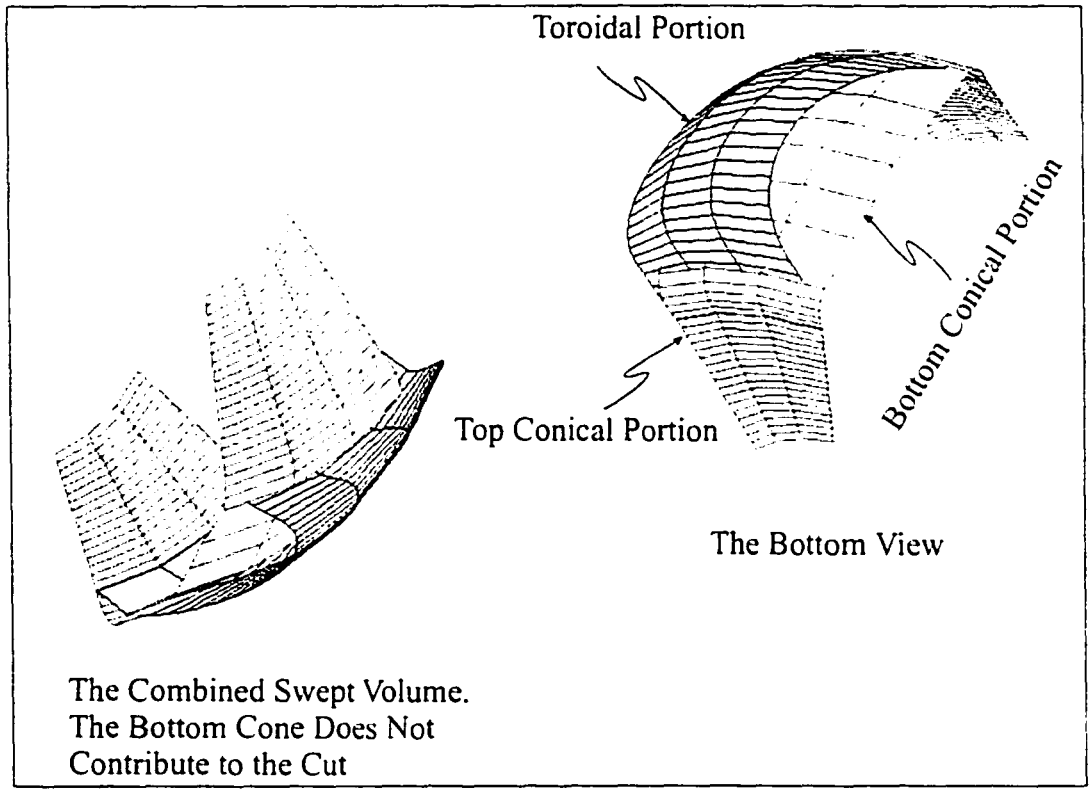


Figure 5.18: A Swept Volume of Four Subsequent Tool Positions When the Feed Direction Angle is Greater than θ_{start}

Chapter 6

Numerical and Experimental Verifications for Generating Curves

The generating curves technique was verified experimentally with the two machined surfaces shown in figures 6.1 and 6.2: a turbine blade surface and another test surface.

The G-codes of the two pieces are simulated using the SVS program and simulation results are compared with the scanned results of the corresponding machined surfaces. The comparison is conducted at different fixed values of the X-axis, along the Y-axis in terms of Z-coordinate. The results are also checked with the simulation results from the Z-map method.

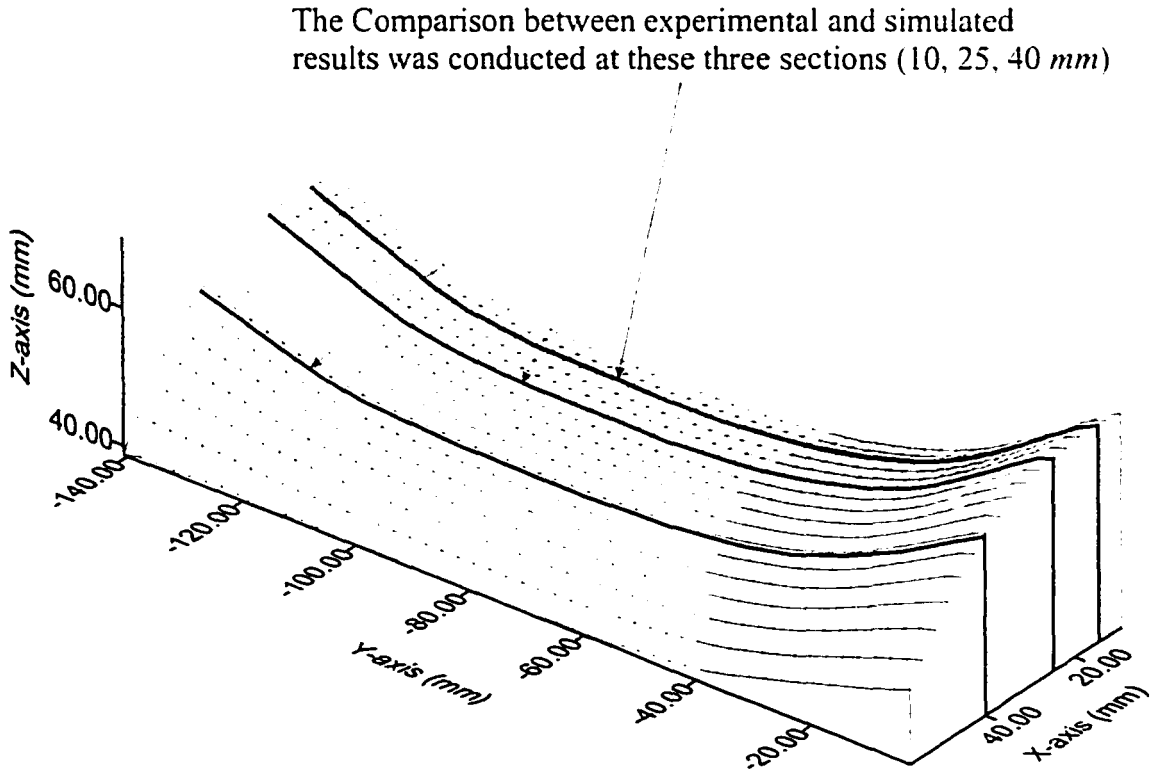


Figure 6.1: The Concave Turbine Blade Surface. Test Surface 1

The Comparison between experimental and simulated results was conducted at these three sections (20, 50, 80 *mm*)

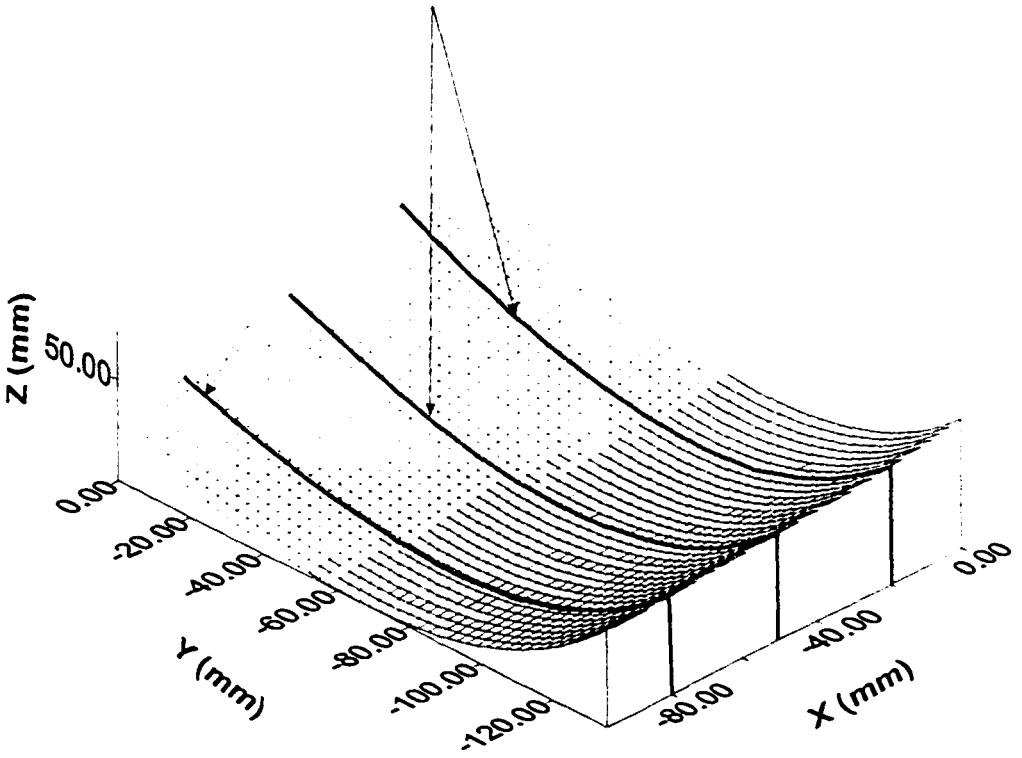


Figure 6.2: Test Surface 2

6.1 Experimental Verifications

The turbine blade surface shown in figure 6.1 was machined by Rao [33] using the Rambaudi CNC machine. The Rambaudi machine was originally a three-axis CNC machine but it was retrofitted to a five-axis machine by adding a tilt-rotary table. Figure 5.8 shows a schematic configuration of the machine. The test piece was fixed on the rotary table. The G-code of this turbine was constructed by combining consecutive tool passes parallel to X-axis. The feed direction in this cut was parallel to the X-axis and the cross feed was 5 mm. The cutting conditions used were: spindle speed $N = 1000$ rpm and feed 200 mm/min.

Rambaudi has been used to machine numerous test surfaces and the typical surface deviation obtained was between $\pm$10-15 μm. The turbine blade surface was scanned using the CMM and the scanned data was compared with the simulation results from the SVS program at three sections parallel to the Y-axis at $X = 10$, 25, 40 mm. The comparison results in all three sections were similar. One of these sections is shown in figure 6.3. The scanning with the CMM was performed with a 2 mm diameter probe and the probe moved vertically across the turbine blade surface. The experimental and simulated results are not expected to have an exact match due to experimental setup errors. The maximum surface deviation in this cut was 15 μm. The high frequency that appears in figure 6.3 could be mainly attributed to the fine step of 0.05 mm used in scanning the turbine blade. The reason behind using this high resolution is to capture the maximum number of points on the surface. The surface deviation in figure 6.3 tends to change from positive to negative. To understand this behavior, the first thing that comes in mind is comparing the frequency of the surface deviation with the tool path cross feed and

try to relate them together. Conversely, the frequency of the surface deviation was about 6.5 mm which is not anywhere close to the tool path cross feed of 5 mm. The surface deviation errors could be attributed to a number of reasons. Firstly, probe of the CMM was scanning the test surface vertically not normal the surface. Secondly, the CMM probe was measuring the center of the spherical probe tip and using an inbuilt offsetting strategy to digitize the surface. This strategy is prone to errors as discussed by Warkentin ??. Thirdly, they could be attributed to errors in locating the exact sections that was used in machining simulations the part in the CNC machine. Finally, they could be also attributed to numerical errors, the accuracy of the Rambaudi CNC machine and experimental setup errors.

The second test surface shown in figure 6.2 is an open form surface typically found in the die industry. The parametric equation of this surface is as follows:

$$S(u,v) = \begin{pmatrix} x \\ y \\ z \\ \end{pmatrix} = \begin{bmatrix} -99.4 + 88.9v + 5.6v^2 \\ -131.3u + 28.1u^2 \\ 5.9(u^2v^2 + u^2v) - 3.9v^2u + 76.2u^2 \\ +6.7v^2 - 27.3uv - 50.8u + 25v + 12.1 \end{bmatrix} \tag{6.1}$$

The surface was machined using the five-axis inclined tool method[1]. The feed direction was parallel to the Y-axis and the cross feed was 3.5 mm. This surface was also machine using the Rambaudi machine, at McMaster University. The toroidal cutter used had 3 carbide inserts and its dimensions were: $R = 12.7$ mm and $r = 6.35$ mm. The cutting conditions used were: spindle speed $N = 1200$ rpm and feed

[1]The inclined tool method is explained in chapter 7.

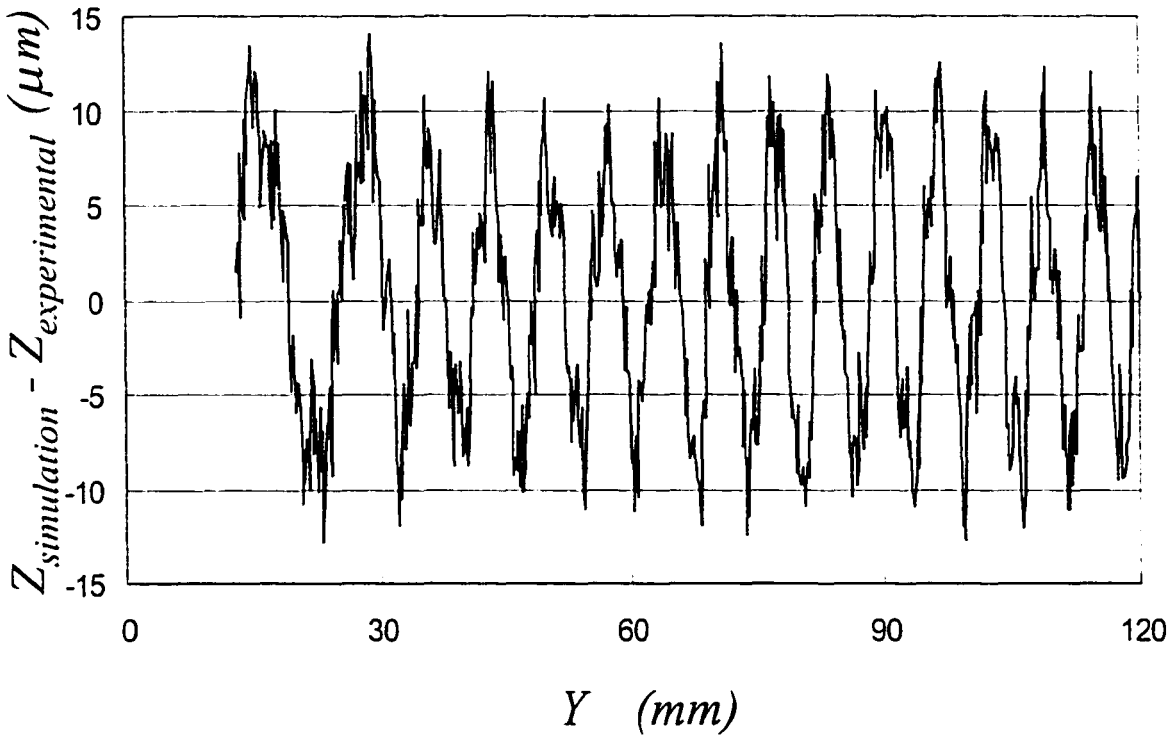


Figure 6.3: The Difference Between Scanned and Simulated Results for the Turbine Blade at $X = 10$ mm and Parallel to Y Axis

150 mm/min.

The second test surface was also scanned using the CMM and the scanned results were compared with the simulation results of the SVS program at three sections parallel to the Y-axis at $X = 20, 50, 80$ mm. Again, the comparison results in all three sections were similar. One of these sections is shown in figure 6.4.

With the exception of one point, the maximum surface deviation was 12 μm. As in the turbine blade, the high frequency that appears in figure 6.4 is mainly attributed to the fine step of 0.05 mm used in scanning the second test part. The frequency of the surface deviation was 12 mm, therefore, the change in surface deviation from positive to negative could not be attributed to the tool path cross feed. Like in the previous cut, the change in surface deviation could be attributed to errors in the measurements using the CMM, numerical errors, the accuracy of the Rambaudi CNC machine and experimental setup errors.

6.2 Numerical Verifications

Both surfaces were tested numerically against the Z-map method. The comparison was conducted at the same sections as those used in the experimental verification.

The grass density was 100 per mm, and the distance between the subsequent tool positions was 1.00 mm. Figures 6.5 and 6.6 show that both methods are in agreement within 3 μm.

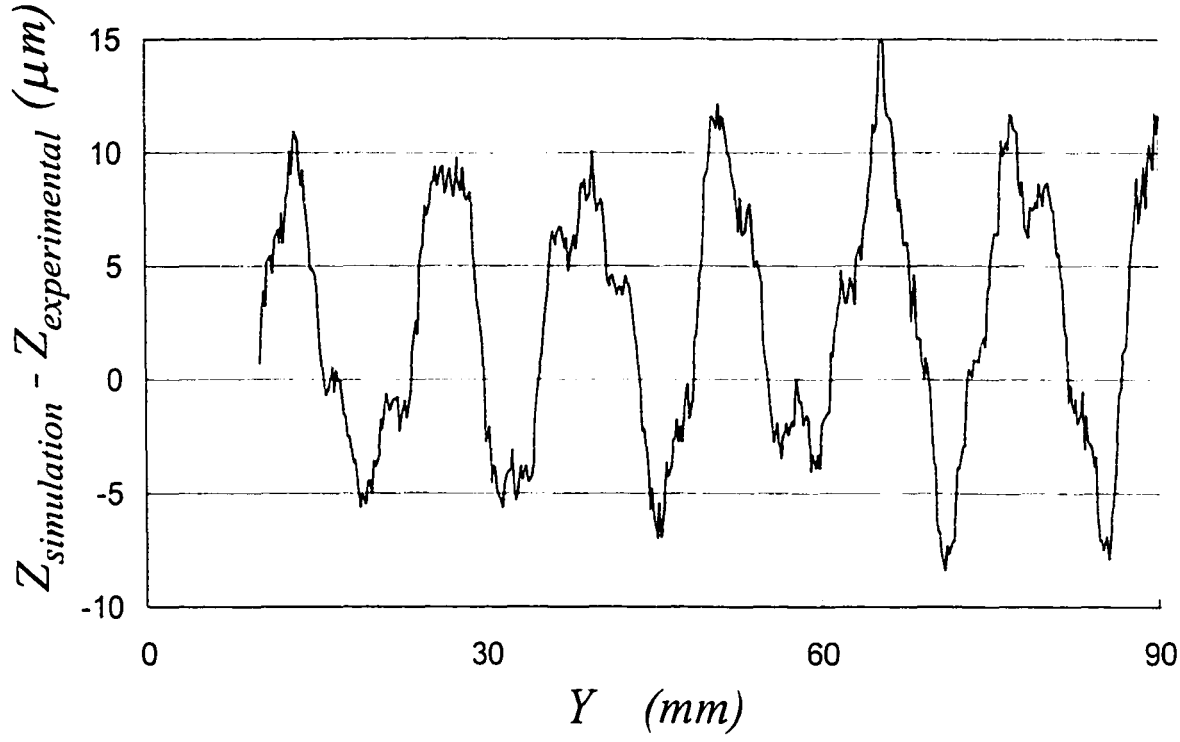


Figure 6.4: The Difference Between Scanned and Simulated Results for the Test Surface at $X = 50$ mm and parallel to Y Axis

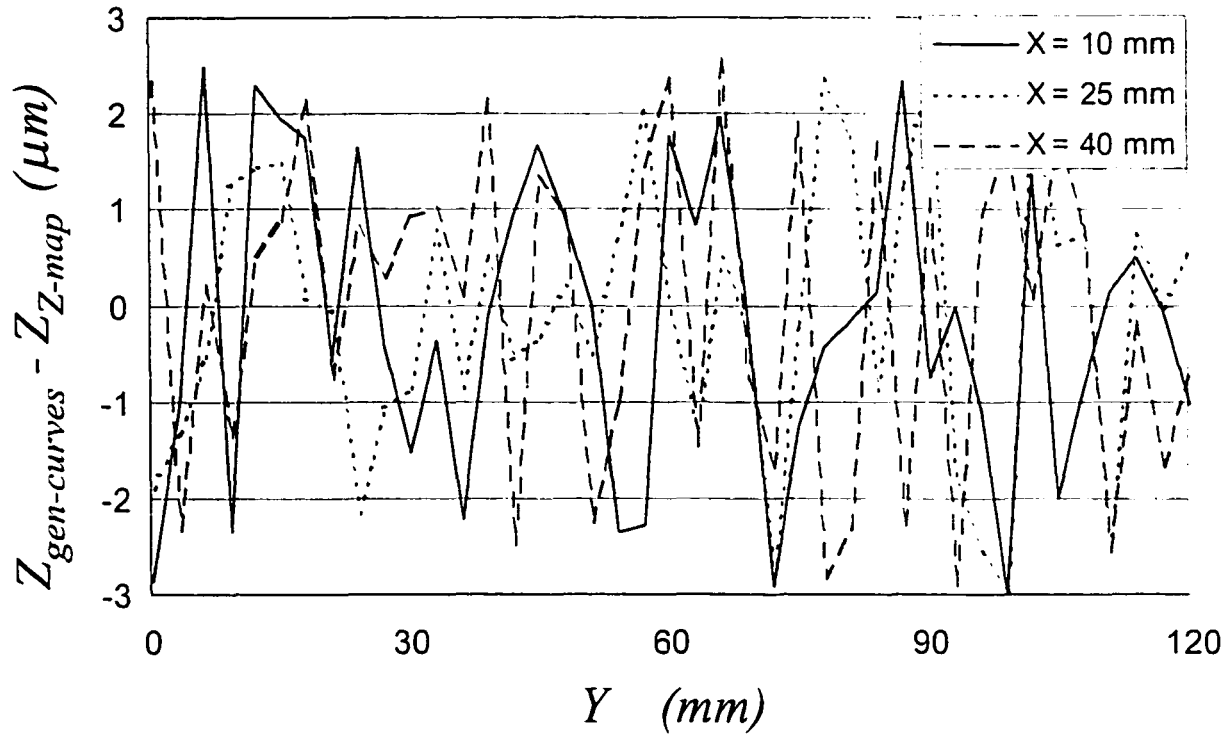


Figure 6.5: Comparison Between the "Generating Curves" and Z-map Techniques for The Turbine Blade at Three Sections

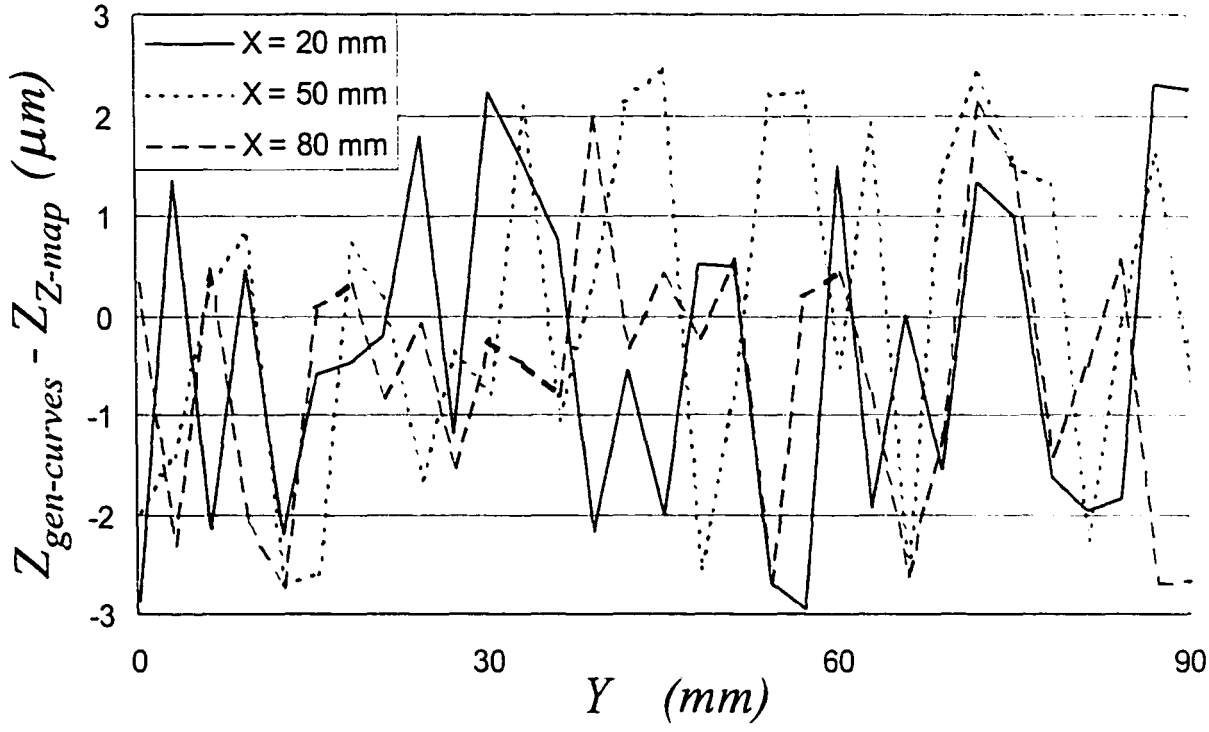


Figure 6.6: Comparison Between the "Generating Curves" and Z-map Techniques for The Test Surface at Three Sections

The simulation time of the turbine blade was about 5 minutes in the SVS program and about 3 hours in the implemented Z-map program for the whole surface. The second test surface took about 4 minutes in the SVS program and about 2.5 hours in the implemented Z-map program. Programming was done in C++ and computations were performed on a Pentium 300 MHz PC.

As explained in chapter 2, the Z-map method is based on placing the tool over the workpiece at all tool positions and then intersecting the tool with rays fired normal to the surface. If the step size between the subsequent tool positions is not small, it will result in a poor surface representation because the Z-map method has no sweeping effects, see figure 6.7. On the other hand, in the generating curves method, corresponding points on the generating curves are joined with straight lines, which leads to a more accurate surface representation as shown in figure 6.7.

The numerical and experimental results indeed verify the generating curves technique as an accurate method to simulate five-axis motion. Also, the new technique is significantly faster than the Z-map method.

The accuracy and the speed of the new technique are exploited in slicing the simulated swept volume into a number of parallel sections. These sections are then utilized in gouge detection and avoidance as explained in the next chapter.

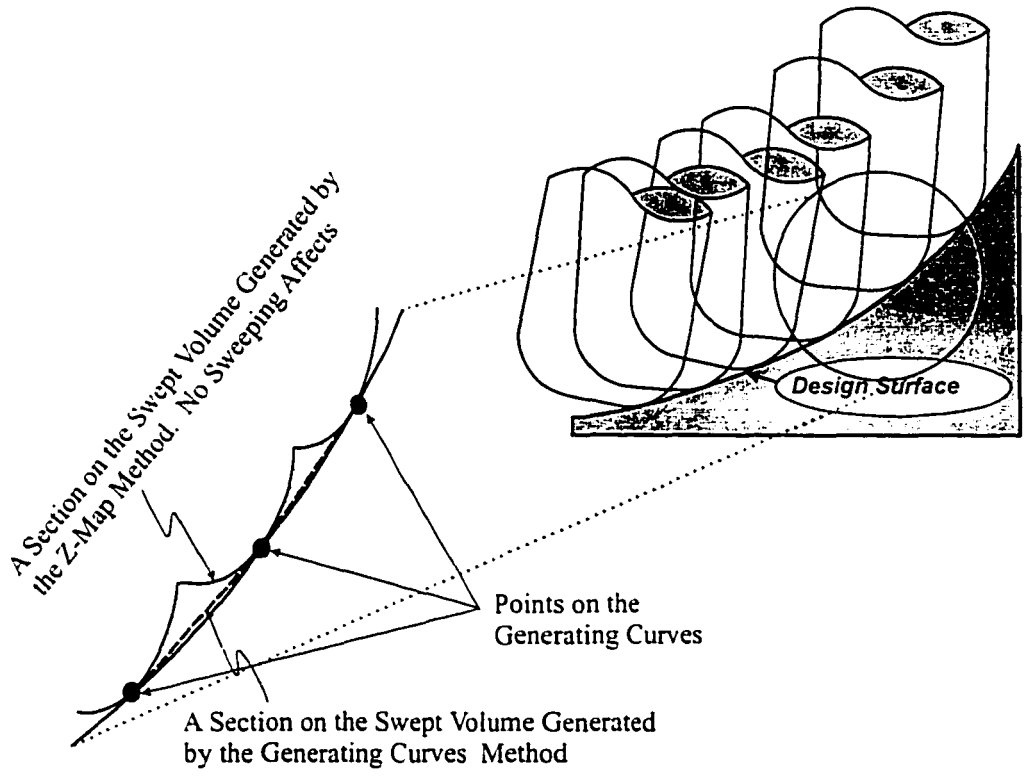


Figure 6.7: Comparison Between Swept Volume Representation in Generating Curves and Z-map Methods

Chapter 7

Gouge Checking and Avoidance Methods

7.1 Introduction

Five-axis CNC machining with toroidal cutters has many advantages over the traditional three-axis with ball-nosed endmills machining such as improved surface finish and faster material removal rate. Nonetheless, the gouging problem in five-axis is a major obstacle researchers are confronted with.

In this chapter a new gouge detection strategy is presented. The new gouge detection method utilizes the points on the generating curves and quickly detects gouging during the design stage of the tool path, as presented in section 7.2. This is followed by gouge correction, which is accomplished by tilting the tool further in the feed plane as explained in section 7.3.1. The new techniques were integrated with the SVS program and produced a new, fast and precise NC verification toolkit.

7.2 The Sectioning Gouge-Detection Method

In the generating curves technique, it is easy to digitize the simulated surface into a number of sections. A comparison is then conducted between the corresponding sections on the design surface to check for gouging and interference, within the desired tolerance, in one plane which reduces the complexity of the calculations, as shown in figure 7.1.

The creation of parallel sections is achieved by slicing the surface into a number of parallel sections, where gouging is going to be checked, and then substituting the x and y values of these sections in the generating curves equations to solve for angle ϕ_j, shown in figure 5.7, to find those particular cutting inserts that generate the surface at the comparison sections. In other words, there is no need actually to compute the whole generating curve; only the points corresponding to points in the checking sections as illustrated in figure 7.1.

After generating the contact points on the comparison sections for one tool movement, gouging is checked instantly for that particular movement. Gouge checking in this method can be accomplished as follows:

- If the equation of the surface is known, which is the case in this study, the x and y values of the contact points on the comparison sections are substituted in the surface equation and then gouging is checked based on the difference of the z values between the simulated contact points and the resulting points from the surface equation.

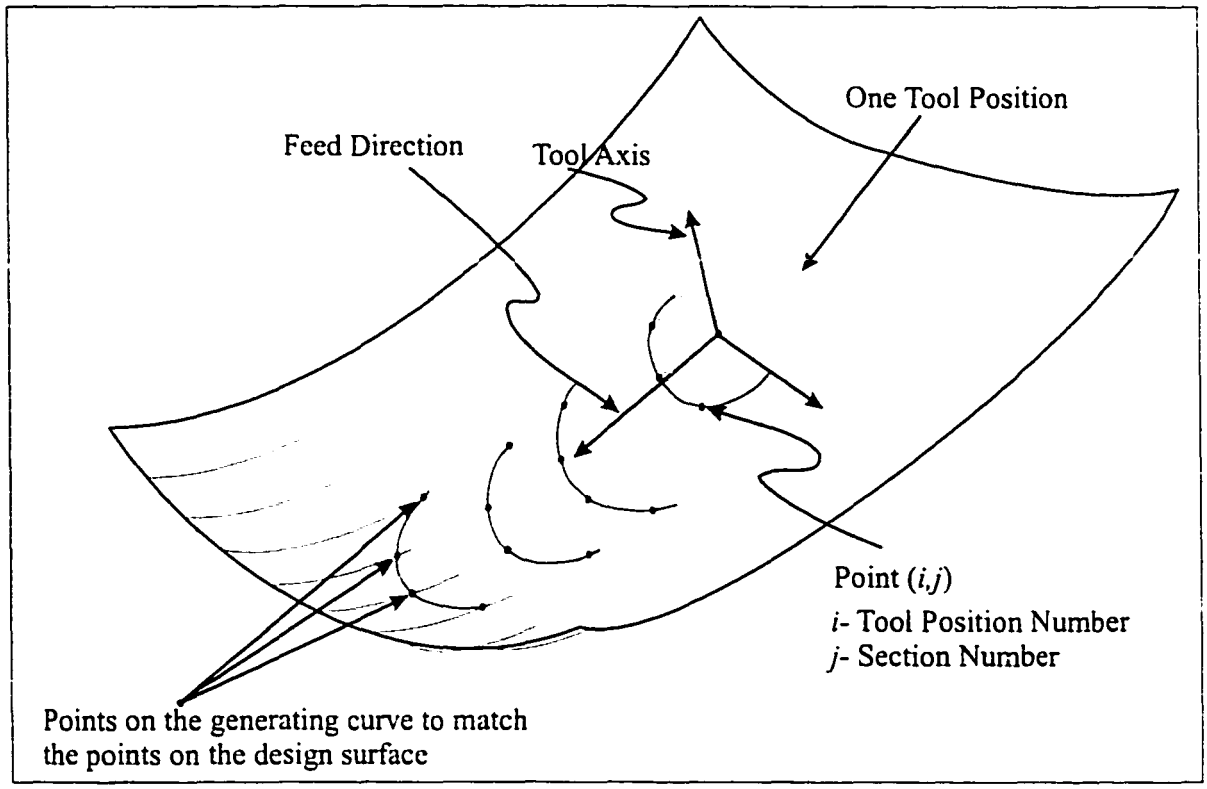


Figure 7.1: Matching the Generating Curves Sections with the Corresponding Sections on the Surface

- If the equation of the surface is not known and only points on the surface are given, regression analysis has to be conducted to generate planar equations at the desired comparison sections to perform the z value check.

The same procedure of gouge checking is used with the back half of the tool after reversing the tool path: so the actual back of the tool will be the front in the reversed tool path.

In the literature, one of the traditional ways of detecting gouging is the triangularization of the surface. In the triangularization method, the whole surface is

simulated and triagularized then rays are fired, normal to the surface, to check for gouging and interference. If there is any gouging or interference; it is corrected and then the entire procedure is repeated. Although easy to implement, the computational time for this algorithm is considerably larger compared to the new method. Note that this procedure has to be repeated for both the front and the back of the tool, which makes it even more time consuming. Also, in the triangularizing of the surface method, using the Z-map as the swept volume tool, the so called inside/outside test is conducted to check for gouging. The inside/outside test is performed by firing rays normal to the surface and checking whether or not these rays lie inside or outside the torus. If they lie inside the torus, this means gouging has occurred and the tool position has to be corrected. In the industrial world, it is common that the equation of the surface is not known and only the CL data or G-code is available as a description of the surface. In addition to the long time required by the Z-map to simulate the contact between the tool and surface, the triangularization of the surface method poses a major difficulty in determining the direction of the surface normal and consequently the source and direction of the fired rays as shown in figure 7.2. Each point in the triangular facets is shared by at least two triangles and without the equation of the surface there is no way of determining the correct surface normal at each point. The assumption that surface normal is the same as the facet normal and then firing rays from the centers of the facets will result in losing some of the surface information since the center of the facet may not actually be a point on the design surface. While in the new gouge detection technique, the direction of the normal is not an issue.

The new method has another advantage over the popular triangularization of the surface method, that is the ability of detecting gouging at every position of

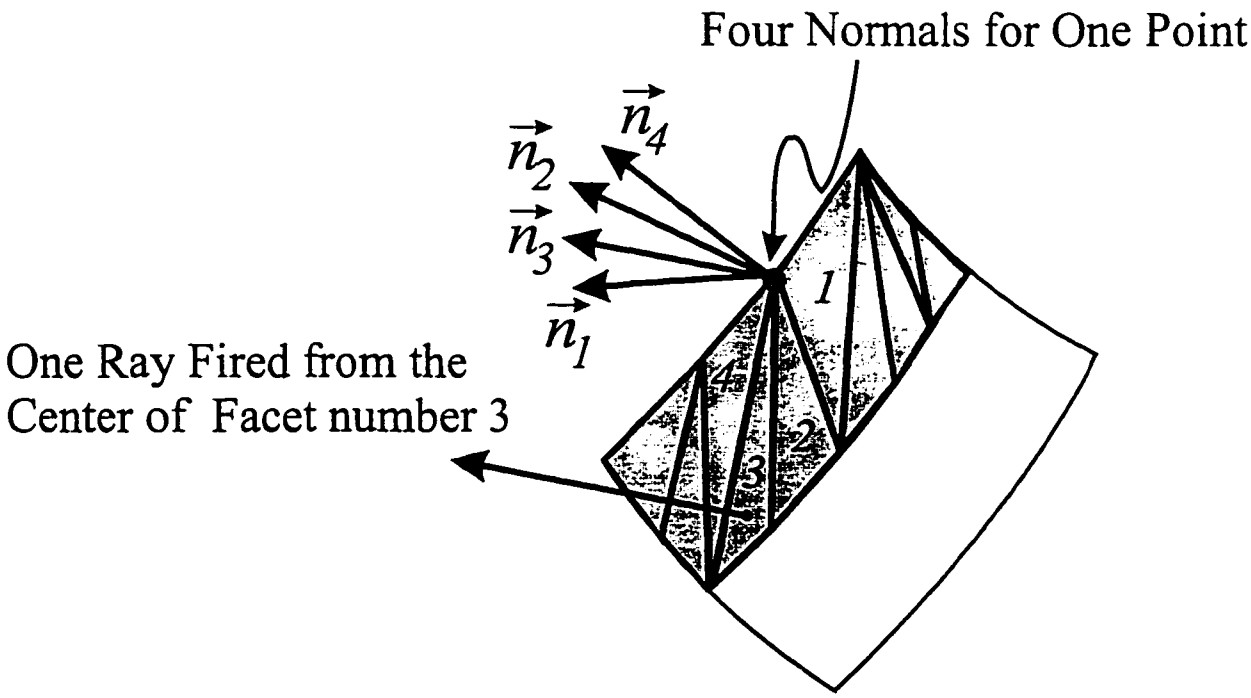


Figure 7.2: Difficulties in Identifying Surface Normals in the Triangularizaion Method

the tool path, before finishing the simulation of the swept volume for the whole surface. If gouging occurs, the positioning of the tool is corrected instantly. This procedure reduces the simulation time significantly and speeds up the tool path planning. The question now is, how many sections are enough to represent the surface? Based on the simulation results, for a good surface representation, the distance between sections can range from 1 *mm* to 3 *mm*. However, depending on the desired accuracy, the density can be increased. The more dense the sections are the more accurate the gouge-detection will be.

7.3 Gouge Elimination

Gouge avoidance in this study is conducted through the *Inclined Tool* method which is one of the most common positioning methods in five-axis. This inclined tool method has been implemented in many CAM tool kits because of its ability of producing tool paths with large cross feeds. The inclination angle however is chosen by the user and normally it remains constant throughout the entire path. It can lead to gouging. In the following section, a modified version of the inclined tool method is presented where gouging detected using the sectioning method is avoided.

7.3.1 Gouge Correction

The inclined tool positioning strategy, also known as Strutz milling, is one of the most appropriate benchmark for other five-axis machining methods. Positioning the toroidal cutter over the surface in this method is shown in figure 7.3. The tool

is inclined in the feed direction by an angle α, the Strutz angle. To calculate the tool position, the tool should be placed in tangential contact with surface at the contact point (CC).

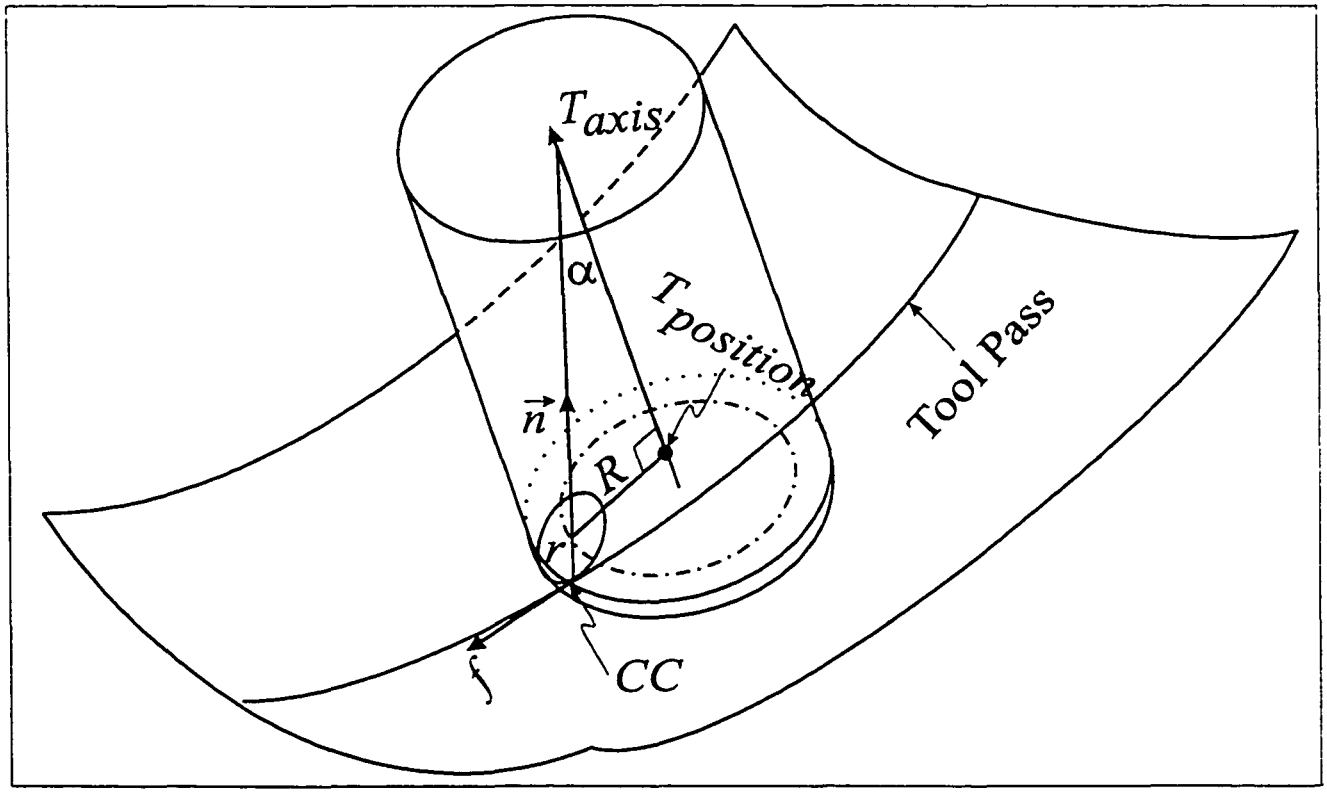


Figure 7.3: Positioning in the Inclined Tool Method

The tangential positioning of the tool can be achieved by dealing with a plane that contains the tool axis, T_{axis}, and feed direction, f, as shown in figure 7.4. A coordinate system is created in this plane at the center of the insert, C_{insert}. C_{insert} can be located as follows:

$$C_{insert} = CC + r\vec{n} \tag{7.1}$$

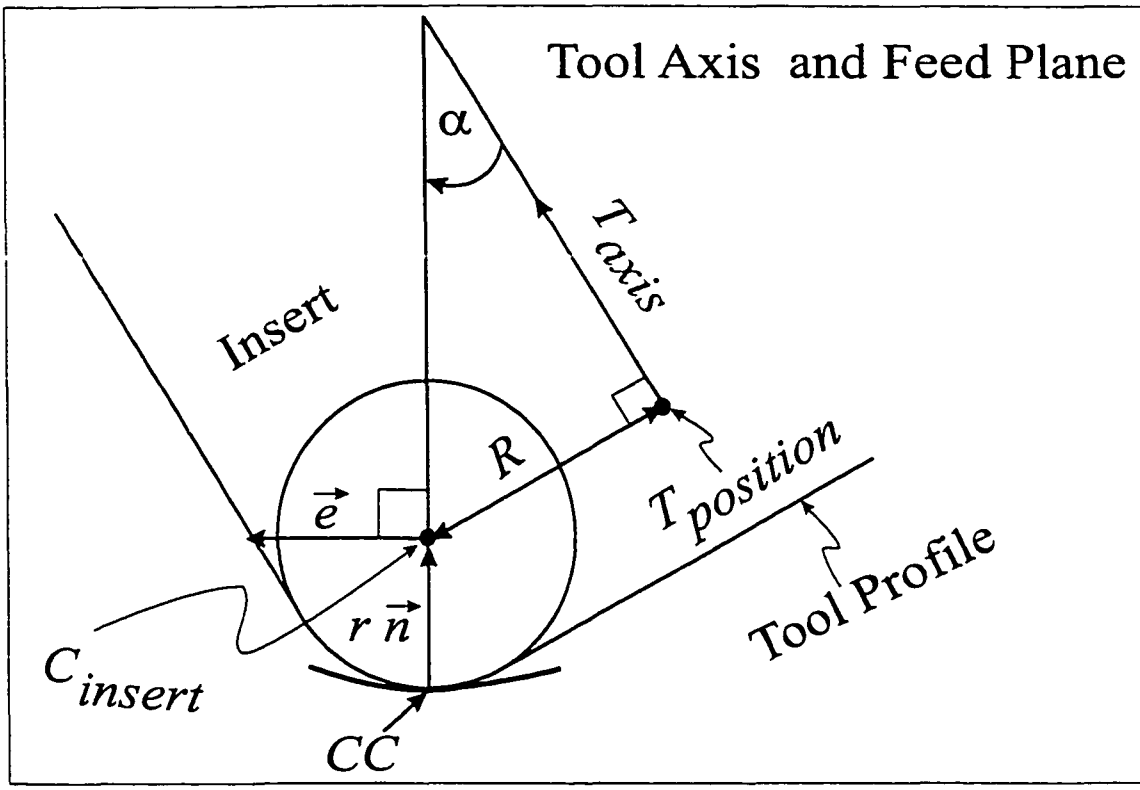


Figure 7.4: Tool Axis Plane for An Inclined Tool

where $\vec{n}$ is the surface normal at CC

To generate the local coordinate system in the tool axis plane, one of the axes should be the normal of the surface, $\vec{n}$. The other axis, $\vec{e}$, should be perpendicular to $\vec{n}$ and at the same time lie in the tool axis plane. $\vec{e}$ can be constructed by taking the following triple cross product:

$$\vec{e} = \vec{n} \times (\vec{n} \times \vec{f}) \tag{7.2}$$

The tool axis is then calculated as follows:

$$T_{axis} = \cos\alpha\vec{n} + \sin\alpha\vec{e} \tag{7.3}$$

The tool position is calculated from:

$$T_{position} = C_{insert} + R(\sin\alpha\vec{n} - \cos\alpha\vec{e}) \tag{7.4}$$

The above equations require the value of Strutz angle α. A fixed value of α is used throughout the whole tool path. A small value of α will generate gouging and a large value will result in large scallops. Therefore, the selection of α is a critical element in the Strutz method.

The gouge correction method is based on changing the orientation of the tool in a plane that contains the surface normal and the feed vector. The value of α is initially set to zero to allow maximum material removal from the surface. The SVS program is then used to produce the desired sections and the sectioning technique is then applied to check for gouging within the desired limits. If gouging occurs, the value of α is progressively increased until gouging is eliminated. Figure 7.5 is a flow chart for the algorithm. The major advantage of this new algorithm is the speed and the ability of detecting gouging instantly rather than having to wait until the whole surface has been simulated.

With the idea behind the new gouge detection and avoidance methods is now clear: the experimental and numerical verification are presented in the next chapter.

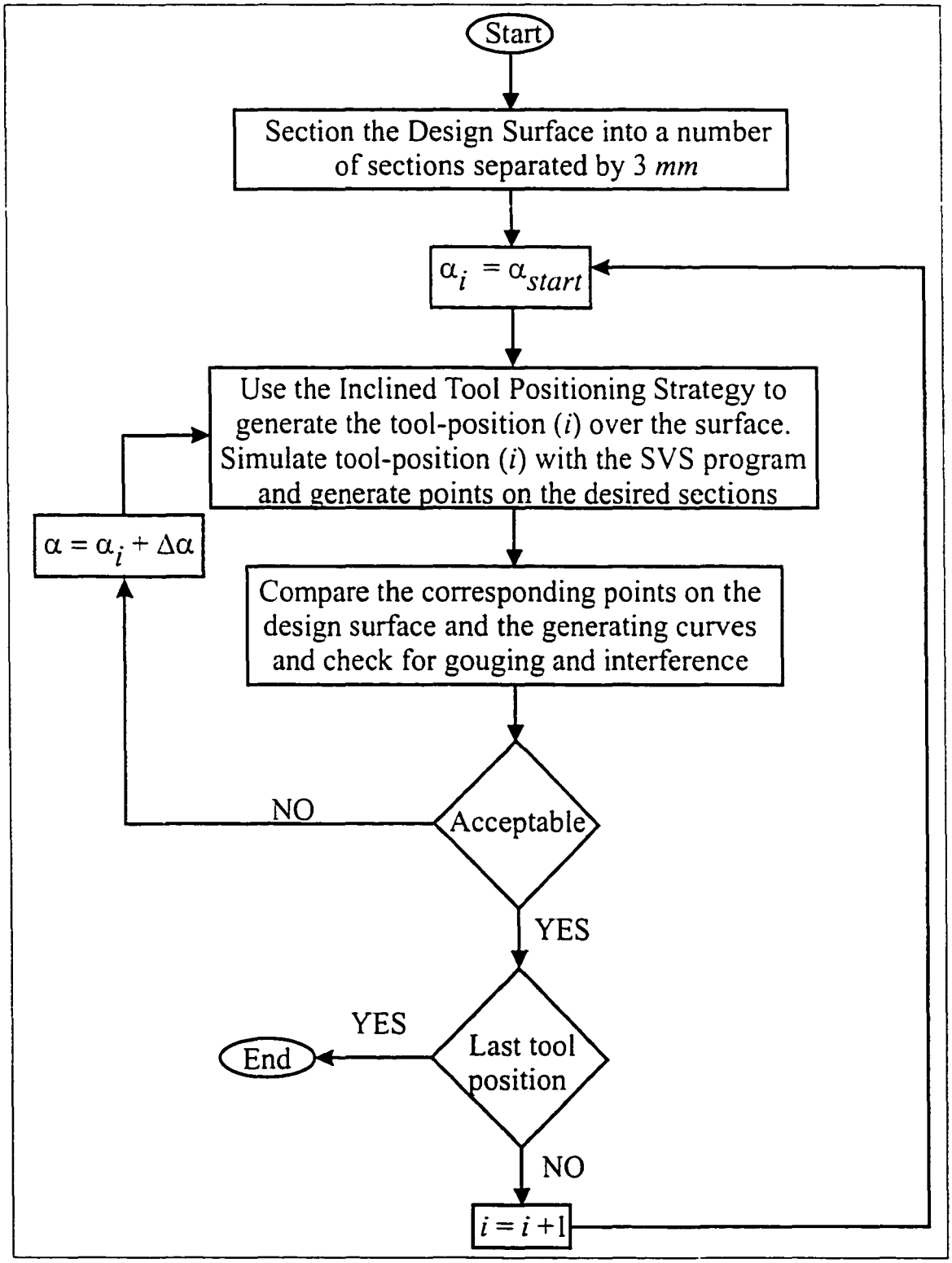


Figure 7.5: The Gouge Detection and Elimination Procedure

Chapter 8

Numerical and Experimental Verifications for Gouge Checking and Avoidance

The new gouge checking and avoidance method was verified experimentally by machining a surface in four different ways. The method used in the first three cuts was the inclined tool, with different angles and feed directions without the gouge avoidance technique involved. In the fourth cut, the surface was machined using the new gouge detection and avoidance technique.

The equation of the test surface used in this chapter is given by equation 6.1. The five-axis machine used in machining the experimental parts was the Fadal VMC 4020 with Tsudokoma Rotary-Tilt table at McMaster University. The toroidal cutter used had 3 carbide inserts and its dimensions were: $R = 12.7\ mm$ and $r = 6.35\ mm$. The cutting conditions used were: spindle speed $N = 1200\ rpm$ and feed rate

150 mm/min. The tool was programmed to machine only with its front using the inclined tool method. Based on that, gouging can be defined as the interference of the back of the tool. G-codes of the four cuts were simulated in the SVS program and checked against gouging.

In the first cut, figure 8.1, the test piece was machined with $\alpha = 3°$, the feed direction was parallel to the Y-axis and the cross feed was 3.5 mm. In this cut, the back of the tool gouged at the middle of the part as it was predicted by the SVS program. The gouging can be seen in figure 8.1 in the area marked (A). The surface simulated on SVS is shown in figure 8.2 with the gouging area drawn in red color.

In order to check the accuracy of the simulation relative to the machined parts, the machined surface was scanned in different sections, parallel to the Y-axis. The maximum amount of gouging was found to be 8 μm at different spots in the marked area in figure 8.1.

Scallop heights in this cut were also scanned (across the feed direction) and simulated in three sections in XZ plane at 20, 70, 110 mm as shown in figures 8.3, 8.4 and 8.5, and the largest scallop height was 67 μm.

The width of the simulated scallop heights is wider than the width of the scanned scallop at the upper part of the scallops. This is because the probe of the CMM approached the scallops vertically, not in the normal direction to the scallops. At the upper part of the scallops, the probe touched the surface by its sides (not by its bottom) which could generate errors. Also, due to experimental errors in

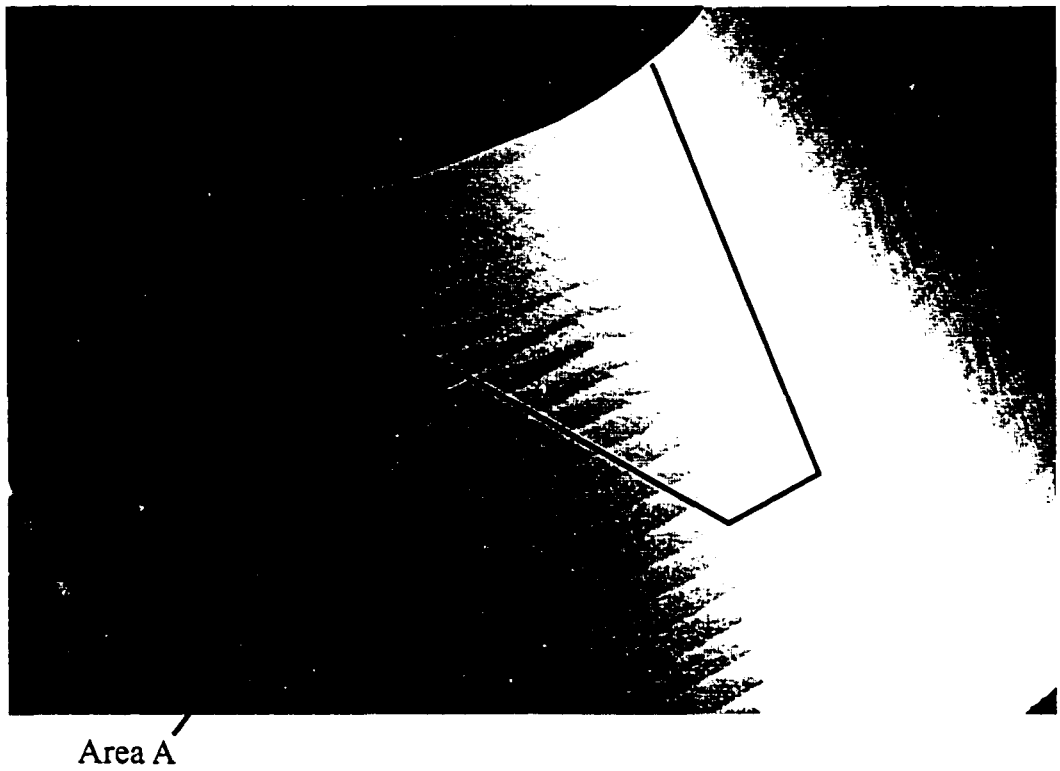


Figure 8.1: A Test Surface Machined with The Inclined Tool Method. $\alpha = 3°$

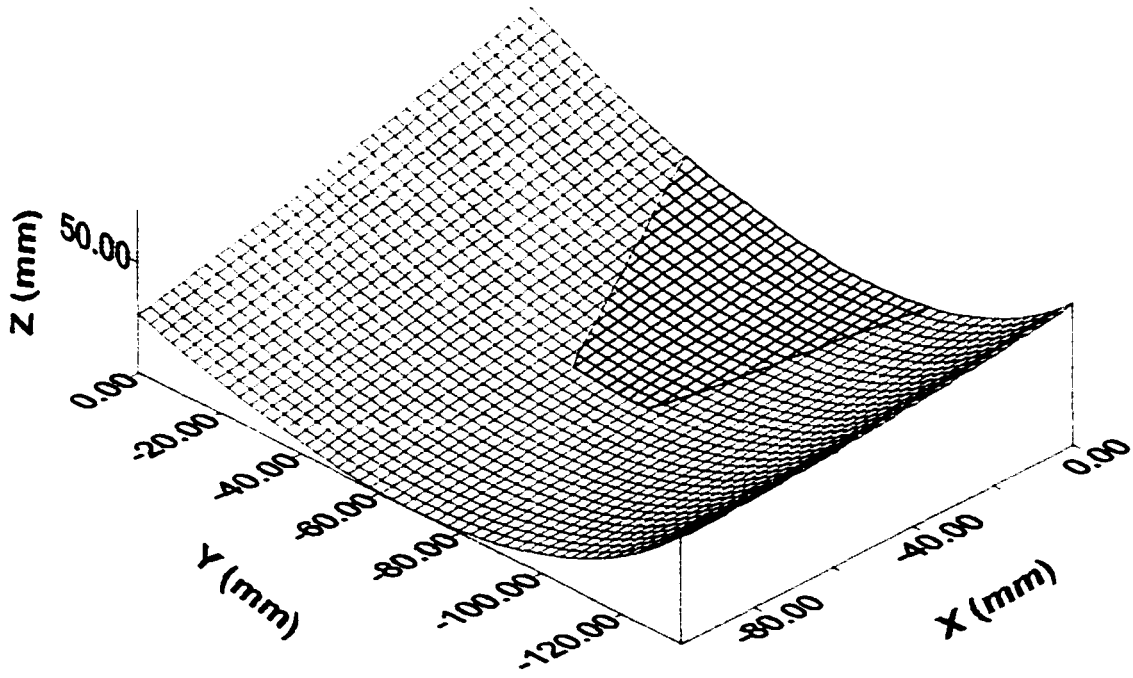


Figure 8.2: The Test Surface Simulated with $\alpha = 3°$

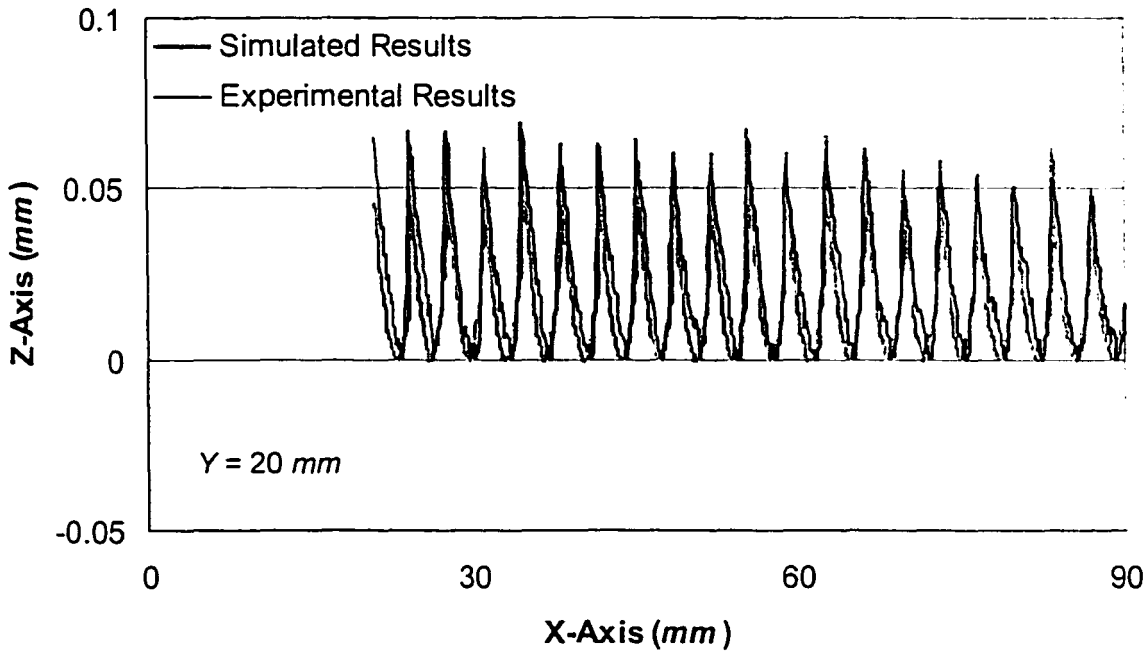


Figure 8.3: Comparison of Scanned and Simulated Results for Inclined Tool Method at $Y = 20\ mm$, $R = 12.7\ mm$, $r = 6.35\ mm$, cross feed $= 3.5\ mm$, $\alpha = 3°$

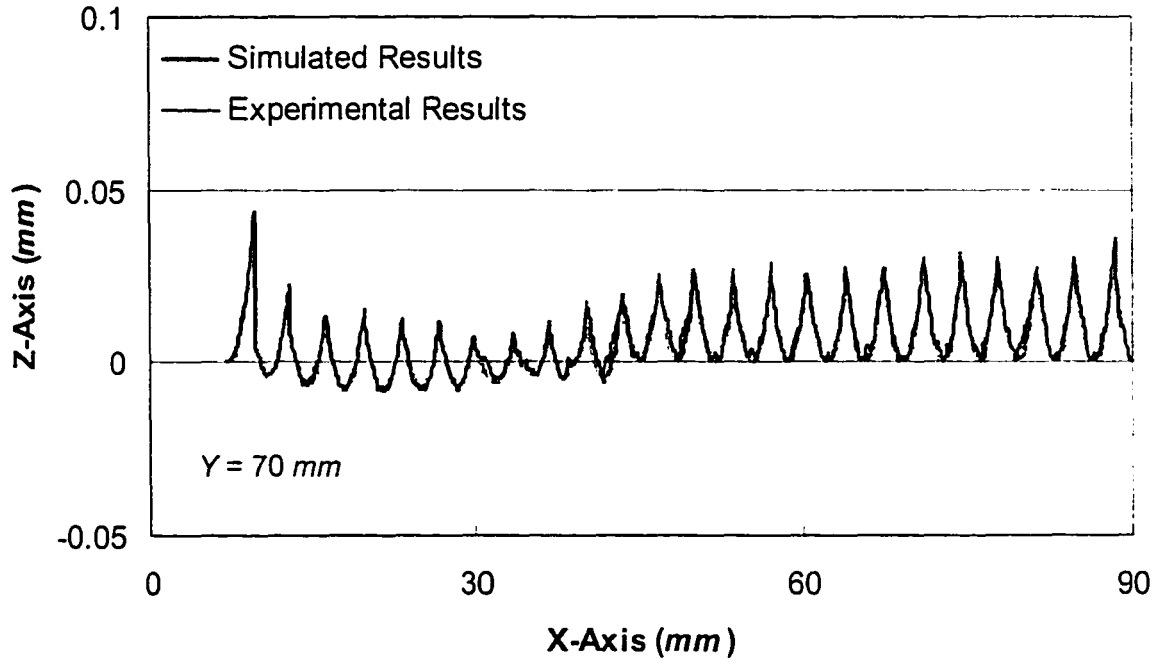


Figure 8.4: Comparison of Scanned and Simulated Results for Inclined Tool Method at $Y = 70\ mm$, $R = 12.7\ mm$, $r = 6.35\ mm$, cross feed $= 3.5\ mm$, $\alpha = 3°$

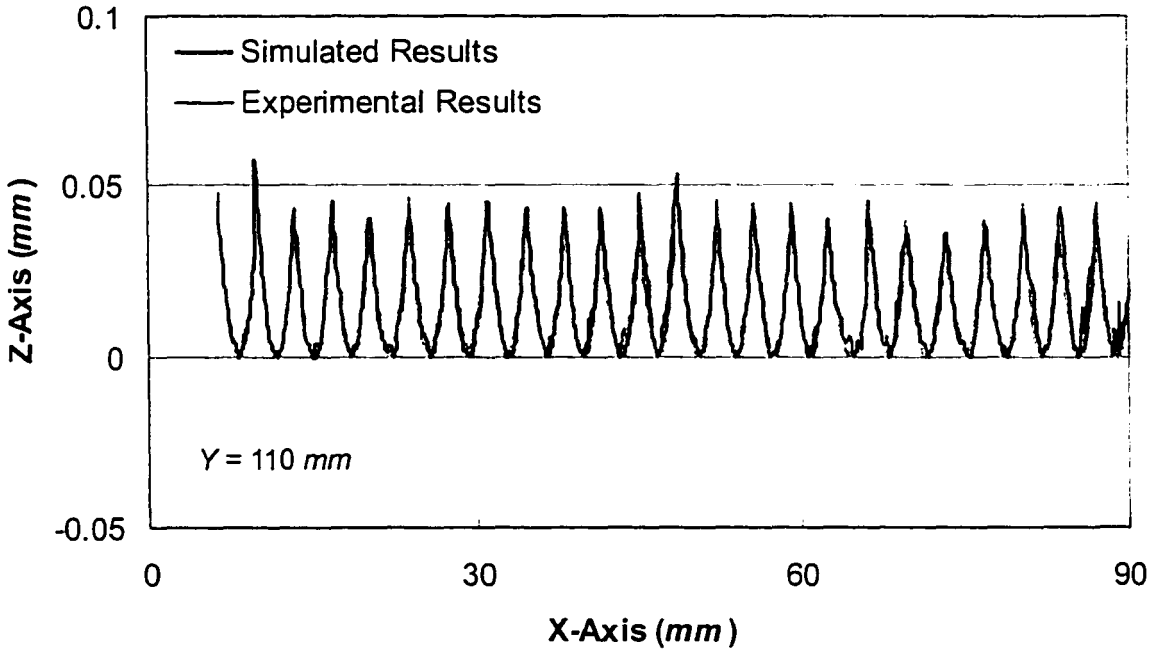


Figure 8.5: Comparison of Scanned and Simulated Results for Inclined Tool Method at $Y = 110\ mm$, $R = 12.7\ mm$, $r = 6.35\ mm$, cross feed $= 3.5\ mm$, $\alpha = 3°$

locating programmed coordinate system during workpiece setup, simulated and experimental results are not expected to match exactly. Errors in the shape of scallop can be also attributed to the CMM measurements. The machined surfaces were scanned at every 0.05 mm to capture the maximum number of points. However, the experimental data are still slightly jagged because of some missing points. Furthermore, the coordinate systems used in machining, and/or in measurements and in simulation may slightly vary.

The second cut, figure 8.6, is similar to the first cut with $\alpha = 6°$. No gouging was detected by SVS and the machined surface was in complete agreement with the simulation results.

Scallop heights were larger in this cut as shown in figures 8.7, 8.8 and 8.9. The large scallop heights in the previous two cuts are attributed to the feed direction in these cuts being parallel to the direction of maximum curvature of the surface. The scanned and simulated results tended to have a parabolic shape that varied across the surface. This variation is due to the changing curvature. Regions of the surface with high curvature had larger scallops than regions with lower curvature.

Warkentin et al. [50] machined the same surface using the inclined tool method with $\alpha = 6°$ and the feed direction was parallel to the direction of minimum curvature. The tool dimensions were $R = 5\ mm$, $r = 3\ mm$ and the cross feed was 8 mm. The cutting conditions were $N = 1200\ rpm$ and the feed rate 70 mm/min. The maximum resulting scallop height was 133 μm. For the purpose of comparisons, Warkentin's simulations were replicated, with the same cutter specifications and the same tool path, and the same magnitude of scallop heights was obtained. So even though the size of the tool was almost half the tool used in the second cut and the cross feed is almost double, the fact that the feed direction in Warkentin's cut

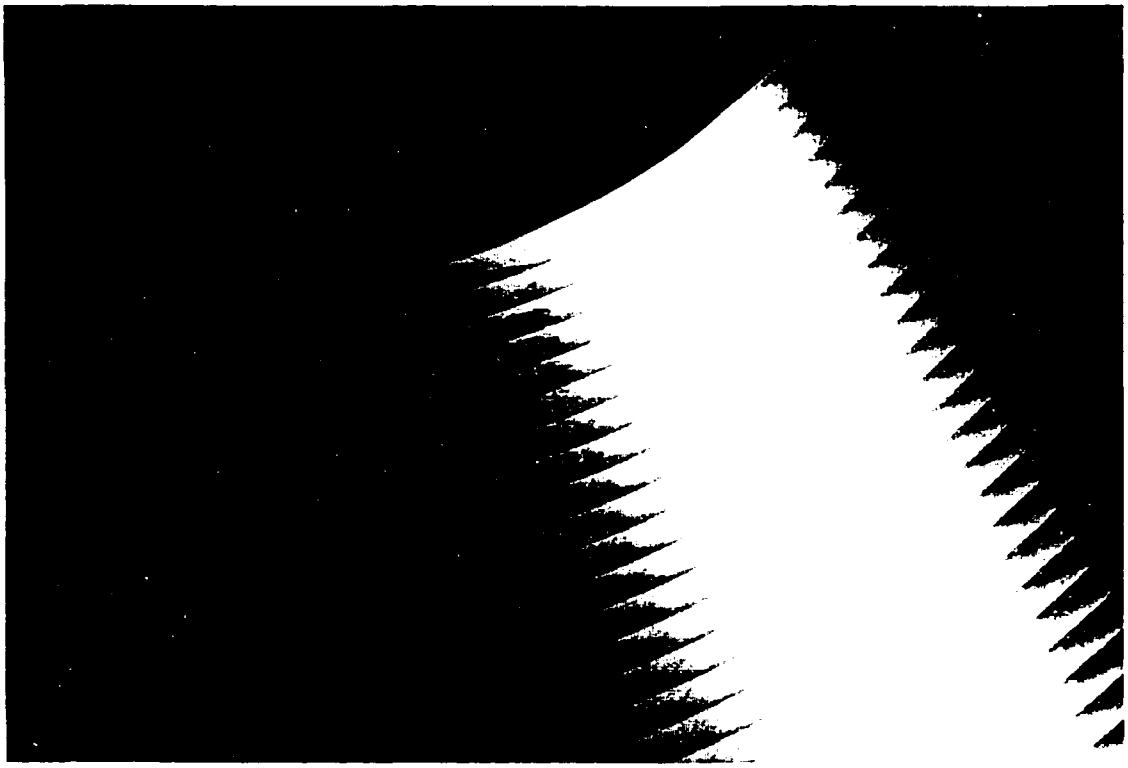


Figure 8.6: A Test Surface Machined with The Inclined Tool Method, $\alpha = 6°$

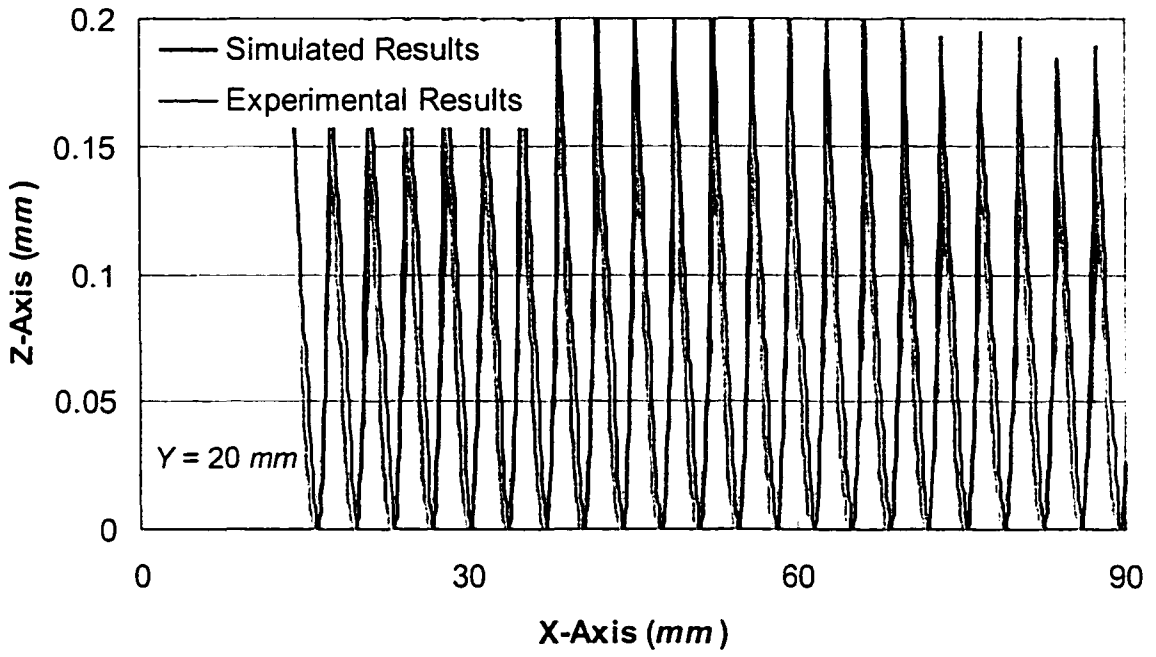


Figure 8.7: Comparison of Scanned and Simulated Results for Inclined Tool Method at $Y = 20\ mm$, $R = 12.7\ mm$, $r = 6.35\ mm$, cross feed $= 3.5\ mm$, $\alpha = 6°$

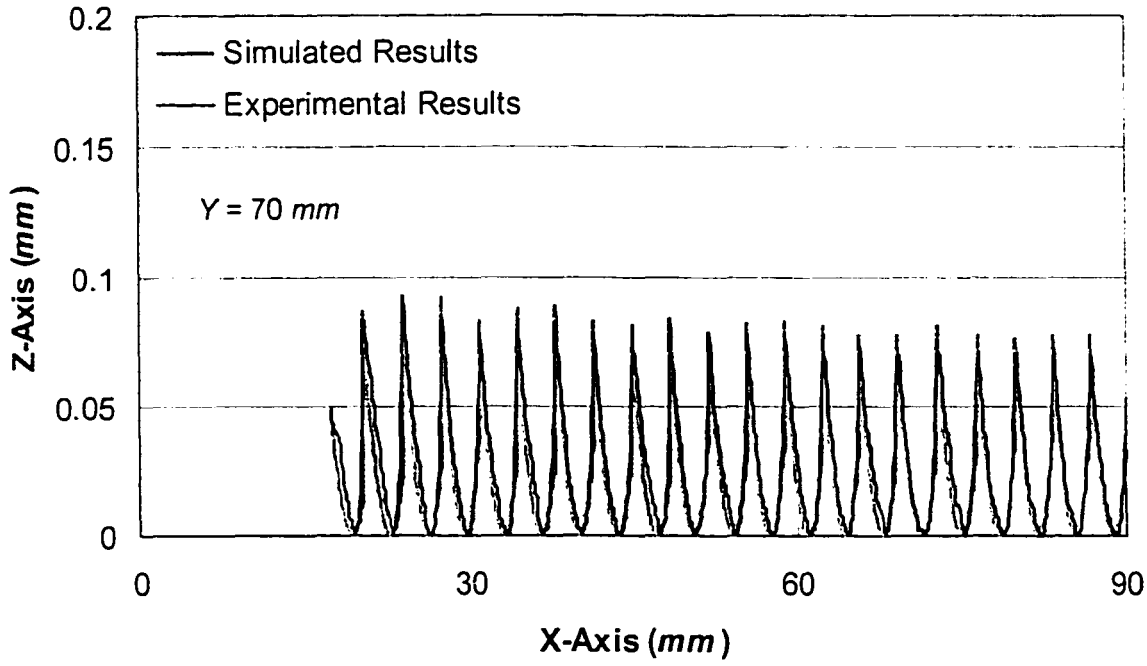


Figure 8.8: Comparison of Scanned and Simulated Results for Inclined Tool Method at $Y = 70\ mm$, $R = 12.7\ mm$, $r = 6.35\ mm$, cross feed $= 3.5\ mm$, $\alpha = 6°$

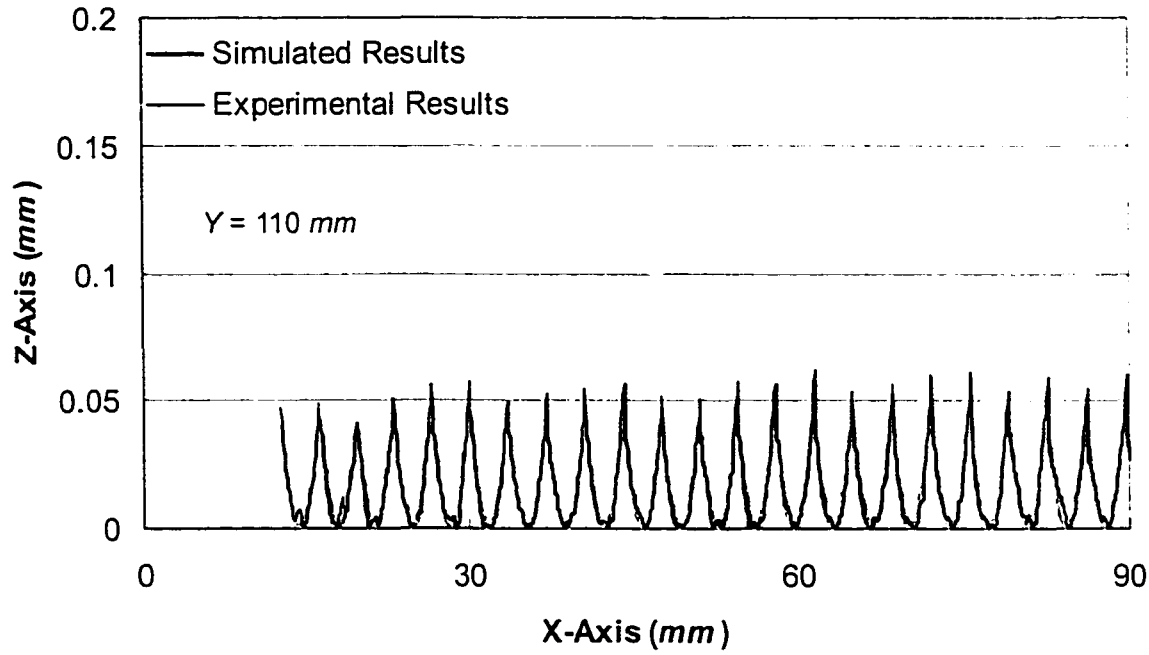


Figure 8.9: Comparison of Scanned and Simulated Results for Inclined Tool Method at $Y = 110\ mm$, $R = 12.7\ mm$, $r = 6.35\ mm$, cross feed $= 3.5\ mm$, $\alpha = 6°$

was parallel to the the direction of minimum curvature reduced the scallop heights by a magnitude of 6.

The third cut, figure 8.10, was also performed with $\alpha = 6°$, however, the feed direction was off the X-axis by 60°. The SVS program did not detect any gouging and it was proven to be correct using the machined part. Scallop heights in this cut were much smaller than the second cut, only 45 μm. Again, this could be directly attributed to the feed direction being close to the direction of minimum curvature.

The fourth cut, figure 8.11, was machined based on the new gouge avoidance method. The feed direction was off the X-axis by 60° and the cross feed was 3.5 mm parallel to Y-axis. At each point of the tool path, the initial value of α was zero and then it was progressively increased to avoid gouging. The maximum value of α in this cut was 5.81°.

As predicted, no gouging occurred on the test surface and the resulting surface finish was much smoother than the previous 3 cuts. The maximum scallop height in this cut was 0.11 μm which is 500 times smaller than the second cut. The generation of the gouge-free tool path in the SVS program took about 20 minutes which is 8 times faster than just generating the swept volume using the Z-map without any gouging analysis.

In summary, the experimental and simulated results were used to check the accuracy of the new gouge detection and avoidance method. The four machined parts were practically identical in appearance. Nevertheless, the surface finish produced

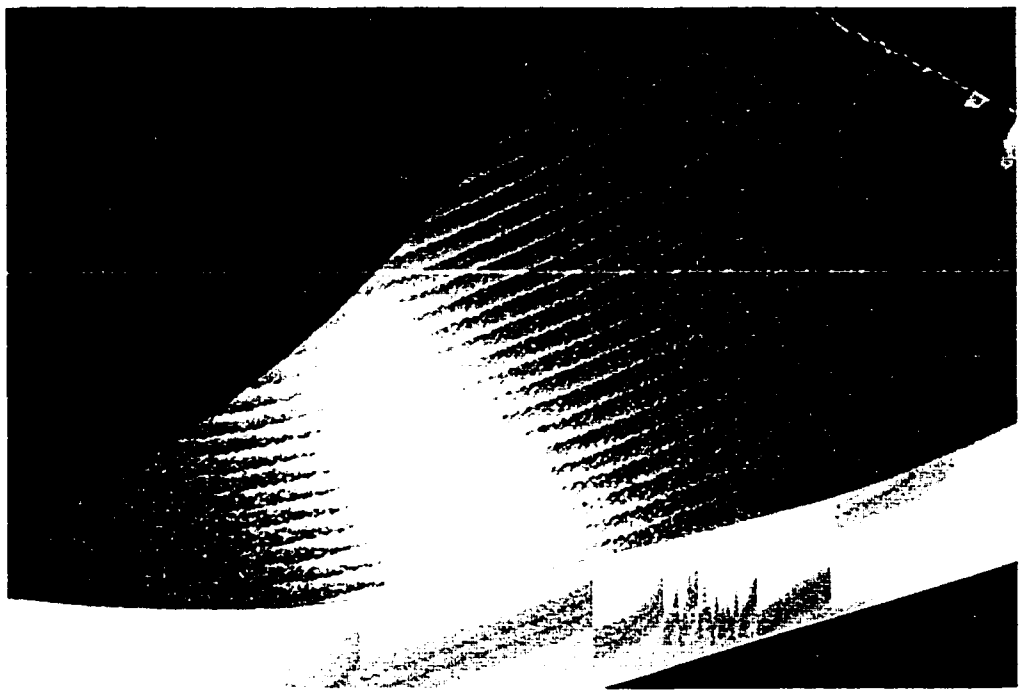


Figure 8.10: A Test Surface Machined with the Inclined Tool Method



Figure 8.11: A Test Surface Machined with the New Antigouging Method

in each cut could be distinguished simply by touch. The second cut felt the roughest and the cut machined by the new technique was the smoothest and virtually had no scallops. Simulation results show that the scallop heights produced by the new technique are 500 times smaller then the second cut, which proves the superiority of the new gouge detection method.

Chapter 9

Conclusions and Recommendations

9.1 Conclusions

Surface machining is a time consuming and expensive process. This process is widely used in a variety of products such as aircraft and automobile components. An accurate, reliable and fast NC toolkit will decrease the production cost and increase the flexibility of producing more complex surfaces with a better surface finish. In this work, the goal was to develop a new, accurate and fast NC toolkit that would significantly reduce the verification time: the SVS program presented in this work has accomplished this goal.

The SVS program is a complete CAD/CAM toolkit, it is composed of four major components:

- **Analyzing the Design Surface Information**

The design surface can be entered into the program either by providing the equation of surface or the CL-data. The SVS program will produce an initial position and orientation for the tool to remove the maximum amount of material along the pass, as explained in chapter 7. The tool position and orientation will be later corrected to avoid gouging.

- **Generating the Swept Volume**

  Most of the time of this research was spent in developing a fast and accurate swept volume technique. Two techniques were developed in chapters 3 and 5. The method presented in chapter 3 deals with special surfaces. Different surface patches (concave, convex, flat) were thoroughly investigated. The technique presented in chapter 7 is more general and it accommodates more general APT tools. Both techniques were verified numerically and experimentally in chapters 6 and 8 and proven to be fast and accurate.

- **Gouge Checking**

  After generating the swept volume, the generating curves are digitized into a number of points. Depending on the desired accuracy, the number of points can be increased or decreased. These points are then used to generate sections across the surface to check for gouging, which allow gouge checking to be performed in two dimensions, which reduces complexity of gouge checking considerably as explained in chapter 7.

  It should be noted that gouging is checked at each point as the tool moves along a pass. If gouging occurs, it will be corrected instantly without having to wait until the whole surface is simulated then checked for gouging, which

is a very costly operation.

- **Gouge Avoidance**

  Gouge avoidance was achieved in this work by positioning the tool with the inclined tool method using different angles. Initially the value of angle α is set to zero then it is progressively increased until gouging is corrected. This procedure will allow the tool to remove the maximum amount of material without gouging the surface which will drastically reduce the scallop heights and consequently the production cost.

9.2 Future Work

The SVS program is indeed more effective to many CAD/CAM softwares in terms of creating gouge-free tool paths. Though it requires some components to make it competitive with the commercial softwares. These components are briefly discussed below.

- **Optimizing the Feed Direction and Scallop Heights**

  As was discussed in chapter 8, the feed direction is crucial in determining scallop heights. Presently, the SVS program does not have a tool to find the best feed direction (direction of minimum curvature). Also, an optimization method has to be integrated with SVS to maintain a certain level of scallop heights.

- **Enhancing the Input/Output**

  The SVS program currently accepts commands from the line mode. A major improvement will be to enhance the program with pop-up windows, drop-down menus, help notes such as material selection, example files and online simulations. This improvement will make sure that users do not have to be very knowledgeable in G-coding and other NC aspects when using the software. Also, expert users should be allowed to manually modify the resulting G-code as required.

- **Adopting Different Kinematics Configurations**

  When the present author started developing the swept volume techniques, it was assumed that all the five axes are on the spindle, which supports some existing five-axis CNC machines. Conversely, when for machining the experimental test pieces, the kinematics had to be changed to adopt the five-axis machine with tilt-rotary table configuration. At the present time, only these two configurations are available in the SVS program. The program should be extended to adopt more kinematics configurations.

It is obvious that a significant amount of research is still needed to draw general conclusions regarding the performance and the best range of application of the new methods. Nonetheless, the results presented in this work for the novel techniques are very encouraging. They have the potential of speeding up the design process and reducing the finish machining time.

Bibliography

[1] Altan, T. .Lilly, B.W.., Kuth, J.P., Konig, W., Toshoff, H.K., Luttervet, C.A., Delft, T.U., Khairy, A.B., *"Advanced Techniques for Die and Mold Manufacturing"*, Annals of the CIRP, vol. 42/2, pp. 707-716, 1993.

[2] Sprow, E.E., *"Should we? Could we? Step Up to Five-Axis Programming?"*, Journal of Manufacturing Engineering, vol. 111, pp. 15-16, November, 1993.

[3] Khalil, Abid and Powell, Anne, *"5-axis model making saves time and money"*, Journal of Production Engineer, pp. 55-60, February, 1987.

[4] Cho, H.D., Jun, Y.T. and Yang, M.Y., *"Five-axis CNC milling for effective machining of sculptured surfaces"*, International Journal of Production Research, vol. 31, pp. 2559-2573, November, 1993.

[5] Roa, N., Bedi, S. and Buchal, R., *"Implementation of the Principal Axis Method for Machining of Complex Surfaces"*, vol. 11, pp. 244-257, 1996

[6] Jensen, C.G. and Anderson, D.C., *"Accurate tool placement and orientation for finish surface machining"*, Journal of Design and Manufacture, October, 1992.

[7] Jensen, C.G., Anderson, D.C. and Mullins S.H., *"Scallop Elimination Based on Precise 5-axis Tool Placement, Orientation, and Step-over Calculations"*, Advances in Design Automation *ASME*, vol. 2, pp. 535-544, February, 1993.

[8] Chou, J.J. and Yang, D.C.H., *"On the Generation of Coordinated Motion of Five-Axis CNC/CMM Machines"*, Journal of Engineering for Industry, vol. 114, pp. 15-22, February, 1992.

[9] Warkentin, A., Bedi, S. and Ismail, F., *"Five-Axis Milling of Spherical Surfaces"*, International Journal of Machine Tools and Manufacture, vol. 36, no. 2, pp. 229-243, 1996.

[10] Vickers, G. W. and Quan, K. W., *"Ball-Mills Versus End-Mills for Curved Surface Machining"*, *ASME* Journal of Engineering for Industry, vol. 111 (22), pp. 22-26, 1989

[11] Bedi, S., Gravelle, S., and Chen, Y., *"Principle Curvature Alignment Technique for Machining Complex Surfaces"*, *ASME* Journal of Manufacturing Science and Engineering, vol. 119, no. 4 pt.B, p.756, 1997

[12] Rao, N., *"Implementation of The Principal Axis Method for Machining of Sculptured Surfaces"*, M.A.Sc. thesis, University of Waterloo, Waterloo, Canada, 1996.

[13] Jerard, R. B., Hussaini, S. Z., Drysdale, R. L. and Schaudt, B., *"Approximate Methods for Simulation and Verification of Numerically Controlled Machining Programs"*, *The Visual Computer*, vol. 5, pp. 329-348, 1989

[14] Blackmore, D. and Leu, M.C., *"A Differential Equation Approach to Swept Volumes"*, Conference on Computer Integrated Manufacturing, *IEEE*, pp. 143-149, Tory, NY, May, 1990

[15] Blackmore, D. and Leu, M.C., *"Analysis of Swept Volume via Lie Groups and Differential Equations"*, International Journal of Robotics Research, vol. 11, no. 6, pp. 516-537, December, 1992.

[16] Blackmore, D., Leu, M.C. and Wang, L.P., *"The Sweep-Envelope Differential Equation Algorithm and Its Application to NC Machining Verification"*, Computer Aided Design, vol. 29, no. 9, Elsevier Science Ltd, pp. 629-637, September, 1997.

[17] Leu, M. C., Wang, L. and Blackmore, D., *"A Verification Program for 5-Axis NC Machining with General APT Tools"*, CIRP Annals - Manufacturing Technology vol. 46, no. 1, International Institute for Production Engineering Research, pp. 419-424, 1997.

[18] F. Warner, *"Foundation of Differentiable Manifolds and Lie Groups"*, Scott-Foresman, Glenview, 1971.

[19] Zeng-Jia Hu and Zhi-Kui Ling *"Generating Swept Volumes with Instantaneous Screw Axes"*, Design Technical Conference, *ASME*, DE-vol. 70, Mechanism Synthesis and Analysis, pp. 7-14, New York, NY, 1994.

[20] Ling, Z.K. and Chase, T.R., *"Generating the Swept Area of a Body Undergoing Planar Motion"*, Advanced in Design Automation, *ASME*, vol. 32, pp. 227-236, 1991.

[21] John D. Weld and Ming C. Leu, *"Geometric Representation of Swept Volumes with Application to Polyhedral Object"*, International Journal of Robotics Research, vol. 9, pp. 105-117, October, 1990.

[22] Leu, M. C., Park, S.H. and Wang, K.K., *"Geometric Representation of Translational Swept Volumes and its Applications"*, *ASME* Journal of Engineering for Industry, vol. 108, pp. 113-119, 1986.

[23] Martin, R.R., *"Swept Volumes in Solid Modellers"*, Conference of Computer-Aided Surface Geometry and Design, 1989.

[24] Sambandan, K., Kedem, K. and Wang, K.K., *"Generalized Planar Sweeping of Polygons"*, Journal of Manufacturing Systems, vol. 11, no. 4, pp. 246-257, 1991.

[25] Wang, W.P. and Wang, K.K., *"Geometric Modeling for Swept Volume of Moving Solids"*, *IEEE* of Computer Graphics and Applications, vol. 6, no. 12, pp. 8-17, 1986.

[26] Staten, M.L., Canann, S.A. and Owen, S.J., *"BMSweep: Locating interior nodes during sweeping"*, Engineering with Computers vol. 15, no. 3, Springer-Verlag London Ltd., London, England, pp. 212-218, 1999.

[27] Liu, S.-S., Uicker, J. Jr. and Gadh, R., *"Dual Geometry - Topology Constraint Approach for Determination of Pseudo-swept Shapes as Applied to Hexahedral Mesh Generation"*, *CAD* Computer Aided Design vol. 31, no. 6, Elsevier Science Ltd, Exeter England, pp. 413-426, 1999.

[28] Narvekar, A.P. and Oliver, J.H., *"Intersection of Vectors With General Five-Axis NC Swept Volumes"*, Manufacturing Group Conference, *ASME*, pp. 99-104, New York, NY, March, 1990.

[29] Wang, W.P. and Wang, K.K., *"Real Time Verification of Multiaxis NC Programs with Raster Graphics"*, *IEEE* Proc. of 1986 International Conference on Robotics and Automation, San Francisco, pp. 166-171, April, 1986.

[30] Van Hook, T., "*Real Time Shaded NC Milling Display*", Computer Graphics, Proc. SIGGRAPH, vol. 20, no. 4, pp. 15-20, Dallas, TX, August, 1986.

[31] Atherton, P.R., Eral, C. and Fred, C., "*A Graphical Simulation System for Dynamic Five-Axis NC Verification*", Proc. Autofact, *SME*, Dearborn, MI, pp. 2-12, 1987.

[32] Menon, J. P. and Robinson, D. M., "*Advanced NC Verification via Massively Parallel Ray Casting: Extensions to New Phenomena and Geometric Domains*", *ASME Manufacturing Review*, vol. 6, no. 22, pp. 141-154, June, 1993

[33] Rao, N., Ismail, F. and Bedi, S., "*Tool Path Planning for five-axis Machining Using the Principal Axis Method*", International Journal of Machine Tools and Manufacture-Design Research and Application, vol. 37, no. 7, pp.1025-1041, 1997.

[34] Kim, C.B., Park, S. and Yang, M.Y., "*Verification of NC Tool Path and Manual and Automatic Editing of NC Code*", The International Journal of Production Research, vol. 33, no. 3 pp. 659-673, 1995.

[35] Jerard, R. B., Drysdale, R. L. and Hauck, K., "*Geometric Simulation of Numerical Controlled Machining*", Proc. *ASME* International Computers in Engineering Conference San Francisco, vol. 2, pp. 129-136, 1988.

[36] Jerard, R. B., Drysdale, R. L., Schaudt, B. and Magewick, J., "*Methods for Detecting Errors in Numerically Controlled Machining of Sculptured Surface*", *IEEE* Computer Graphics and Applications, vol. 9, no. 1, pp. 26-39, 1989.

[37] Drysdale, R. L., Jerard, R. B., Schaudt, B. and Hauck, K., "*Discrete Simulation of NC Machining*", *Agorithmica*, vol. 5, no. 1, pp. 33-60, 1989.

[38] Bedi, S., Ismail, F., Chen, Y. and Mahjoob, M., *"Toroidal versus Ball Nose and Flat Bottom End Mills"*, International Journal of Advanced Manufacturing Technology, vol. 13, no. 5, pp.326-333, 1997.

[39] Sheltami, K., Bedi, S. and Ismail, F., *"Swept Volumes of Toroidal Cutters Using Generating Curves"*, International Journal of Machine Tools and Manufacture vol. 38 pp. 855-870, 1998.

[40] Martti Mantyla *"An Introduction to Solid Modeling"*, Text Book, Helsinki University of Technology, 1988.

[41] Kieffer, J. and Litvin, F.L., *"Swept Volume Determination and Interference Detection for Moving 3-D Solids"*, Journal of Mechanical Design, vol. 113, pp. 156-163, 1991.

[42] Roth, D., Bedi, S. and Ismail F., *"Generation of the Swept Volume of Toroidal Endmills in Five-Axis Motion Using Space Curves"*, 5^{th} ACM Symposium on Solid Modeling and Applications, Ann Arbor, MI, , USA, Sponsored by: Association for Computing [Machinery], New York, NY, USA, pp. 306-311, Jun 9-11, 1999.

[43] Yu, Daoyuan, Deng, Jianchun, Duan, Zhengcheng and Liu, Jinling, *"Generation of Gouge-Free Cutter Location Paths on Freeform Surfaces for non-Spherical Cutters"*, Computers in Industry vol. 28 pp. 81-94, 1996.

[44] Li, F., Wang, X. C., Ghosh, S. K., Kong, D. Z., Lai, T. Q. and Wu, X. T., *"Gouge Detection and Tool Position Modification for Five-Axis NC Machining of Sculptured Surfaces"*, Journal of Materials Processing Technology vol. 48 pp. 739-745, 1995.

[45] Li, S. X. and Jerard, R. B., *"5-Axis machining of sculptured surfaces with a flat-end cutter"*. Computer Aided Design vol. 26 no. 3 Published by Butterworth-Heinemann Limited pp. 165-178, 1994.

[46] Takeuchi, Y. and Idemura, T., *"5-Axis control machining and grinding based on solid model "*. Annals of the CRIP vol. 40 no. 1 pp. 455-458, 1991.

[47] Veeramani, Dharmaraj and Gau, Yuh-Shying, *"Issues in patch-by-patch machining of compound sculptured surfaces"*. *IIE* Transactions (Institute of Industrial Engineers) vol. 30 no. 4 Chapman & Hall Limited, pp. 341-355, April, 1998.

[48] Wang, Yu and Tang, Xiaowei, *"Five-axis NC machining of sculptured surfaces"*. International Journal of Advanced Manufacturing Technology vol. 15 no. 1 Springer-Verlag London Limited, pp. 7-14, 1999.

[49] Chung, Yun C., Park, Jung W., Shin, Hayong and Choi, Byoung K., *"Modeling the Surface Swept by a Generalized Cutter for NC Verification"*. Computer Aided Design, vol. 30, pp. 587-593, 1998.

[50] Warkentin, A., Ismail, F., and Bedi, S. *"Comparison Between Multi-Point and Other 5-axis Tool Positioning Strategies"*. International Journal of Machine Tools and Manufacture, vol. 40, no. 2, pp. 185-209, 2000.